2009

Molecular dynamics simulation of shock waves in laser-material interaction

Sobieslaw Stanislaw Gacek
Iowa State University

Molecular dynamics simulation of shock waves in laser-material interaction

by

Sobieslaw Stanislaw Gacek

A dissertation submitted to the graduate faculty

in partial fulfillment of the requirements for the degree of

DOCTOR OF PHILOSOPHY

Major: Mechanical Engineering

Program of Study Committee:
Xinwei Wang, Major Professor
Palaniappa A. Molian
Song-Charng Kong
Zhi Jian Wang
Qingze Zou

Iowa State University

Ames, Iowa

2009

TABLE OF CONTENTS

LIST OF TABLES

LIST OF FIGURES

ACKNOWLODGEMENTS

Above all, I would like to express my appreciation to my major advisor, Professor Xinwei Wang without whose valuable assistance in providing continuous support in the Ph.D. program and endless help this work would not have been possible. The invaluable discussions with him encouraged me to approach research problems from different perspectives and motivated me to be persistent to accomplish any goal.

Besides my advisor, I would like to thank other Professors from my thesis committee: Palaniappa A. Molian, Song-Charng Kong, Zhi Jian Wang, Qingze Zou for their insightful comments and careful review of this manuscript on a very short notice.

My great appreciation also goes to Lijun Zhang for initial introduction to the original MD program for shockwave simulation and other great colleagues from this laboratory.

During the course of this work, at University of Nebraska Lincoln (2006-2007), I was supported by the Nebraska Research Initiatives. At Iowa State University support to my work from ONR under the MURI program is gratefully acknowledged.

Last, but not least, I am in depth grateful to my Family for believing in me, and especially I thank my Godmother – Krystyna Pawelec, for unconditional encouragement and unceasing incentives to study and research.

ABSTRACT

In recent decades, laser technology has been widely used in manufacturing, non-destructive measurement processes, and has been extensively implemented in medical applications. The detailed knowledge of the laser-target interaction along with accompanied effects in background environment is absolutely essential due to the significance of the intricate existing occurrences. Therefore, in this discourse, a number of phenomena in laser-material interaction at nanoscale are studied thorough.

Firstly, the dynamics and internal structure of shock waves in picosecond laser-material interaction are explored at the atomistic level. The pressure of the shock wave, its propagation, and interaction zone thickness between the plume and ambience are evaluated to study the effect of the laser absorption depth, ambient pressure, and laser fluence. Sound agreement is observed between the molecular dynamics simulation and theoretical prediction on shock wave propagation and mass velocity. Due to the strong constraint from the compressed ambient gas, it is observed that the ablated plume could stop moving forward and mix with the ambient gas, or move backward to the target surface, leading to surface redeposition. Under smaller laser absorption depth, lower ambient pressure, or higher laser fluence, the shock wave will propagate faster and have a thicker interaction zone between the target and ambient gas.

Secondly, the effects of shock driven process of the laser-ablated argon plume in the background gas environment are explored via molecular dynamics simulations. The primary

shock wave propagation and its influence on the backward motion of the target material are delineated. It has been observed that the strong pressure gradient inside the main shock wave overcomes the forward momentum of the plume and some compressed gas, leading to backward movement and re-deposition on the target surface. Reflection of the backward moving gas on the target surface results in the secondary shock wave. Detailed investigation of the secondary shock wave phenomenon is provided, which gives, for the first time, an insight into formation and evolution of the internal gaseous shock at the atomistic level.

Thirdly, the physics of plume splitting in pico-second laser material interaction in background gas are studied with MD simulations. The velocity distribution shows a clear split into two distinctive components. For the first time, detailed atom trajectory track reveals the behavior of atoms within the peaks and uncovers the mechanisms of peak formation. The observed plume velocity splitting emerges from two distinguished parts of the plume. The front peak of the plume is from the faster moving atoms and smaller particles during laser-material ablation. This region experiences strong constraint from the ambient gas and has substantial velocity attenuation. The second (rear) peak of the plume velocity originates from the larger and slower clusters in laser-material ablation. These larger clusters/particles experience very little constraint from the background, but are affected by the relaxation dynamics of plume and appear almost as a standing wave during the evolution. Density splitting only appears at the beginning of laser-material ablation and quickly disappears due to spread-out of the slower moving clusters. It is found that higher ambient pressure and stronger laser fluence favor earlier plume splitting.

Finally, the conclusions are drawn and author's contributions from performed work are delineated.

1. INTRODUCTION

The number of applications of the laser ablation of materials in background gas has thrillingly increased in recent years, especially having widely usage in photolithography, integrated optics, and last, but not least, the micro/nanofabrication.

Specifically, laser–induced ablation results from the conversion of an initial electronic or vibrational photoexcitation into kinetic energy of nuclear motion, leading to ejection of atoms, ions molecules, and even clusters from a surface. The formation of an ablation plume – a weekly ionized, low-to-moderate density expanding gas cloud – normally is accompanied by complex plasma-surface interactions, gas dynamics, and laser-induced photodynamics. The kinetics and dynamics of this conversion depend critically on the mechanism of light absorption, electron-lattice interactions characteristic of the laser-irradiated solid, such as scattering of free electrons by phonos with phonon emission, localized lattice rearrangements and configuration changes such as self trapping of holes and exitons, defect formation and defect reactions as well as surface decomposition due to the electronic interactions of defects with lattice ions (Miller and Haglund, 1998).

Unquestionably, great popularity of this technological genre is owed to the contemporarily developed techniques such as laser micromachining (Fogarassy and Lazare, 1992), laser shock peening (Hill *et al.*, 2003), and pulsed laser deposition (PLD) (Chrisey and Hubler, 1994). In these methods, ambient medium is frequently used to improve the desired characteristics of the obtained materials as well as qualities of the final surfaces produced.

However, presence of background environment significantly affects the formation of intricate kinetic and dynamics processes, which among others may incorporate the plume backward motion, plume oscillation with plume splitting, and generation of the primary and secondary shock wave front. Therefore, the dynamical behavior of the plume, along with accompanied effects in such environment (shock waves) are of fundamental significance in obtaining the detailed knowledge about these intriguing phenomena.

A considerable number of techniques have been used to provide information about the interaction of laser light with solids so far. The great interest is to measure many parameters in laser ablation process. They may include: the shape and velocity of the plume at various times after the ablating laser pulse, the spatial distribution of density, and temperature at various times after the ablating laser pulse, and the spatial variation of the plume composition, in terms of the atoms, molecules, excited states, and clusters presence (Phipps, 2007). A very extensive literature describing a wide range of experimental techniques to diagnose laser ablation plumes exist. These have been reviewed by various authors in particular by Chrisey and Hubler (1994) or Eason (2007). The methods include a variety of optical spectroscopies, electron and mass spectrometry, time-of-flight studies, optothermal techniques and pressure and momentum transfer measuring techniques, all of which have been applied for the study of the event during and immediately following the light pulse.

Therefore, in order to establish any optimization of the film deposition process it requires then, a comprehensive knowledge of the plume processes during the expansion.

Since the breakthrough in preparation of thin films of Y-Ba-Cu-O superconductor using pulsed excimer laser evaporation of a single bulk material target in vacuum (Dijkkamp *et al.*, 1987) the optimization of the film deposition immensely progressed in nineties. Dyer *et al.* (1990) studied plume dynamics for excimer laser ablation of Y-Ba-Cu-O in an O_2 atmosphere using streak photography and spectroscopy. They observed that at pressures greater than 1 mbar the expansion resembles a blast wave driven by the ablation products with mixing and reaction at the contact surface. Scott *et al.* (1990) investigated the luminous ablation plume formed by laser irradiation of the superconductor $YBa_2Cu_3O_{7-x}$ by high-speed framing photography. They reported the formation of shock waves and instabilities on the shock front for pressures above 0.25 mbar and found that changing the pressure of the background oxygen gas influences significantly the velocity distribution of ejected products. Lichtenwalner *et al.* (1993) presented the results on how the ablated flux characteristics of PZT, LSC, and MgO strongly dependent the ablation time, the laser energy, and the oxygen (or noble gas) pressure.

The knowledge of plume's behavior has advanced tremendously from the many recent spectroscopic studies with fast imaging techniques (Geohegan and Puretzky, 1995; Harilal *et al.*, 2002, 2003; Amoruso *et al.*, 2005, 2006), but Langmuir probe studies have also contributed to the understanding of plume dynamics (Geohegan and Puretzky, 1995; Wood *et al.*, 1997; Hansen *et al.*, 1999; Amoruso, *et al.*, 2005, 2006). Furthermore, the study by Ashfold *et al.* (2004) focused on aspects of the fundamental chemical physics of PLA and PLD processes and deposition, and has attempted to track the evolution of material from the target through to the deposited film.

The detailed theoretical or computational treatment has been also performed and a number of numerically based models have been developed for laser ablation processes. The theoretical description of the adiabatic expansion has been considered by Anisimov *et al.* (1996). His original model was extended to describe an expansion into a background gas with a low pressure. Arnold *et al.* (1999) derived an analytical model for the plume dynamics during the expansion into a background gas. Their model is based on a spherical expansion in forward and backward direction from a fictive target surface without any assumptions of a background gas of low pressure. Pathak *et al.* (2007) developed the method that can capture multiple plume roll-up, interaction of plume with shock waves and they claimed that the combination of nonlinear Godunov and linearized Roe methods for discretization of plume gas dynamic equations is suitable for modeling plume dynamics in laser ablation of carbon.

Gaining a better understanding of the factors governing thermal and physical phenomena under laser irradiation is of special importance for material interaction process. Essential knowledge of the dynamics of the shock wave and transient plume's behavior can serve for controlling the laser material interaction process, optimizing the efficiency of laser assisted micro-machining, and minimizing the laser induced material damage. These brief chapters give separate introductions in number of laser material interaction processes and techniques that involve generation of the shock wave.

1.1 Shock Wave Phenomena in Laser Material Interaction in Background Gas

The study of laser ablation processes is absolutely essential since it has been one of the key laser technologies of recent years. It constitutes a sequence of particularly convoluted and multiplex phenomena inclusive of laser-solid interaction, evaporation of target material due to the implemented laser energy, plasma plume formation combined with its intrinsic generation of high kinetic energy region of the ejectants, transportation and evolution of the intense, very short time scale shock waves associated with intense processes in the ejected front cloud, along with plume-solid interaction at the deposited surface. Of special importance and intricacy is the dynamics evolution of shock waves in laser-material interaction. When a background gas instead of a vacuum environment is present, considerable new processes arise such as deceleration, attenuation and thermalization of the molten particles, as well as diffusion, recombination and formation of the shock waves (Le *et al.*, 2000). Often observables are also generation of multiple fronts, nanoclusters frequently combined with plume backward motion occurrence and phenomenon of 'plume splitting' all resulting in significant impact on the deposition process.

The nanoscale shock wave phenomenon has long fascinated researchers all around the world and has been the subject of intensive investigation in recent years. Shock waves are fast mechanical transients generated by violent impacts or explosions associated with the fast compression inherently violent increase in pressure and temperature. According to Zel'dovich and Raizer (2001) shock wave formation is the result of a growing hydrodynamic interaction between the plume and the background gas and becomes important when the mass of the displaced gas is comparable to the mass of the plume. The study of the internal structure of

shock fronts is of interest for many and recent progress in combining the techniques of time-resolved molecular spectroscopy with shock compression science gave profound insight in studying physical chemical phenomena that involve large-amplitude displacements (Dlott, 1999).

The accompanying issue of plume splitting in low pressure background gases has been reported in the profound experimental (Geohegan and Puretzky, 1995, 1996) and numerical work by Leboeuf *et al.* (1996) and Wood *et al.* (1997). Work by Voevodin *et al.* (2000) presents results of laser ablation deposition of yttria stabilized zirconia films in a low pressure oxygen and argon ambient environment. One significant study by Harilal *et al.* (2003) shows the effect of ambient air pressures on the expansion dynamics of the plasma generated by laser ablation of an aluminum target. Mason and Mank (2001) investigated how laser parameters, especially laser fluences affect crater size and shape formation. Moreover, Russo *et al.* (2000, 2002) performed sound research on how laser fluence, the induced recoil pressure and radiating heating of the substrate influence the amount of ablated material mass.

The subject of laser ablation in background gas and consecutively shock waves formation is also extensively treated in prior theoretical and numerical literatures. Analysis of multiple shock waves has been well documented in a theoretical study by Bulgakov and Bulgakova (1995). In Le *et al.*'s study (2000) the physical phenomena involved in laser-induced plasma expansion into a background gas was numerically studied. The authors developed a model which considers diffusions, thermal conduction, viscosity, and ionization effects. A new theoretical model has been developed by Zhang and Gogos (2004) to explain

the influence of ambient gas and laser intensity in laser ablation. Another theoretical study by Bulgakov and Bulgakova (1998) paid particular attention to the analogy between an ablation plume and a supersonic under expanded gaseous jet.

Nevertheless, none of those fully stated about shock wave formation, propagation and attenuation, interaction of the shock wave with the ablation plume, effect of the optical absorption depth on the shock wave, or the effect of the laser pulse width, laser fluence, background pressure, and species of the background gas. It would be of considerable significance to have a compendium of those compelling processes.

In chapter 3 is presented quantitative explanations for a number of gas-dynamics effects when the interaction between the picosecond laser ablated argon plume and background gas occurs in a very short of time - up to 5 ns.

1.2 Secondary Shock Wave Phenomenon in Laser Material Interaction in Background Gas

In laser-assisted material processing an ambient gas is frequently used to improve the desired characteristics of the obtained materials as well as qualities of their final structure. The presence of background gas and the induced shock wave significantly affects the dynamic behavior of the ablated plume. In prominent research on the dynamics of laser ablation plume by Geohegan *et al.,* experimental investigation (Geohegan and Puretzky, 1995) as well as theoretical study (Leboeuf *et al.*, 1996 and Wood *et al.*, 1997) of the plume splitting in low pressure background gases has been performed. Interesting theoretical study

on gas dynamics of pulsed laser ablation by Han *et al.* (2002) was conducted on shock wave formation in helium ambient gas and reflection of the shock front on the silicon substrate. Recent measurements of the internal structure and expansion dynamics of laser aluminum plumes have been reported in work of Harilal *et al.* (2003). Work by Singh *et al.* (2005) provided study on the effect of ambient pressure on the redeposition of debris and the plume backward motion. Furthermore, the issue of pulse characteristic of the plume expansion was reported by Bulgakov *et al.* (1996) Time-of-flight (TOF) signal oscillations according to generation of the primary and secondary shock wave in the plume-background gas interaction was observed in their experimental work (Bulgakov *et al,*. 1996), and that exceptional feature has been covered also empirically (Bulgakov and Bulgakova, 1995).

Although extensive experimental and theoretical work has been done on the shock wave phenomena in laser ablation, the formation of the secondary shock wave has not been explained satisfactorily. As a matter of fact, to the author's knowledge, the internal shock wave formation at atomistic level has scarcely been studied in literature so far.

One of the objectives of chapter 4 is to explicate the process of formation, and particularly structure with thermodynamic and physical states of the secondary shock wave in nanoseconds range at molecular level.

1.3 Plume Splitting in Laser Material Interaction under the Influence of Shock Wave

A wide spectrum of applications for pulsed lasers in material processing, thin film growth, and laser-assisted manufacturing has brought overwhelming interest to the field of laser-material interaction. The techniques are complicated and the dynamics of expanding laser ablation plume in background gas consists of many successive elaborated phenomena (Chrisey and Hubler, 1994; Eason, 2007). At a certain distance from the target, the fraction of atoms from the plume that penetrate the surrounding gas as a freely expanding plume decreases strongly with the increasing gas pressure. This decrease is accompanied by a large enhancement of the slow component which leads to the so-called plume splitting.

Over the last decade plume splitting in laser-material interaction has received much attention in literature and a preponderance of previous work has studied the phenomena both experimentally and theoretically. The most in-depth one that gives very detailed accounts of the concerned effect is given by Geohegan and Puretzky (1995) who provided first time compelling evidence of the plume splitting for yttrium in argon environment , and compared with results in several other systems, including Si/Ar, Si/He, YBCO/O_2 (Geohegan and Puretzky, 1995) Furthermore, the authors interpreted the experimental results using hydrodynamic model that includes multiple scattering to exemplify this occurrence (Leboeuf *et al.*, 1996 and Wood *et al.*, 1997). The nature of plume double-peaked arrangement in the background gas has been widely investigated by Bulgakov *et al.* (1995, 1996, 1998, 2000) based on superconductor YBCO in oxygen and an endeavor of the respectable gas-dynamical modeling has been conducted. In prominent study by Harilal (2001) the plume splitting has been observed also in carbon/helium system for different laser fluences, and the plume

splitting effect was observed only in a particular pressure range in an Al/air system (Harilal *et al.*, 2002). Moreover the twin-peak distribution formation has been studied for different air pressures (Harilal *et al.*, 2003). In recent years the work performed by Amoruso *et al.* (2005, 2006, 2008) provides remarkable investigation of the clearly observed metallic plume splitting in a variety of gases such as helium, oxygen, argon and xenon for UV laser irradiation.

Various analytical techniques based on gas dynamics have been developed to study the laser ablation regime. These models provide somehow insufficient insight into the physical picture. To that subject more suitable appears to be the molecular dynamics or Monte Carlo simulation approach. One account of the strength of the atomistic investigation is to provide detailed explanation of nanoscale phenomena. Analysis from Itina *et al.* (2002) numerical modeling based on the combined large-particle direct Monte Carlo simulation has provided compelling evidence on the existence of the double peaked character in Al/O_2 system. In their work the physics of plume splitting from the atomistic view were attempted to explain.

The chapter 5 of this study represents an early attempt to exemplify the fundamentals of plume splitting at atomistic level under the influence of shock wave.

1.4 Laser Shock Peening

The rapid progress in laser material interaction regime contributed to development of one special, derivative technique – laser shock peening (LSP), which performance is strongly influenced by shock wave. The introduction of this technology brought a broad application in the material surface manufacturing and consequently recent decade its full commercialization. Generally, LSP is a process in which a laser beam is pulsed upon a metallic surface, producing a planar shock wave that travels through the workpiece and plastically deforms a layer of material (Hill *et al.*, 2003). It uses a strong laser impulse to impart high compressive residual stresses in the surface of material components. The laser pulse ignites a blast from the specially coated surface of the component. The expansion of the shock wave then creates a traveling acoustic wave that is coupled into the component, thereby compressing the material's lattice microstructure. The achievable strengthening results are a significant improvement in the high cycle fatigue properties of the component and greatly increase its surface mechanical properties.

The method has already found wide range of commercially available applications and continuously extends its potential. Not only in military, aerospace (metal shaping of Ti airfoils in high-performance aircraft), medical and automotive industries is used, but in treatment and forming of components used in healthcare delivery, nuclear power generation, and drilling for petroleum products. Overall the laser peening treatment has proven to be robust and reliable, meeting severe, high performance industrial requirements.

One of the characteristics of this technique is that target surface is usually coated with

protective layer of the dark paint and the process is performed under a thin overlay of transparent material, like water in order to generate higher plasma pressure than that in the air. When a nanosecond laser pulse passes through the transparent tamping water layer, focuses on the top surface and is absorbed by the dark paint. Due to the fact, that the mean free path in metals of visible and near infrared laser radiation is less than 1 μm, only a very thin surface layer of material is heated when a laser beam of sufficient intensity strikes a metal surface. Sudden energy deposition time, limits thermal diffusion of energy away from the interaction zone to at most, a few micrometers. The heated material is ejected, vapor rapidly achieves extremely high temperatures, and electrons are ionized from the atoms which all in result give rise to a rapidly expanding, high pressure plasma cloud. The ablated plasma plume is tamped to the surface by the water layer (it acts like a lid on a pot to help contain the shock). If the plume is not confined to the metal surface, pressures of only a few tenths of GPa are achieved. However, if an overlay transparent to the laser light is pressed against the metal surface, the hydrodynamic expansion of the heated plasma in the confined region between the metal target and transparent overlay creates the high amplitude-short duration pressure pulse required for laser and shock processing (Clauer *et al.*, 1981). Therefore, the plasma pressure is enhanced by water. The interaction creates a pressure shock wave in the range of few GPa to build up on the workpiece surface over 10 to 100 ns that in turn creates a deep compressive stress layer directly underneath the focused pulse and exceeds the yield stress of metals. The plasma is spatially contained from spreading across the surface area by layer of tamping water and thus transmits a shock wave directly forward into the metal. After the passage of the high amplitude shock wave in the material, the permanent strain remains and the surrounding metal material constrains the strained region

due to elastic strain, and thus forms a compressive residual stress on the metal surface. Each laser pulse imparts GPa range pressure pulse at the component surface by generating a plasma in a thin layer of protective tape or paint on the metal surface. The high rate of deformation during laser peening produces a layer of plastically deformed material and the depth of plastic deformation and resulting compressive residual stress are significantly deeper than possible with most other surface treatments. LSP does not have the kinetic energy limitations of metal or ceramic shot. As a result, it can induce a compressive stress layer more than 1 millimeter thick, some four times deeper than that obtainable with traditional shot (Hill *et al.*, 2003). The increased depth effectively extends the service lifetime of parts some three to five times over that provided by conventional treatments, an increase essential for preventing cracking on blades, rotors, and gears.

A unique offered advantage of some techniques of laser shot laser pulse is its square profile. A typical laser's round output beam requires overlapping spots on a metal surface in an inefficient manner, but the new systems allows full coverage of each square spot directly adjacent to the next. Furthermore, the systems are capable to automatically maintain the laser-pulse wavefront near the physically allowable limit, enabling higher power without worry of laser glass damage or damage to the treated part (Hill *et al.*, 2003).

The hardening of the some materials is a result of a significant increase in dislocation density caused by the shock wave. However, some metals do not respond to a single laser shot at the peak pressures achievable by laser. For that reason multiple shots can produce a progressive increase in hardness. The increase in hardness is caused by an increase in the

dislocation density with increasing laser shock repetitions (Clauer *et al.*, 1981).

Large number of literature has been devoted to the laser shock peening phenomena. A number of metals and alloys have been treated by LSP, including steels, aluminum alloys, titanium alloys, nickel-base superalloys, cast irons and a powder metallurgy iron alloy. In some of these cases, the investigations include both residual stresses and fatigue results, or directly compare LSP and shot peening (Everett *et al.*, 2001). The results of tensile testing and hardness depth-profiling indicated that the laser treatment significantly improved the mechanical properties of cast titanium by improving the surface integrity of the cast surface contamination (Watanabe *et al.*, 2009). The thickness of the plastic deformation layer near the surface generated by the shockwave in LSP is higher than 2.0 mm. With increasing the number of the laser impacts in LSP, the compressive residual stresses and the microhardness at the surface of the LY2 aluminum alloy specimen increases (Zhang *et al.*, 2009).

The laser shock peening process has been covered also in theoretical divagations. A numerical model for the simulation of LSP of materials which includes coupled elastic–plastic wave propagation—structural analysis at each time step has been performed. Finite difference method has been used for the elasto-plastic wave analysis due to recoil pressure loading at the surface; whereas the plastic deformation and the resulting residual stresses developed in the laser-treated region of the substrate are computed by using non-linear FE method (Arif, 2003). A finite element analysis method adopting dynamic analysis with LS-DYNA and static analysis performed by ANSYS is described in detail to attain the simulation of single and multiple laser shock processing. The method is used to simulate

shock wave propagation and predict the distribution of the residual stresses in the metal alloys of 35CD4 50HRC steel treated by LSP with square laser spot (Hu *et al.*, 2006).

1.5 Molecular Dynamics of Laser Material Interaction

Despite a substantial amount of research on laser ablation has been conducted, the underlying effects and the mechanism of laser induced plume expansion in an ambient environment still remains relatively unclear. Great difficulties exist in the analytical study, as well as in experimental investigations such as measurements of the transient surface temperature, the velocity of the solid-liquid interface, and the material ablation rate. The continuum approach of solving the heat transfer problem becomes questionable under the above extreme situations. To gain further insights into these fascinating phenomena, molecular dynamics (MD) simulation is necessary, which allows people to directly track the movement of molecules/atoms. Additionally, this method is capable of revealing the thermally induced processes down to atomistic levels for investigating the ultrashort laser material interactions (Wang, 2005). At nanosecond time scale, it can provide more appropriate quantitative description of the shock wave behavior.

A vast amount of commitment has been devoted to the usage of MD to study laser-material interaction and simulation of shock wave–induced phase transitions. In nineties due to the growing computer capabilities small systems were investigated. A significant development for MD in the last 20 years has been the design of more realistic semi-empirical interatomic interactions, not only for monatomic metals, but also for reactive condensed molecular systems (Holian, 2004). Shock wave experiments are particularly well suited for

molecular dynamic simulations because in such experiments sample sizes are small and time scales are short (Belonoshko, 1997). Robertson *et al.* (1991) performed MD simulations for a 2D diatomic molecular solid for less than 5000 atoms, and reported that those exhibit a shock-induced phase transition and concomitant split shock wave. Hakkinen and Landman (1993) investigated dynamics of superheating, melting, and annealing processes at Cu surfaces induced by laser-pulse irradiation using molecular dynamics simulation. Belonoshko (1997a, b) performed a three-dimensional molecular dynamics simulation of shock wave loading to investigate the Hugoniot equation of state at the transition of argon from solid to liquid. His calculations with different numbers of atoms showed that the system consisting 6000 atoms is sufficient to obtain reliable results. Etcheverry and Mesaros (1999) studied laser material interaction of crystal argon model and the production of acoustic waves in a material irradiated by a pulsed laser, by means of molecular-dynamics simulation for 500000 atoms. Lorazo *et al.* (2003) investigated the mechanisms of laser ablation in silicon close to the threshold energy for pulse durations of 500 fs and 50 ps which was achieved using a unique model coupling carrier and atom dynamics within a unified Monte Carlo and molecular-dynamics scheme. Zhigilei (2003) investigated the dynamics of the early stages of the ablation plume formation and the mechanisms of cluster ejection in large-scale molecular dynamics simulations (more than 1 million molecules). Ivanov *et al.* (2003) presented the first atomistic simulation of a shock propagation including the electronic heat conduction and electronphonon coupling. Their computational model was based on the two-temperature model that describes the time evolution of the lattice and electron temperatures by two coupled non-linear differential equations. Perez and Lewis (2004) studied the variations in the thermodynamic paths followed by materials during fs and ps laser ablation using a simple

two-dimensional molecular-dynamics model. They investigated the thermodynamic evolution of a material after irradiation by femto and ps pulses using a simple 2D Lennard–Jones model. Lorazo *et al.* (2006) investigated the thermodynamic pathways involved in laser irradiation of absorbing solids in silicon for pulse durations of 500 fs and 100 ps. This was achieved by accounting for carrier and atom dynamics within a combined Monte Carlo and molecular-dynamics scheme and simultaneously tracking the time evolution of the irradiated material in ρ-T-P space. Of special significance is work by Zhigilei *et al.* (2003) where a combined MD-DSMC computational model has been developed for simulation of the long-term plume expansion of organic systems. Zhigilei's in-depth study revealed a number of physical phenomena, including temperature and pressure evolution, phase change/explosion, structural change, and ablation rate change in laser ablation of molecular systems including organic materials. Investigations on thermal transport, phase change, thermal stress development and propagation, and nanoparticle formation in laser-material interaction can also be found in other literatures (Wang and Xu, 2002, 2003a, b; Wang, 2005). It needs to be pointed out that in these MD studies of laser-material interaction the emphasis was placed on the plume behavior during laser ablation in vacuum (without shock wave). The effect of shock wave on plume evolution has not been studied in these works.

In recent years, more emphases have been placed on the exploration of kinetic and physical properties of nanodomain shock wave in near-field laser material interaction (Feng and Wang, 2007) and its dynamic structure with mass penetration under picosecond laser irradiation (Zhang and Wang, 2008).

1.6 Problem Statement and Objectives

The overall objective of this work is to study the thermophysical and dynamical phenomena in laser material interaction with ambient environment under single picosecond laser pulse by molecular dynamics (MD) simulations. The study has three specific goals.

First goal is to study the shock wave phenomenon in laser material interaction. Since blast wave accompanies the physical phenomena in laser ablation in presence of the background gas, the study is focused on the formation, propagation and evolution along characterization of its thermal, physical and thermodynamical properties/parameters.

Second objective is to study the secondary shock wave in laser material interaction. Due to the strong interaction with background gas, plume re-deposits on the target surface which causes backward movement of ambient gas and reflection from the target surface eventually results in formation of the secondary shock wave. The study is focused on both pressure/velocity and temperature/density distribution within process of formation of the internal shock wave.

The last goal is to study the phenomenon of plume splitting in laser material interaction influenced by the shock wave. When the fraction of atoms from the expanding plume that penetrate the surrounding gas decreases with the increasing gas pressure, a large enhancement of the slow component is being formed, which leads to the plume splitting. It is of special interest to perform atoms track which allows monitoring the behavior of atoms within the peaks in order to reveal the mechanisms of peak formation.

2. METHODOLOGIES OF MD SIMULATION

Molecular Dynamics simulation is a computational method to investigate the behavior of materials by simulating the atomic motion governed by a interatomic potential. For the purpose of this study, the computational domain has been designed to resemble a free-standing target material placed in a gas environment irradiated by a laser pulse (Fig. 2.1a). Argon material is selected for the film target in the simulations because it is well characterized physically and chemically, and it has been thoroughly studied in the laser-material interaction using MD. Argon crystal structure as the target has an initial temperature of 50 K, and the lattice constant *a* of the face-centered-cube (fcc) is 5.414 Å. The melting and boiling temperatures of argon at one atmosphere are 83.8 K and 87.3 K, respectively, while its critical temperature is 150.87 K. The background gas shares similar properties as the target, such as the molecular mass, but has a modified interatomic potential which considers only repulsive force between atoms. Except this, the model gas is arranged to have the same parameters as argon for MD simulation. As a result, this approach significantly simplifies the computation and reduces the computational time. The computational domain measures 32.5×2.7×3627 (nm) ($x \times y \times z$) and consists depending of the considered case of 262708, 375,000, and 630,000 atoms. The solid target material is 108 nm long in the *z* direction, below which there is a gas domain 271 nm long. Periodic boundary conditions are imposed to the boundaries in the *x* and *y* directions, and free boundary conditions to the boundaries in the *z* direction.

The basic problem of MD simulation involves solving the Newtonian equation for

each atomic pair interaction with the usage of the Lennard-Jones potential

$$m_i \frac{d^2 r_i}{dt^2} = \sum_{j \neq i} F_{ij} \,, \tag{2.1}$$

where m_i and r_i are the mass and position of atom *i*, respectively, F_{ij} is the pair force between atoms *i* and *j* which is calculated as $F_{ij} = -\partial \phi_{ij} / \partial r_{ij}$. The Lennard-Jones (12-6) potential is in the form

$$\phi_{ij} = 4 \cdot \varepsilon \left[\left(\frac{\sigma}{r_{ij}} \right)^{12} - \left(\frac{\sigma}{r_{ij}} \right)^{6} \right] \tag{2.2a}$$

where ε is the LJ well depth parameter, σ is referred to as the equilibrium separation parameter, and $r_{ij} = r_i - r_j$. . Therefore, the force F_{ij} can be expressed as

$$F_{ij} = 4 \cdot \varepsilon \cdot \left[-12 \frac{\sigma^{12}}{r_{ij}^{14}} + 6 \frac{\sigma^{6}}{r_{ij}^{8}} \right] \cdot r_{ij} \tag{2.2b}$$

A finite difference approach is a standard method for solving ordinary differential equations. The general idea behind MD is to obtain the atomic positions, velocities, etc. at time $t+\delta t$ based on the positions, velocities, and other dynamic information at time *t*. The equations are solved on a step-by-step basis, and the time interval δt is dependent on the method applied. However, δt is usually much smaller than the typical time taken for an atom to travel its own length. Many different algorithms have been developed to solve Eqs (2.1) and (2.2). In this calculation they are solved by applying the modified Verlet algorithm to the velocity, which is commonly identified as the half-step leap-frog scheme with a time step of 25 fs. Verlet algorithm is widely used due to its numerical stability, convenience, and

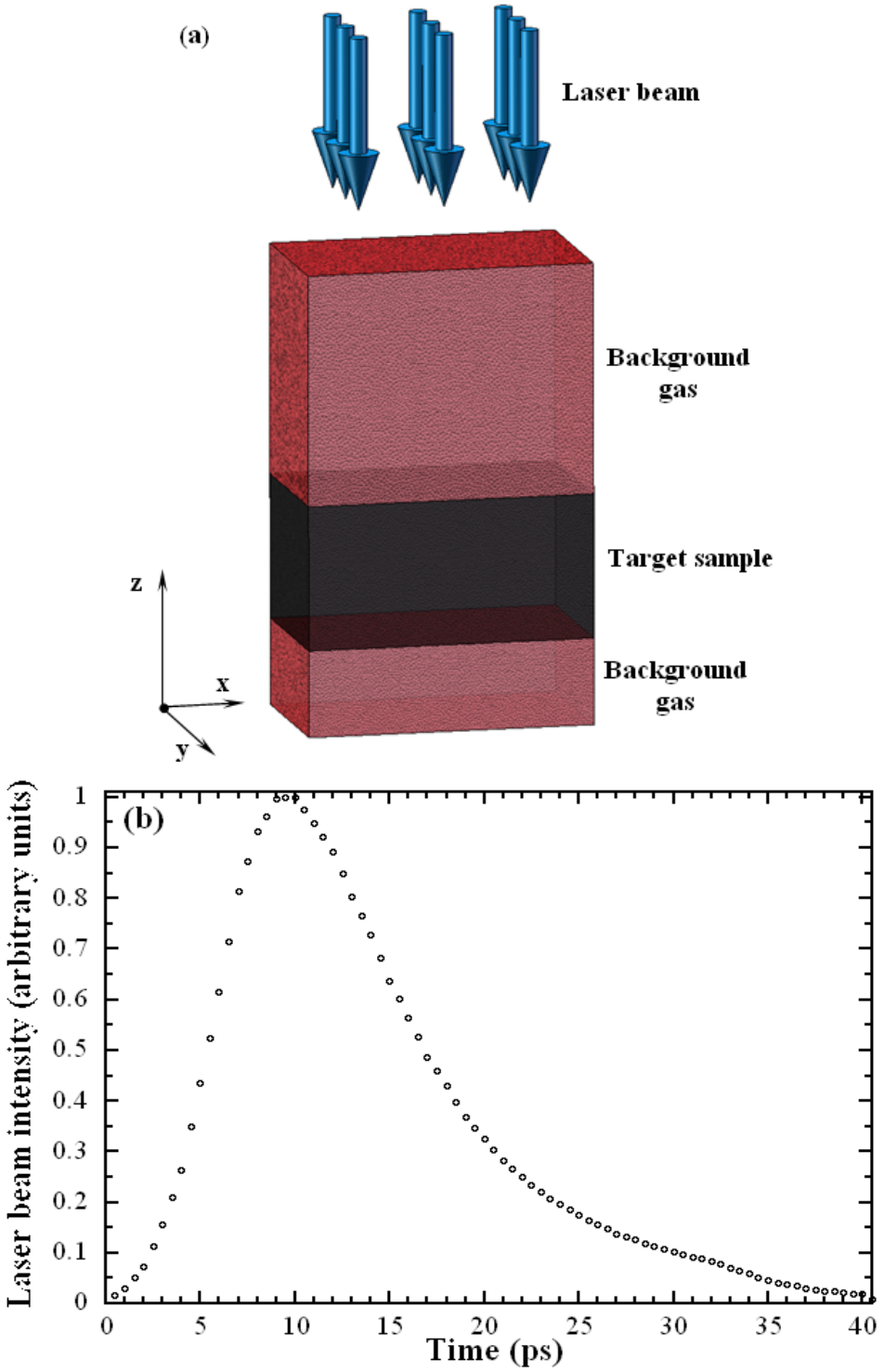

Figure 2.1 (a) Schematic of the domain construction for shock wave simulation; (b) temporal distribution of the laser intensity.

simplicity (Allen and Tildesley, 1987). The velocity Verlet algoritm is expressed as

$$v(t+\delta t/2) = v(t-\delta t/2) + \frac{F_{ij}(t+\delta t)}{m_i}\delta t \tag{2.3a}$$

$$r_i(t+\delta t) = r_i(t) + v(t+\delta t/2)\delta t \tag{2.3b}$$

$$F_{ij}(t+\delta t) = -\frac{\partial \phi_{ij}(t+\delta t)}{\partial r_{ij}} \tag{2.3c}$$

$$v(t) = \frac{1}{2}(v(t+\delta t/2) + v(t-\delta t/2)) \tag{2.3d}$$

During computations, most time is spent on calculating forces. When atoms are far away enough from each other, the force between them is negligible. The interaction between atoms is neglected when their distance is beyond the cutoff distance, $r_c = 2.5\sigma$ meaning the distance between atoms is first compared with r_c and only when the distance is less than r_c the force is calculated. The comparison of the atomic distance with r_c is organized by of the cell structure and linked list method (Allen and Tildesley, 1987). In this method the computational domain is divided into regular cells with a size a little greater than the cutoff distance. The cell structure and the linked list method are demonstrated in Fig. 2.2, which shows cells and atoms into their appropriate cells based on their positions. The method involves sorting all atoms into their appropriate cells based on their positions (Wang, 2001).

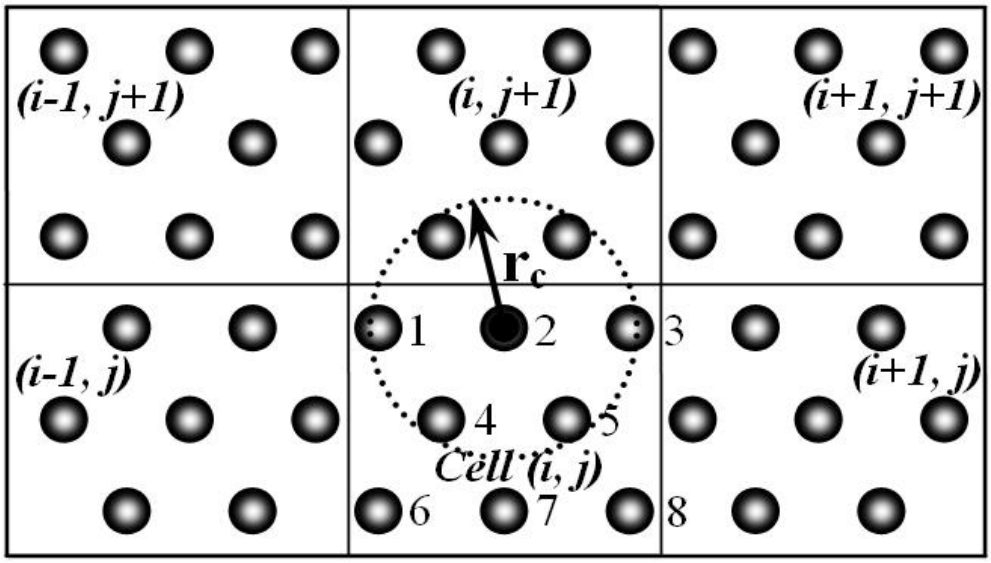

Figure 2.2 Cell structure and linked list in a 2-D space.

During the first 200 ps (8000 steps), the velocity of molecules is being scaled up to 100 ps. Initial velocities of atoms are specified randomly from a Gaussian distribution based on the specified temperature of 50 K using the following formula

$$\frac{1}{2}m\sum_{i=1}^{3}v_i^2 = \frac{3}{2}k_B T \tag{2.4}$$

where k_B is the Boltzmann's constant. During the equilibrium calculation, due to the variation of the atomic positions, the temperature of the target may change because of the energy transform between the kinetic and potential energies. In order to allow the target to reach thermal equilibrium at the expected temperature, velocity scaling is necessary to adjust the temperature of the target at the early stage of equilibration. The velocity scaling approach proposed by Berendsen *et al.* (1984) is applied in this work. At each time step, velocities are scaled by a factor

$$\chi = \left\{1 + \frac{\delta t}{t_t}\left(\frac{T}{\zeta} - 1\right)\right\}^{0.5} \tag{2.5}$$

where ζ is the current kinetic temperature, and t_t is a preset time constant, which is taken as 0.4 ps in the simulation. This technique forces the system towards the desired temperature at a rate determined by t_t, while only slightly perturbing the forces on each atom. After scaling the velocities, the calculation is continued to reach thermal equilibrium and to make sure that the disturbance caused by the velocity scaling is eliminated. Towards the end of the equilibration, the ambient gas reaches a pressure of 0.22 MPa, close to the ideal gas condition (0.27 MPa). In this work, different ambient pressures ranging from 0.051 MPa to 0.87 MPa are used for studying shock waves. These pressures are higher than those used in PLD, and are close to open-air laser-assisted surface nanostructuring, and pulsed laser-assisted material machining (polishing, welding, and drilling).

The target top surface is uniformly irradiated with a single laser pulse which has a temporal Gaussian distribution (Fig. 2.1b) and a fluence of 3, 5 and 7 J/m^2, depending on considered case. The laser pulse has 11.5 ps the full width at half maximum (FWHM) and is peaked at 10 ps. The laser beam heating is applied on the top target surface after 200 ps equilibrium calculation, and the irradiation is volumetrically absorbed in the material. This incident laser beam within each time step (δt) is assumed to be absorbed exponentially with an artificial optical absorption depth (τ) and is expressed in the following formula (Wang, 2005)

$$\frac{dI}{dz} = -\frac{I(z)}{\tau} \tag{2.6}$$

The incident laser energy within a time step (δt) is $E_1 = \delta t \cdot I \cdot A$ where A is the area of the

target surface. The laser energy absorbed inside the material is

$$\Delta E = E_0 \cdot \left(1 - \exp\left[-\frac{\delta z}{\tau_0}\right]\right) \tag{2.7}$$

where δz is the layer thickness, and E_0 is the energy incident on one single layer in the z direction. The domain is divided into such layers whose thickness is a little larger than the cutoff distance used in force calculation. $\tau_0 = \tau \cdot \rho_0/\rho$ is the adjusted real optical absorption depth, where ρ_0 and ρ are the bulk density and true density of the target, respectively. Finally, laser beam absorption in the target is achieved by exciting the kinetic energy of atoms, and is accomplished by scaling the velocities of atoms by a factor which is expressed by (Wang, 2005)

$$\chi = \left\{1 + \frac{\Delta E}{\frac{1}{2}\sum_{i=1}^{N} m_i \cdot \left(\left(v_{i,1} - \bar{v}_1\right)^2 + \left(v_{i,2} - \bar{v}_2\right)^2 + \left(v_{i,3} - \bar{v}_3\right)^2\right)}\right\}^{0.5} \tag{2.8}$$

where $v_{i,j}$ and $\bar{v}_j$ (j = 1, 2, 3) are velocities of atom i and the average velocity in the x, y, and z directions for atoms in a layer normal to the laser beam. The new velocity, $v'_{i,j}$ of atom i is calculated as follows

$$v'_{i,j} = \left(v_{i,j} - \bar{v}_j\right) \cdot \chi + \bar{v}_j, \qquad j = 1, 2, 3. \tag{2.9}$$

In order to make computations more approachable the non-dimensionalized parameters are used which are listed in Table 2.1 (Wang, 2001).

Table 2.1 Non-dimensionalized parameters

Quantity	**Equation**
Time	$t^* = t/\left(\sqrt{m/4\varepsilon}\sigma\right)$
Length	$r^* = r/\sigma$
Mass	$m^* = m/m = 1$
Velocity	$v^* = v/\sqrt{4\varepsilon/m}$
Potential	$\phi^* = \phi/4\varepsilon$
Force	$F_{ij}^* = F_{ij}/\left(4\varepsilon/\sigma\right)$
Temperature	$T^* = k_B T/4\varepsilon$

On the other hand, the parameters used in the calculation are listed in Table 2.2 (Lukes *et al.*, 2000).

Table 2.2 Values of the parameters used in the calculation

Parameter	**Value**
ε, LJ well depth parameter (J)	1.653×10^{-21}
σ, LJ equilibrium separation (nm)	0.3406
m, Argon atomic mass (kg)	6.63×10^{-26}
k_B, Boltzmann constant (J/K)	1.38×10^{-23}
a, Lattice constant (nm)	0.5414
r_c, Cut off distance (nm)	0.8515
x-direction domain size (nm)	32.484
z-direction domain size (nm)	3627.38
z-direction target size (nm)	108.28
δt,Time step (fs)	25
τ, Laser beam absorption depth (nm)	5, 10, 15
E, Laser energy fluence (J/m^2)	3, 5, 7
Number of atoms	262708, 337500, 630000

Moreover, in the simulations conducted in this work a force elimination procedure needs to be considered as follows. In laser interaction with the target material, a strong stress wave will form and propagate throughout the target in the laser incident direction. When this laser-induced stress wave reaches the opposite side of the target, it can tear off the material and induce unrealistic damage, or the stress wave can be reflected and may induce unexpected artifacts in the liquid-vapor zone, causing changes in the generation and behavior of the shock wave. In our approach, a special boundary treatment is used at the back side of the target to eliminate the above phenomena. A terminating force is applied to the atoms in the affected boundary region, and it can be expressed following the work by Zhigilei and Garison (1999) as

$$F_t = -\frac{\rho \cdot v \cdot c \cdot A}{N} \tag{2.10}$$

where ρ is the density of the target in the selected region, v is instantaneous average velocity of the atoms within the boundary, and c is the speed of propagating stress wave. N is the number of molecules/atoms confined by the affected region. Wang's previous simulations (Zhang and Wang, 2008) proved that the above stress boundary treatment works well in terms of eliminating stress wave reflection and avoiding undesired material damage in the boundary region.

3. DYNAMICS EVOLUTION OF SHOCK WAVES IN LASER MATERIAL INTERACTION

3.1 Shock Wave Formation and Evolution: a General Picture

Consideration of the shock wave formation and evolution is presented on the basis of the situation when the laser energy is 3 J/m^2, the absorption depth is 5 nm, and ambient gas pressure is slightly above 2 atm. A series of snapshots of atomic positions in the simulated domain (*x*-*z* plane) at different times are shown in Fig. 3.1a. At 0.5 ns a denser region in red color is already visible, which represents the expansion front of the shock wave (marked with arrows). The applied laser beam forces the target material to evaporate because its energy intensity exceeds the material ablation threshold, leading to generation of an evidently strong shock wave composed of compressed adjacent gas above the target. In the initial stages, the ejected plume immediately exerts forward, being induced by the high pressure mainly from intense phase explosion (Wang and Xu, 2003) and expands into the background gas until the end of laser pulse. As can be noticed in later stages, nanoparticle-like clusters are formed, mainly due to phase explosion and condensation (Harilal *et al.*, 2003). When the high energy plume propagates through the background gas, the interrelation between solid and gas becomes more significant. More mass of the ambient gas is being entrained in the shock wave front. Meanwhile, the ejected plume is being restrained due to increasing repulsive effect from the ambient gas. This restraint prevents the plume from developing freely in space. Consequently, thermalization of the plume occurs because slowing of the plume velocity converts its kinetic energy into thermal energy. With the time evolving, the co-existing length between the plume and the background gas increases because of the relative

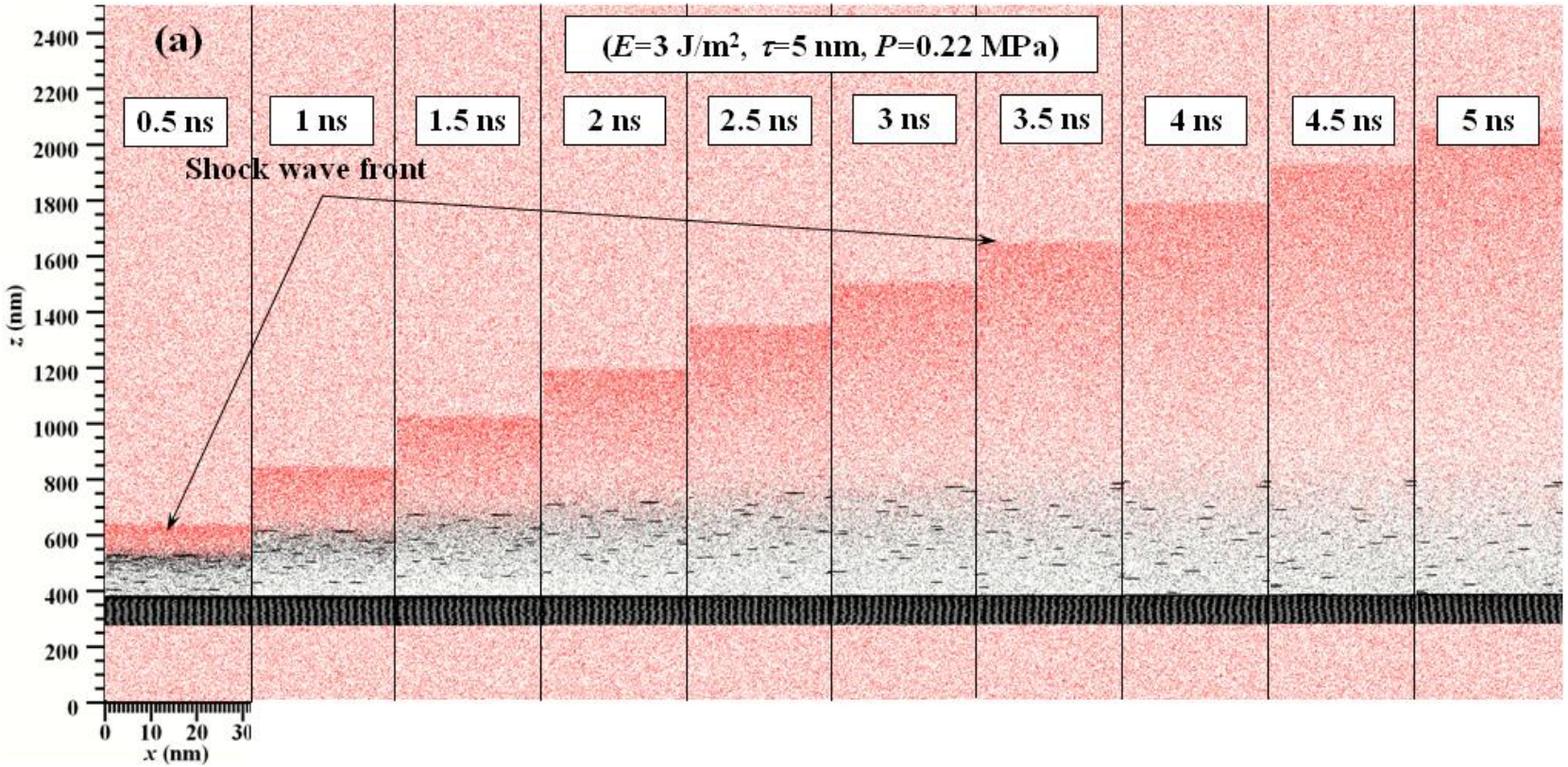

Figure 3.1 Comparison of snapshots for the dynamics of shock wave formation and evolution for E=3 J/m^2, at P = 0.22 MPa, and three different absorption depths: (a) τ=5 nm, (b) τ=10 nm, and (c) τ=15 nm. Black color: target material, red color: background gas.

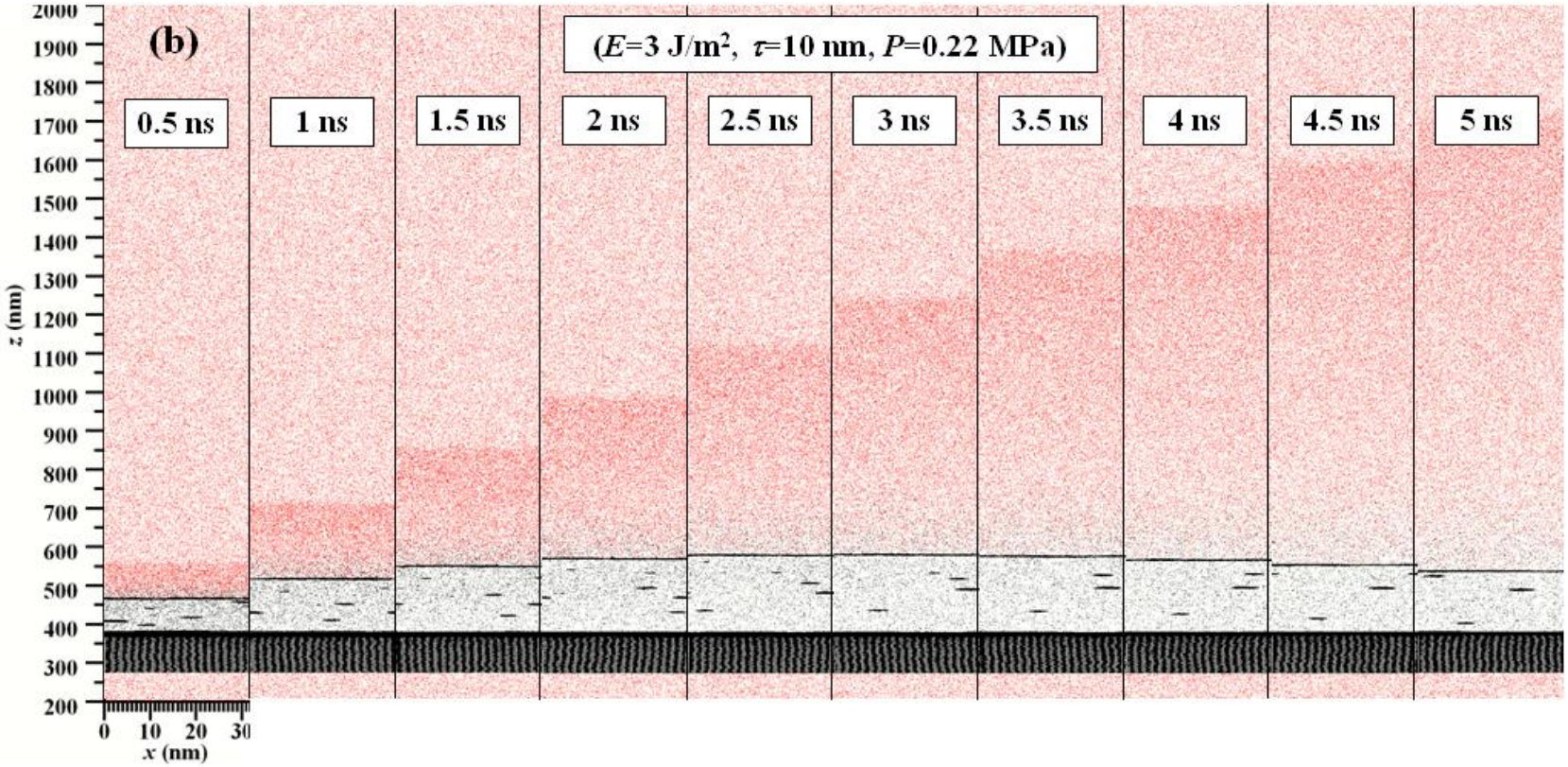

Figure 3.1 Continued.

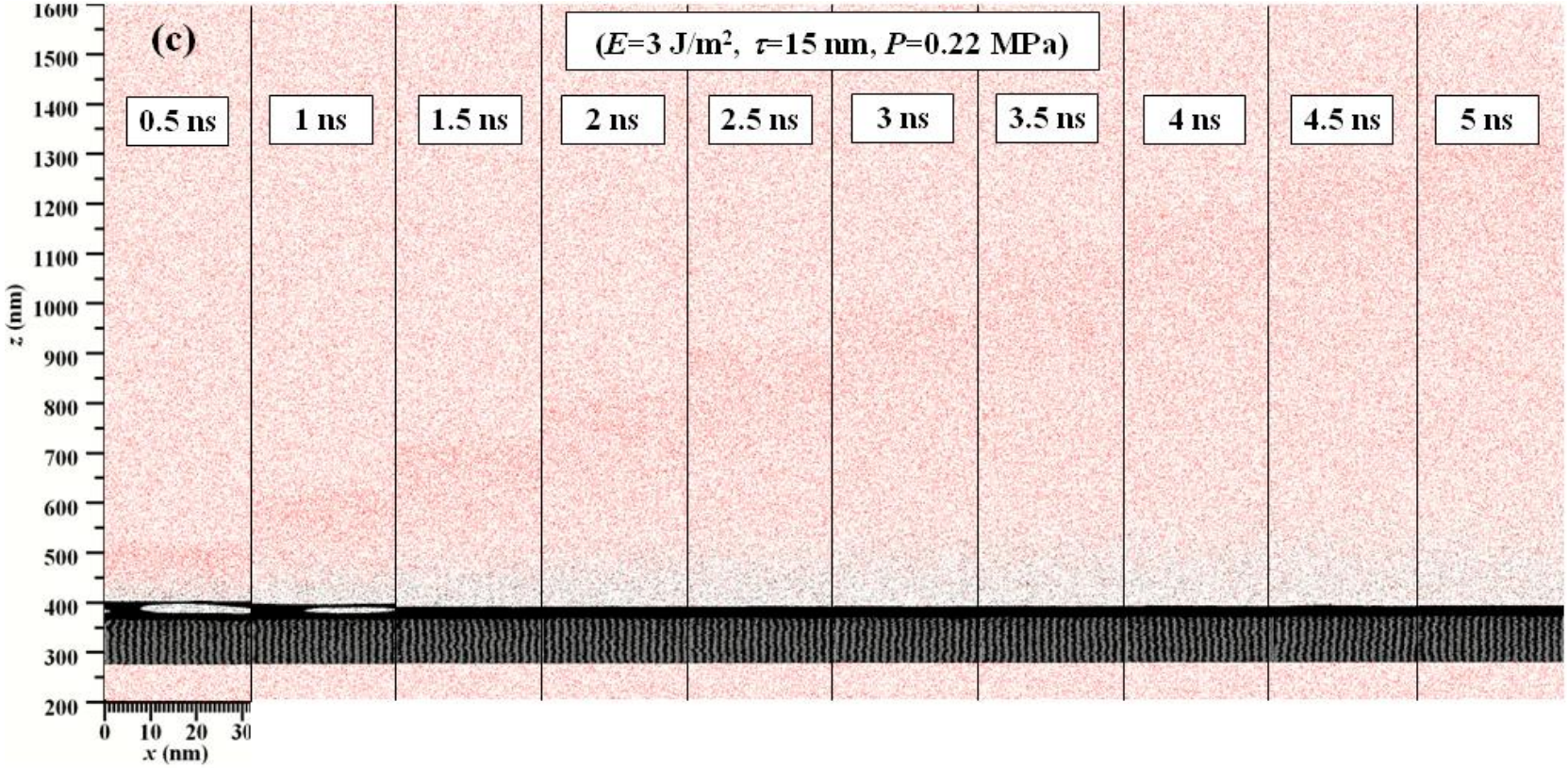

Figure 3.1 Continued.

movement between the plume and the ambient gas. A very interesting phenomenon observed in Fig. 3.1a is that starting from 3 ns, the expansion of the plume in space is significantly slowed down. Moreover, some of the particles/clusters in the plume start to move down toward the target surface although the shock wave front continues to propagate out. This type of backward movement of the plume is being studied in our group by further processing the MD data of a wide spectrum of calculations. From 3 to 5 ns, it is also observed that some clusters/particles stop moving out. Instead, they float and mix with the ambient gas.

3.2 Atomic Velocity inside the Shock Wave

For shock waves generated in laser-material interaction, very little knowledge has been obtained in the past about the average atomic velocity distribution inside the shock wave. This is probably due to the large experimental difficulty in internal velocity probing. Figure 3.2 shows the average velocity distribution of the target materials and the gas for the computational case discussed above. Several interesting phenomena are noticed in the internal velocity distribution, and are discussed below.

In the figures at 0.025, 0.05, and 0.1 ns, a negative velocity wave is observed in the solid target. This velocity wave moves to the backside of the target. It is induced by the local stress wave. This negative velocity is not the local stress wave propagation velocity, but is related to the dislocation of the local atoms under the influence of the stress. When this velocity wave reaches the backside of the target, it just disappears and is not reflected back. This is because in the simulation a stress-absorbing boundary condition is applied on the left boundary. When the stress wave is absorbed by this special boundary condition, the net

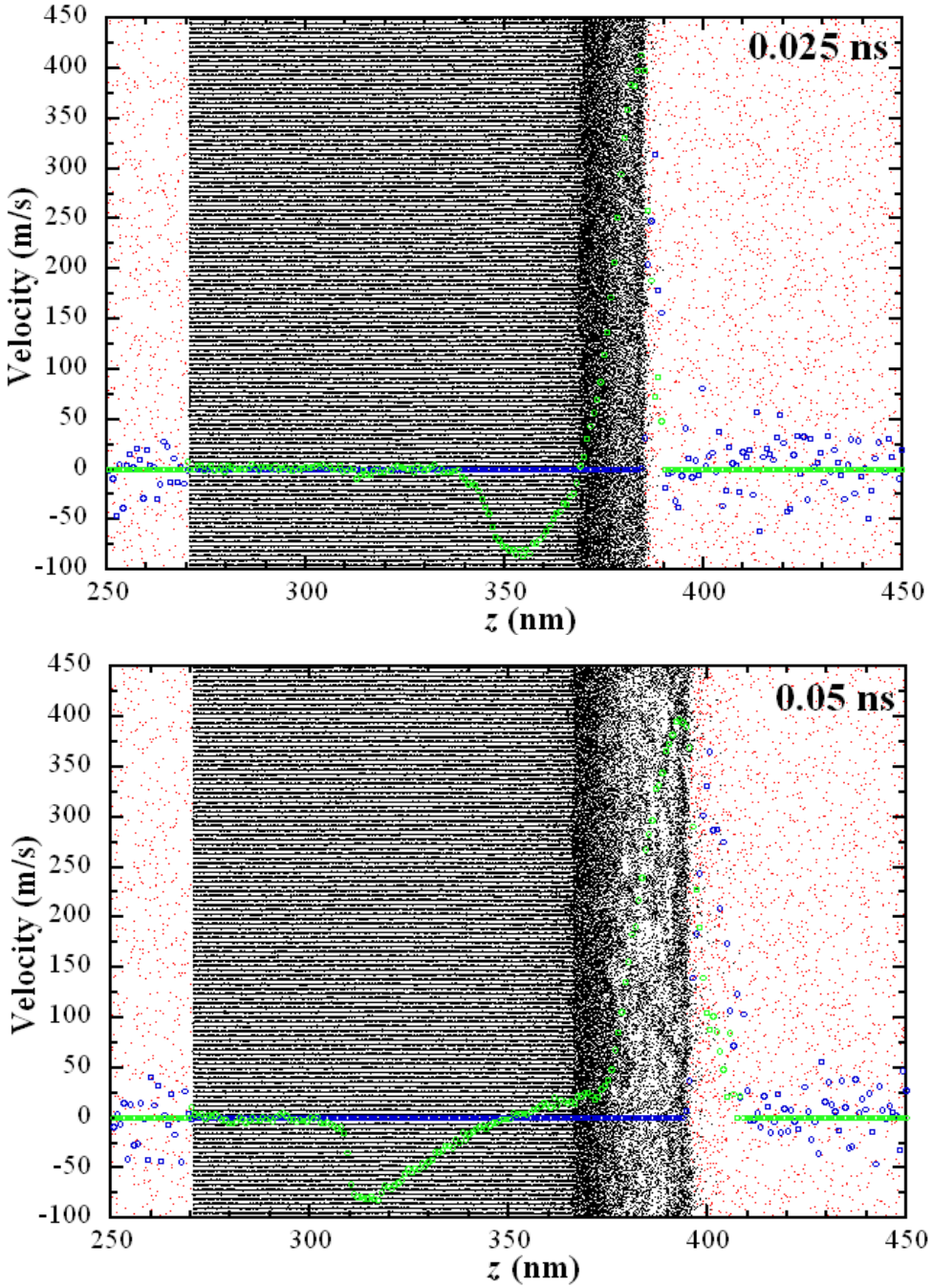

Figure 3.2 Snapshots of atomic positions combined with the evolution of target and gas velocity distribution along the *z* direction (E=3 J/m^2, τ=5 nm, P = 0.22 MPa). Green color: target material velocity; blue color: background gas velocity; black dots: target atoms; red dots: ambient gas atoms.

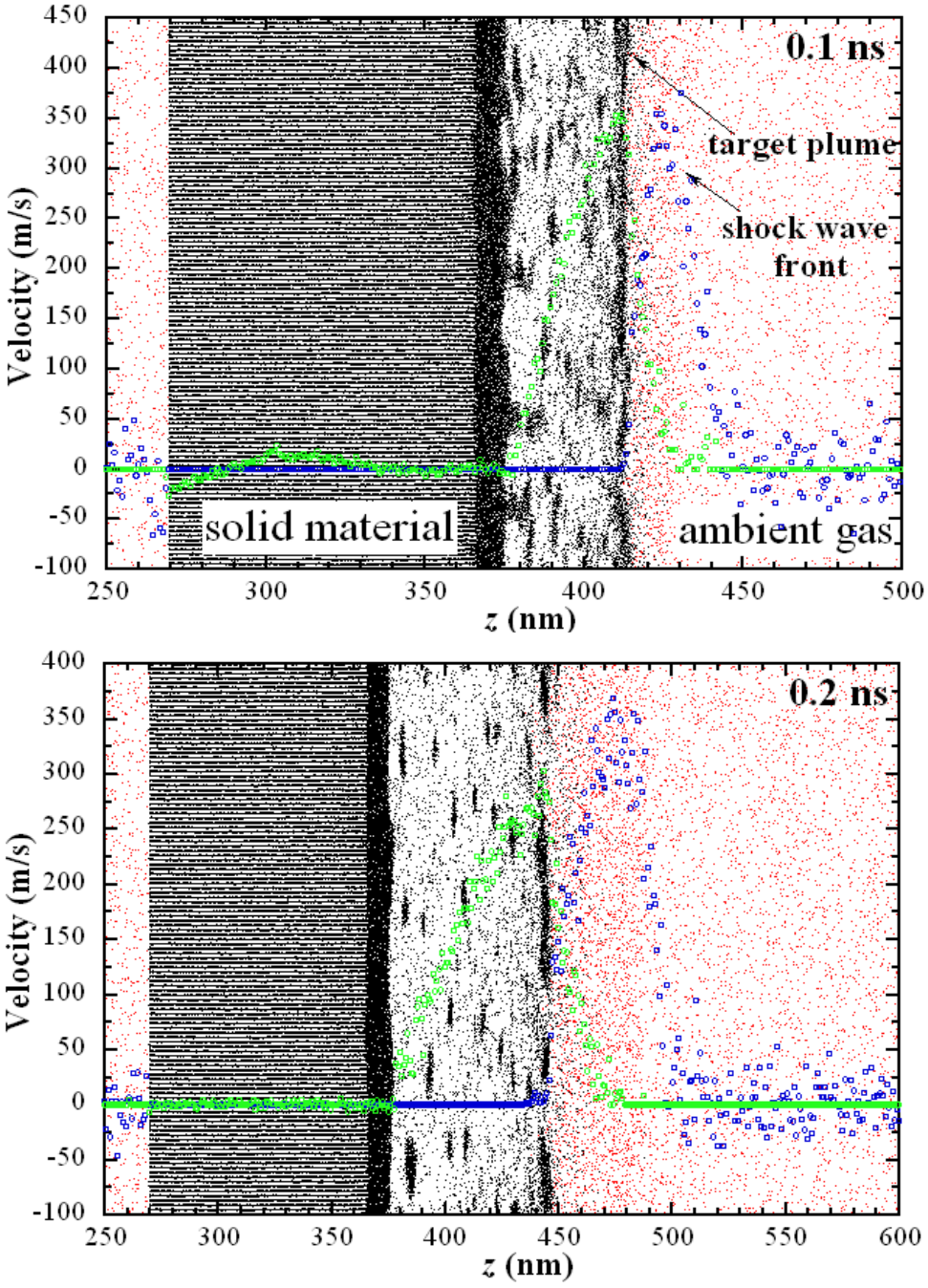

Figure 3.2 Continued.

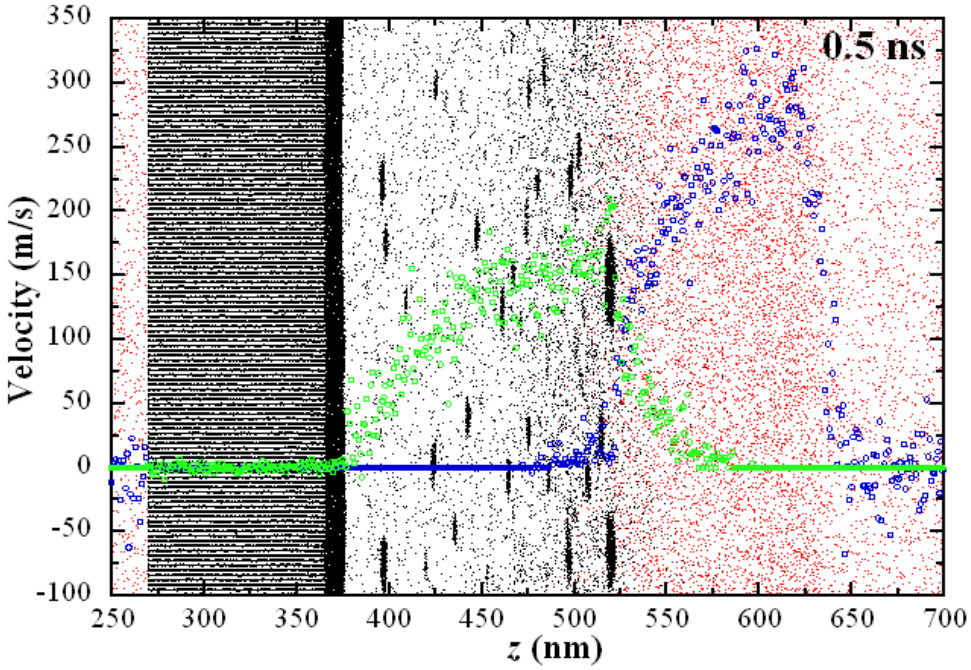

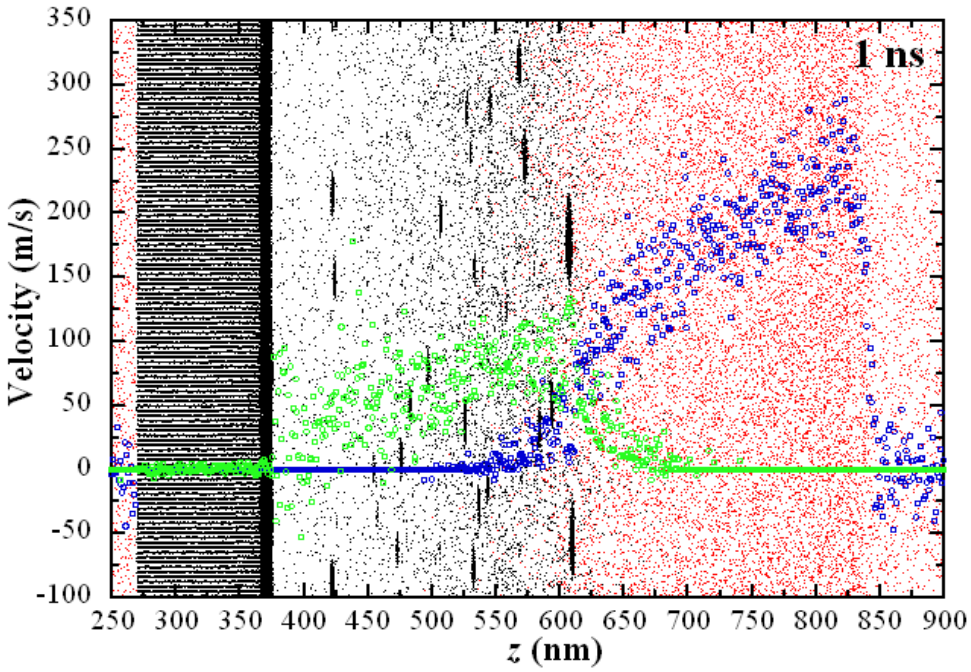

Figure 3.2 Continued.

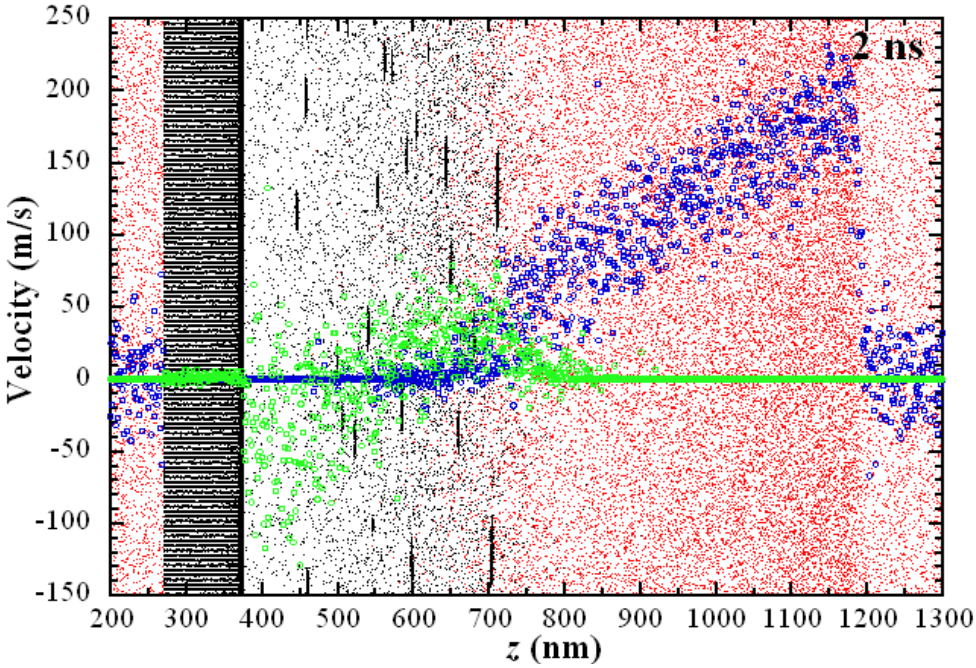

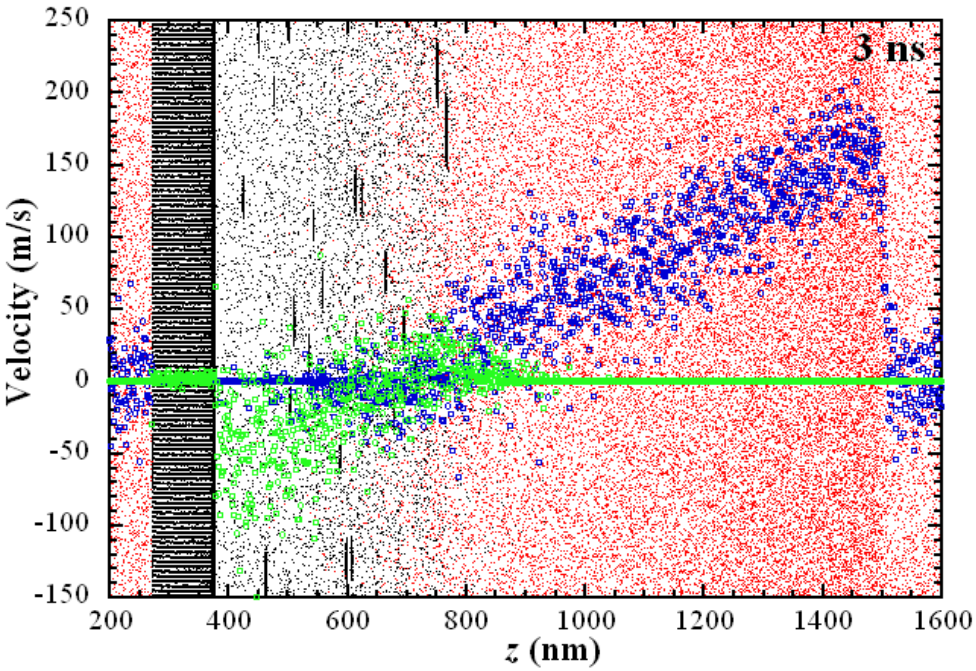

Figure 3.2 Continued.

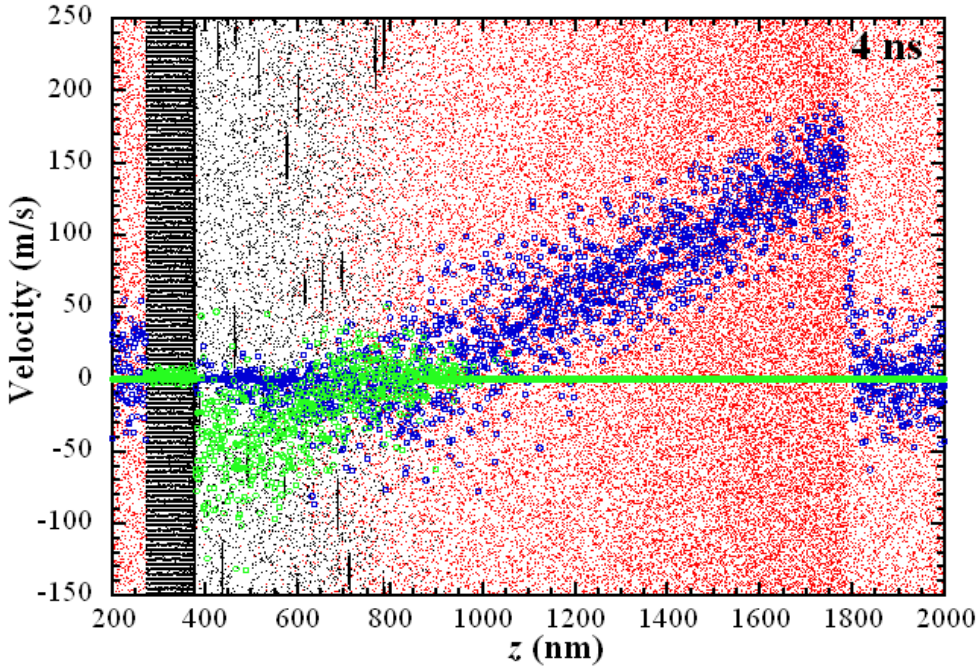

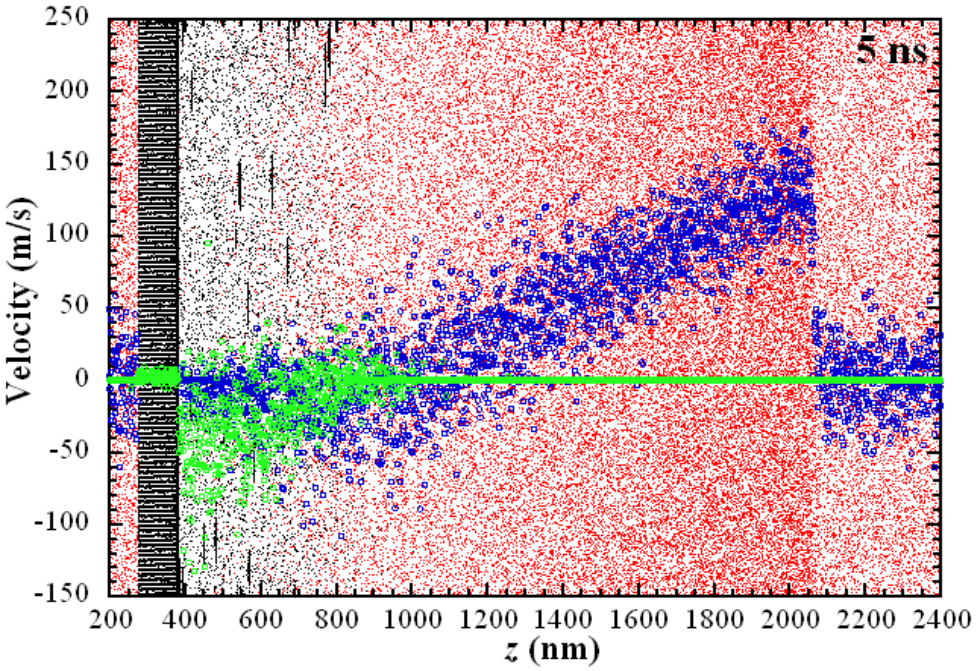

Figure 3.2 Continued.

velocity of atoms disappears. This proves that the applied stress-absorbing boundary condition works well to eliminate stress wave reflection.

The initial velocity of the plume in the surface region is positive due to ablation. If the plume is able to induce a shock wave, its velocity must be much higher than the sound speed of the background gas. The study depicts that initially (0.025 ns) the ejected plume propagates with a supersonic front velocity slightly above 400 m/s which is about 3 times the sound speed in the ambient gas (132 m/s at 50 K). In the initial snapshots it is clearly discernible that solid atoms fly out from the target with high speed accompanying intense phase explosion. The adjacent gas region is eminently compressed because the plume front pushes with great impact on the surroundings, resulting in the formation of the highly energetic shock wave. The shock wave front is already visible at 0.1 ns when the plume transfers a large portion of its kinetic energy to the shock wave, and both travel with an enormous velocity around 350 m/s. It is important to notice that a velocity discontinuity exists at the plume/compressed gas interface. This is physically reasonable because momentum and energy transfer occurs from the ejected plume to the generated shock wave at the initial instant of time. A lot of gas atoms have been pushed out quickly with analogy to a supersonic piston. So the not-pushed or slightly-pushed gas atoms stay behind the shock wave front. This also gives rise to the non-uniform velocity distribution in the compressed ambient gas, where the shock wave front features the maximum speed.

At 0.2 ns the shock wave already gains the momentum to expand, whereas the plume begins to decelerate. At this moment, the peak velocity of atoms in the compressed ambient

gas is even higher than that of the plume. Deceleration of the plume is induced by the accumulated mass of the compressed ambient gas, which becomes comparable to the plume mass. The slowdown effect by the ambient gas reduces the velocity of the expansion plume. It is interesting to notice that at the later steps it happens that the velocity of the plume becomes negative (2 to 5 ns). This means the plume starts to move back to the target surface and could re-combine with it. The accelerated denser shock wave front propagates with a sharp velocity peak, while the rarefied 'tail' undergoes increasing scattering/diffusion with the plume constituents. It is clearly visible that deceleration and 'quenching' of the shock wave front occurs due to the momentum loss to the stationary background gas. At 5 ns, the atomic velocity inside the shock wave front is very close to the sound velocity in the ambient gas (132 m/s).

3.3 Effect of Laser Beam Absorption on Shock Wave

In this work, the volumetric laser energy absorption model is incorporated into the simulations. It de-emphasizes the details of laser material interaction in which quantum mechanical effects need to be taken into account. The time scale of laser energy absorption (< 1 ps) is much smaller than the time scale associated with the laser pulse. Therefore, without knowing the details of laser material interaction, the thermal and mechanical effects, as well as shock wave formation can be investigated using this absorption model (Wang and Xu, 2002, 2003a,b; Wang, 2005). Here the results of simulation for optical absorption depth of 5, 10, and 15 nm are presented, which reflects the fact of different volumetric absorption of the laser beam.

Figures 3.1a-c show the snapshots of the dynamics and evolution of the propagating shock wave for the same laser fluence of 3 J/m^2 , and the same ambient pressure of 0.22 MPa, but with different absorption depths. It is clearly visible that the absorption depth significantly affects the characteristics and generation of the shock wave. The amount of ablated material is an important parameter in laser material interaction. The specific rate of the ablation is dependent on several factors including laser wavelength, laser fluence, and moreover on the properties of the target material (Mason and Mank, 2001; Russo *et al.*, 2000, 2002). In the first case $\tau = 5$ nm (Fig. 3.1a) which has more shallow absorption depth, the shock wave forms and propagates predictably in the way as has been already described in the previous sections. Interesting and startling things occur when we increase the absorption depth. Due to the longer absorption depth the laser beam penetrates deeper inside the sample, resulting in thicker material removal for that more mass is ablated from a larger volume but with lower velocity. As it can be seen in Fig. 3.1b ($\tau = 10$ nm case), a thin layer of target material is ejected out and stays mainly on the plume front. As previously stated, the background gas is extruded and pushed forward by the much higher-density plume, leading to a strong shock wave. Nanoclusters are also visible in the "tail" region of the expanding plume. Starting from 3 ns, it is very obvious that the ablated thin layer starts to move back toward the target surface. This motion is caused by the high pressure in the compressed ambient gas, which prevents the nanoclusters/plume from moving out. Such phenomenon is also observed in the case of E=3 J/m^2, τ=5 nm as discussed above.

Of special attention is the third case shown in Fig. 3.1c. When the laser absorption depth is too large (15 nm), the formation of the plume is hardly visible. At the initial stages it

is observed that a thin layer of film is ejected out a little bit (0.5 and 1 ns), and quite a large bubble forms beneath the surface. But it seems that the ejected material has not gained sufficient energy to overcome two forces: the attraction force from the molten material, and the restraint force from the ambient gas. Therefore, at 1 ns it is being pushed back and at later steps there are only a discernible minority of particles flying out. Although a shock wave has formed, it has very low energy of propagation and it is quickly diffusing in the ambient gas, which can be noticed at 5 ns when the shock wave front becomes very difficult to distinguish.

In order to establish a further understanding of the kinetics in the nanoscale shock waves, their dynamic parameters are studied in great detail. Figure 3.3 is a juxtaposition of the shock wave propagation velocity, the shock wave front position (Fig. 3.3a), as well as mass velocity of atoms in the shock wave front (Fig. 3.3b), for three absorption depths. For comparison and demonstration purposes, different Mach number lines have been marked (Fig. 3.3a), which are multiplications of the sound speed of the ambient gas (132 m/s). The shock wave thickness is the largest (1.6 μm at 5 ns) for the $\tau = 5$ nm case. The mass velocity of atoms in the shock wave front is determined by calculating the average velocity of atoms in a thin layer (about 2 nm thick) close to the shock wave front. The propagation velocity of the shock wave front is totally different from the mass velocity and is specified by using the time derivative of shock wave front position. From Fig. 3.3 it is seen that at 5 ns, the shock wave front still propagates with a Mach number larger than 1. When the absorption depth is smaller, the shock wave front propagates faster. This is because a shorter absorption depth will result in a smaller amount of ablation, but with higher velocity, leading to a faster movement of the shock wave front. For comparison with literatures, front propagation

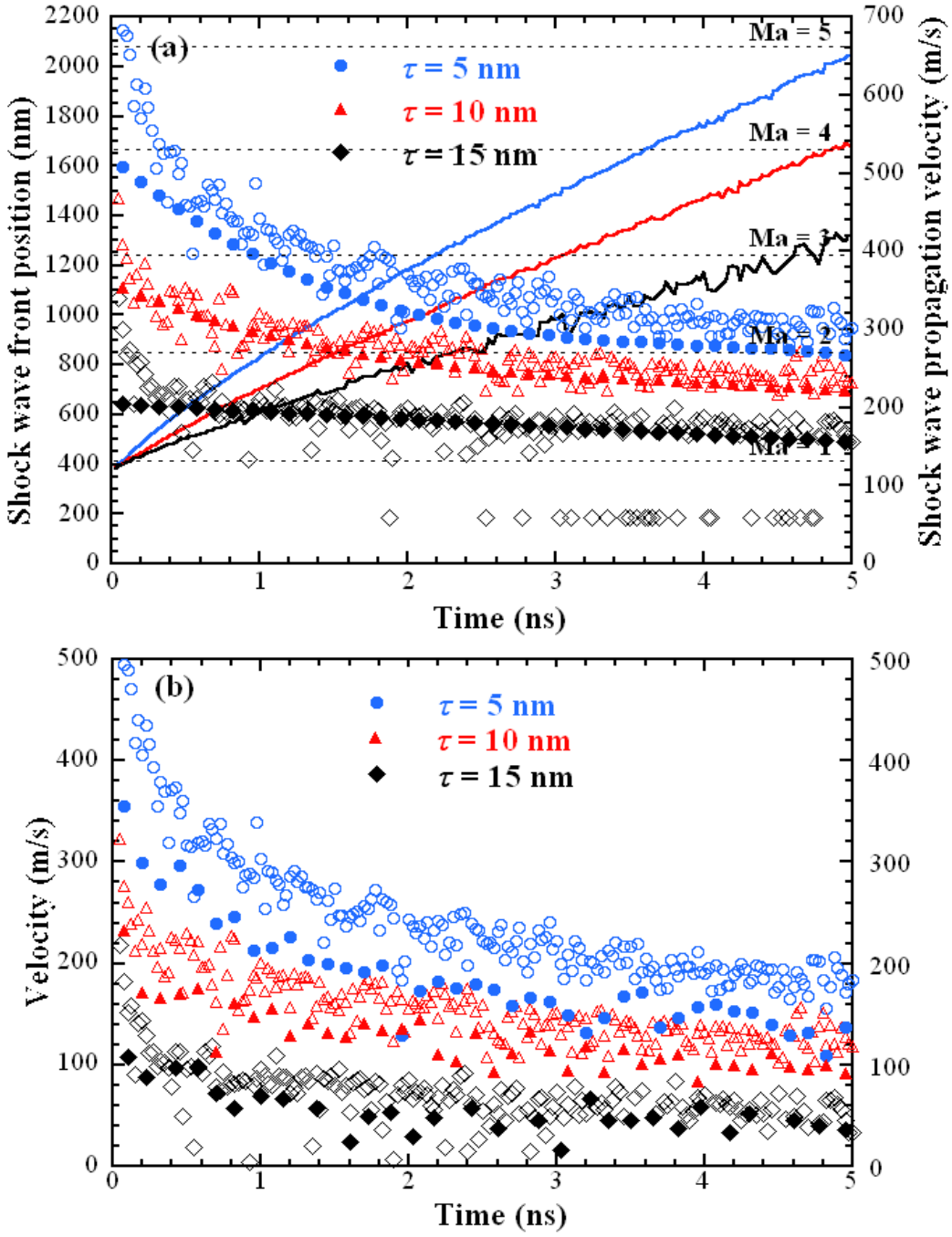

Figure 3.3 Comparison of the shock wave velocities by MD vs. Eqs. (3.1) and (3.2) for three absorption depths: 5 nm, 10 nm, and 15 nm, (E=3 J/m^2, P = 0.22 MPa): (a) shock wave front position and shock wave propagation velocity; (b) mass velocity of atoms in the shock wave front. Solid symbols: MD velocities; hollow symbols: velocities from Eqs. (3.1) and (3.2); solid lines: shock wave front position.

velocity (Fig. 3.3a) and the mass velocity of the shock wave (Fig. 3.3b) are provided. The theoretical velocity distributions in that plot are based on the theoretical equations taken from (Zhang and Gogos, 2004) as

$$M = \frac{u_f}{a} = \sqrt{\frac{\gamma+1}{2\gamma}\left(\frac{p_2}{p_1}-1\right)+1} \;\rightarrow\; u_f = a\sqrt{\frac{\gamma+1}{2\gamma}\left(\frac{p_2}{p_1}-1\right)+1} \tag{3.1}$$

$$u_{av} = \frac{a}{\gamma}\left(\frac{p_2}{p_1}-1\right)\sqrt{\frac{\frac{2\gamma}{\gamma+1}}{\frac{p_2}{p_1}+\frac{\gamma-1}{\gamma+1}}} \tag{3.2}$$

where u_f and u_{av} are shock wave propagation and mass velocity, respectively, M is the Mach number, a is the speed of sound in the ambient gas, p_1 is the ambient pressure, and $\gamma = 5/3$ is the ratio of specific heats for the ambient gas. Those equations use the pressure p_2 which is the pressure of the shock wave front and its distribution is shown in Fig. 3.4. This pressure is calculated based on our MD data using the following equation (Wang, 2005)

$$p_2 = p_{mm} = \frac{1}{\Delta V}\left(\sum_{i\neq j}^{N} r_{ij,m}F_{ij,m} + Nk_bT\right), \quad m = 1, 2, \text{ or } 3 \tag{3.3}$$

where ΔV is the volume of a small domain of interest, k_b the Boltzmann constant, and Nk_bT the pressure induced by the movement of atoms. The characteristic of velocity evolution is in good agreement, despite some slight difference between velocity profiles obtained from literature equations and those obtained from MD simulations. These deviations probably are due to the statistical uncertainty in determining the shock wave front pressure and the position of the shock wave front. Comparing Fig. 3.3a and b concludes that the average mass velocity of atoms in the shock wave front is always less than the propagation speed of the shock wave front. This is because the shock wave front propagation consists of two

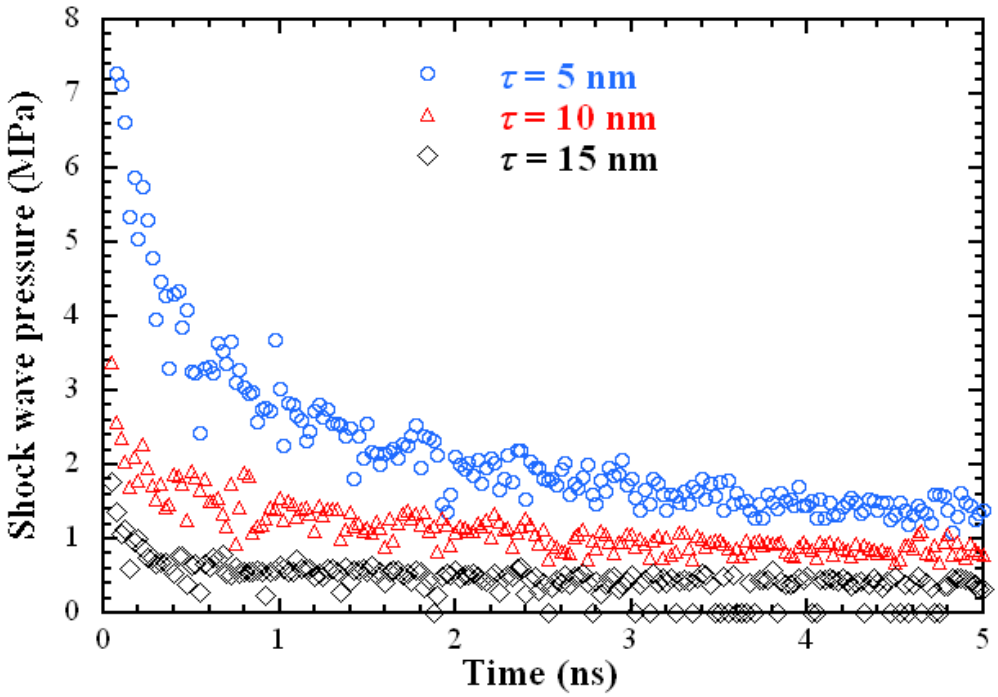

Figure 3.4 Shock wave front average pressure distribution versus time for three absorption depths: 5 nm, 10 nm, and 15 nm (E=3 J/m^2, P = 0.22 MPa).

processes: one is the movement of atoms in the shock wave front, and the other one is the process to entrain the stationary adjacent ambient gas into the shock wave front to make it thicker. Therefore, the shock wave front propagation is always faster than the local mass velocity of atoms.

Another great interesting kinetic parameter which is difficult to obtain experimentally, but relatively easy to determine with MD, is the thickness of the interaction zone between the plume and background gas. The inside of the shock wave is comprised of strongly compressed background gas and fast moving plume. These two species initially will have very little mixing, and will penetrate into each other because of mass diffusion and

relative movement. It is expected strong mixing will lead to appreciable interaction between them. Figure 3.5 illustrates how the thickness of the interaction zone changes with time for three different absorption depths.

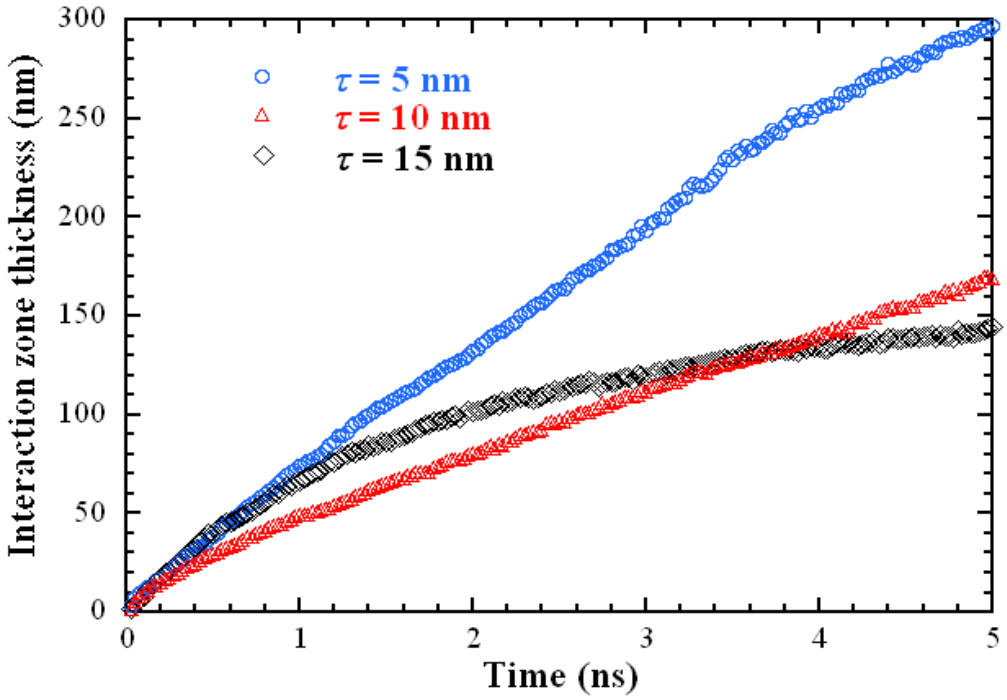

Figure 3.5 Interaction zone thickness between the target and the ambient gas for three absorption depths: 5 nm, 10 nm, and 15 nm (E=3 J/m^2, P = 0.22 MPa).

The definition of the interaction zone thickness was detailed in Wang's previous paper (Zhang and Wang, 2008) where it was designed in the following form

$$L_{mix} = \int \frac{n_t \cdot n_g}{\left[\left(n_t + n_g\right)/2\right]^2} \cdot \delta z \tag{3.4}$$

where n_t=N_{target}/(N_{target}+N_{gas}) and n_g=N_{gas}/(N_{target}+N_{gas}). Symbols n_t and n_g denote the fraction of the target and gas atoms in a small layer δz. N_{target} and N_{gas} are the number of target and gas atoms in a thin layer, respectively.

Generally speaking, when the optical absorption depth is smaller, the shock wave features a much larger interaction zone between the plume and the ambient gas. This is due to the faster movement of the plume, which makes it possible for the plume atoms to penetrate more into the ambient gas. In our past work, it has been proven that the increase of the interaction zone thickness is largely due to the relative movement between the plume and gas atoms (Zhang and Wang, 2008). For $\tau = 5$ nm and $\tau = 10$ nm the thickness changes almost linearly with time. In the situation when a thin layer film is ejected, the density of the plume front is large, but it does not allow penetration by scattered background gas constituents ($\tau =$ 10 nm case). Therefore, only the small clusters/particles in front of this layer mix with the ambient gas molecules. This results in a relative small interaction zone between the plume and background gas. For the case $\tau = 15$ nm it is predictable that the interaction zone is close to saturation at very early stages owing to the weakness of the plume and the shock wave.

3.4 Effect of Ambient Pressure on Shock Wave

Changing of the ambient pressure distinctly affects the controlling parameters of the plume characteristics such as spatial distribution, deposition rate, and kinetic energy distribution of the depositing species, which greatly vary due to plume scattering, attenuation, and thermalization (Chrisey and Hubler, 1994). Figure 3.6 displays snapshots of the spatial plume and shock wave evolution under three different ambient pressures. It is evident that raising the background gas pressure results in denser shock wave formation, greater strength, and considerable sharpening of its front. In fact, increase in the ambient pressure strengthens interpenetration collisions on the plume expansion front with the background gas. When the pressure is 0.87 MPa, it is obvious that the plume does not expand much to the space.

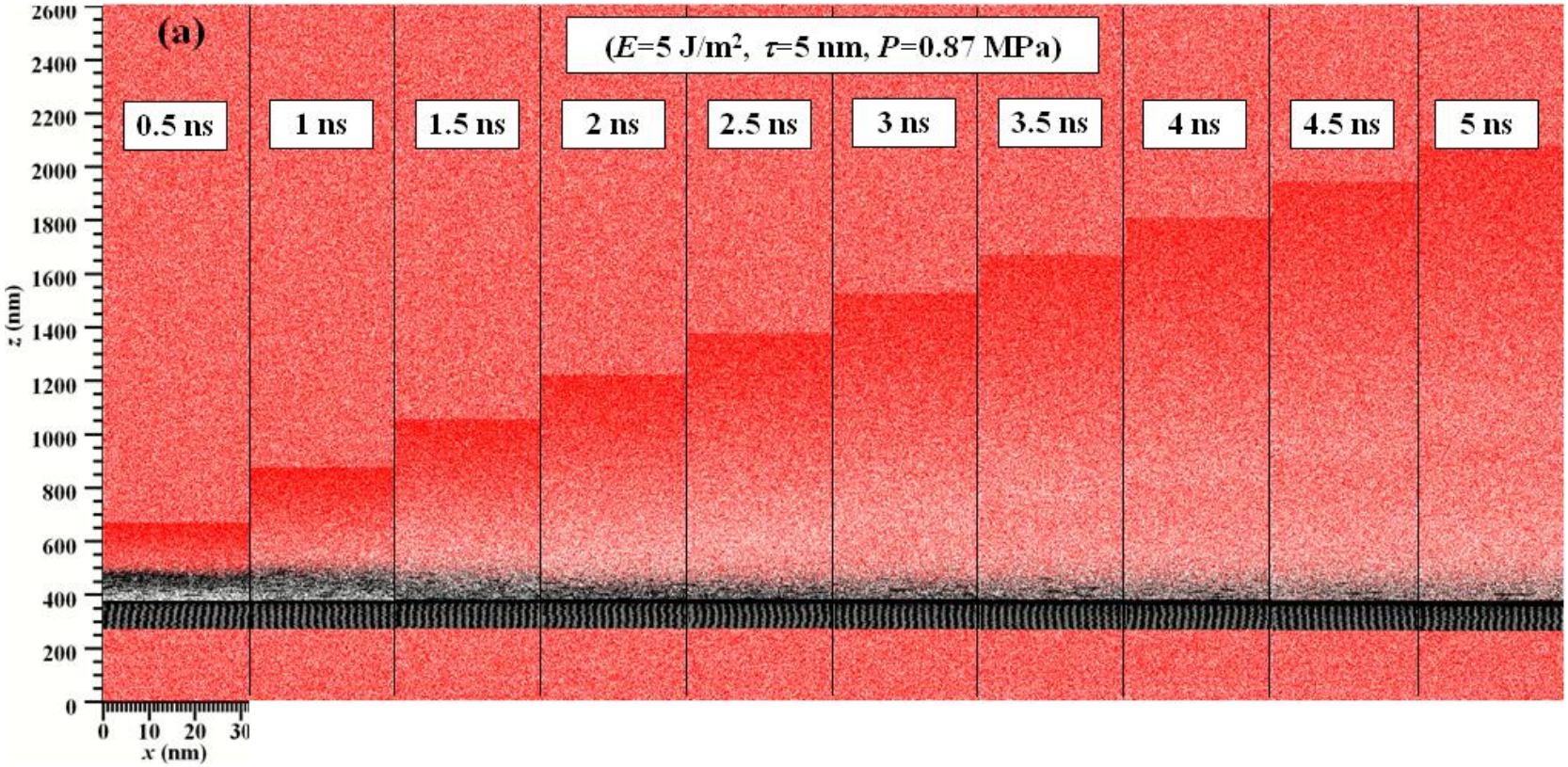

Figure 3.6 Comparison of snapshots for the dynamics of shock wave formation and evolution for E=5 J/m^2, τ=5 nm, and three different ambient pressures: (a) P = 0.87 MPa, (b) P = 0.22 MPa, and (c) P = 0.051 MPa.

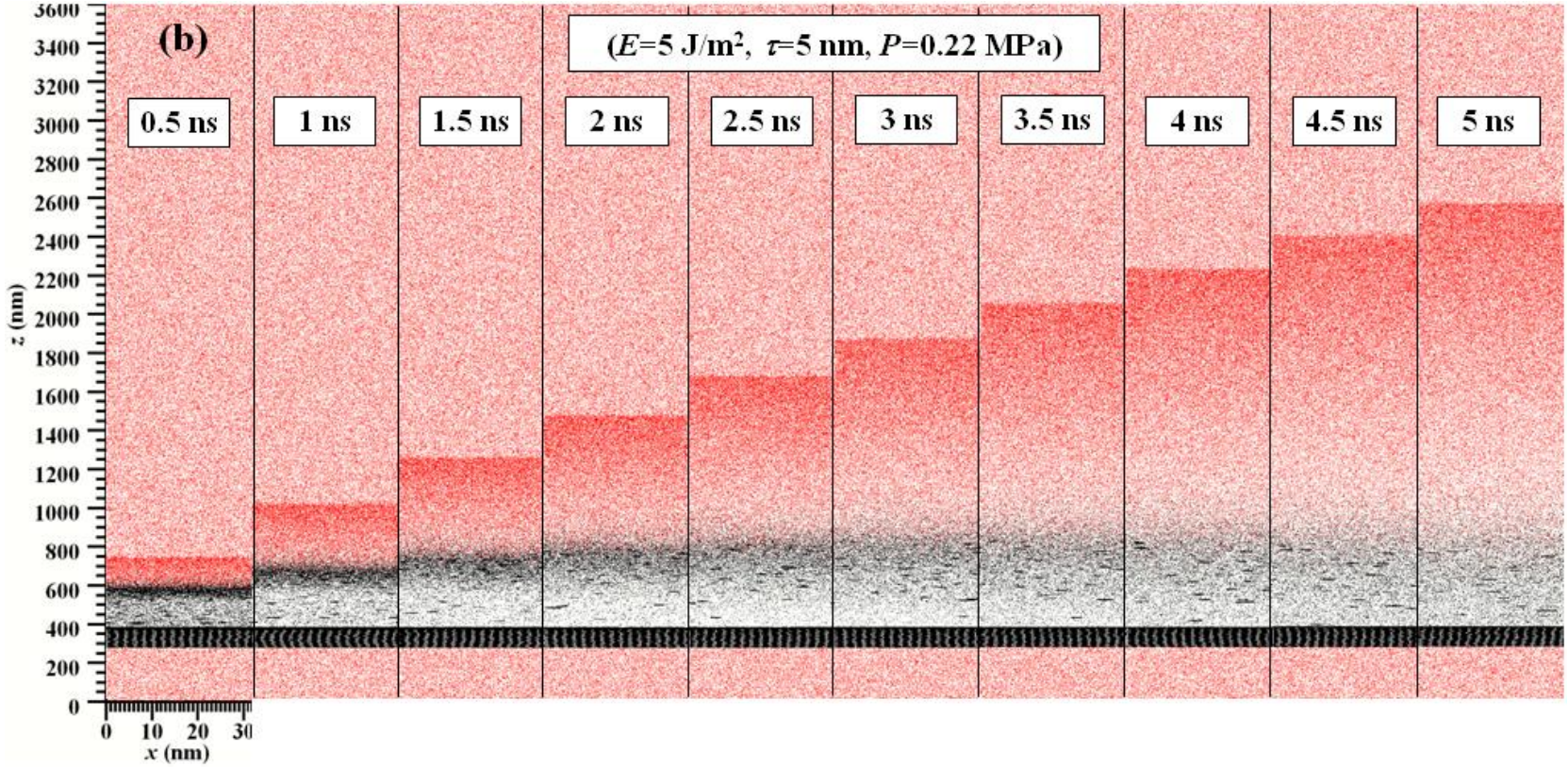

Figure 3.6 Continued.

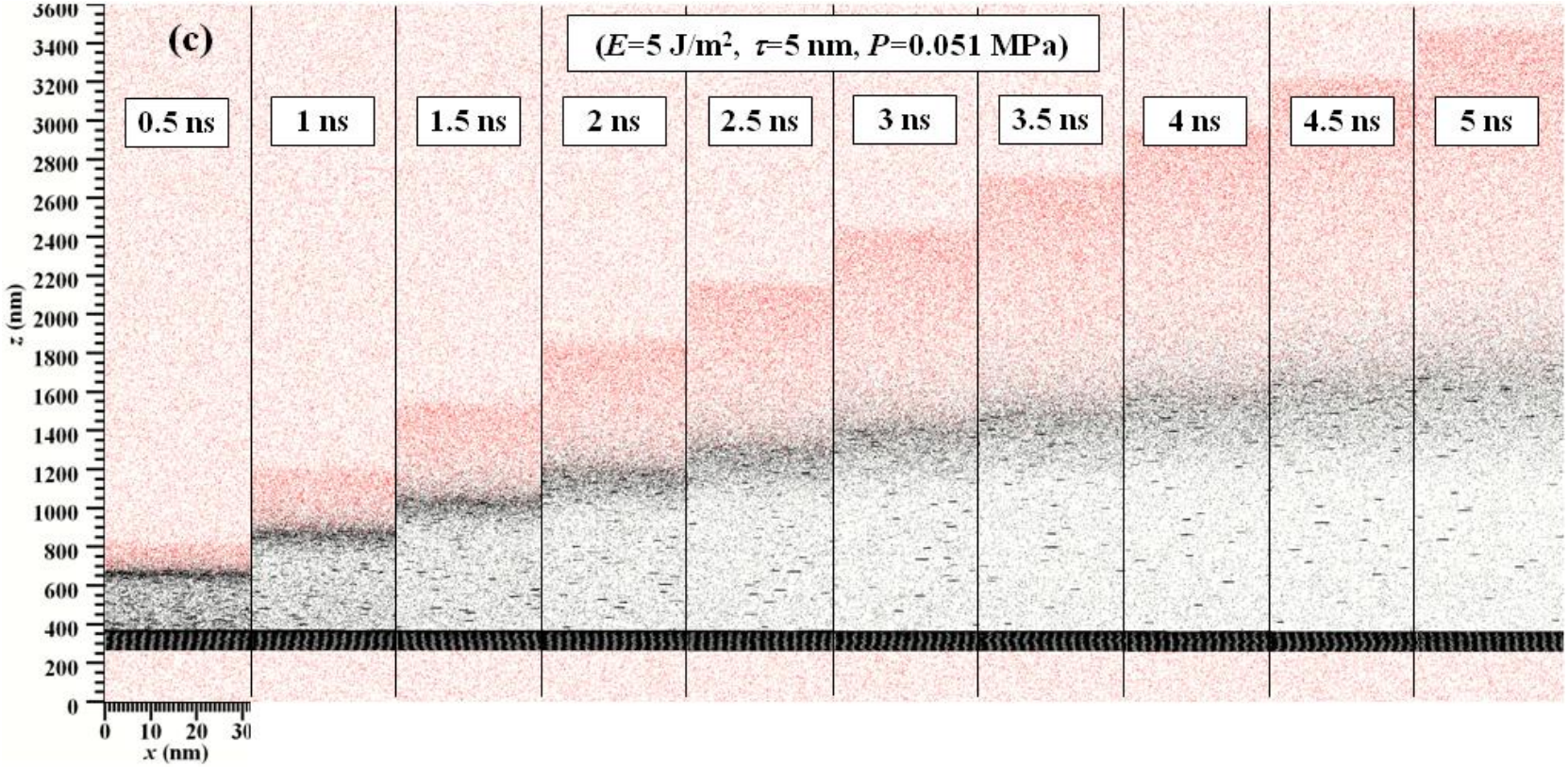

Figure 3.6 Continued.

Starting from 1 ns, the plume moves back to the liquid surface. At 5 ns, only very little plume is observed in space. Such back movement of the plume is also observed for 0.22 MPa, but happens much later (starting from 3.5 ns). Much more plume is ejected when the ambient pressure is 0.22 MPa. Stronger forward movement of the plume in lower pressure is more obvious when it is reduced to 0.051 MPa, under which the plume flies to the space as much as 1.6 μm at 5 ns.

In order to extract more valuable information about the ambient pressure effect on the shock wave dynamics, Fig. 3.7 is provided to illustrate the shock wave propagation velocity, the mass velocity of atoms in the shock wave front, the shock wave front position for three background gas pressures (Fig. 3.7a), and shock wave front average pressure distribution in time (Fig. 3.7b). It can be inferred that the shock wave forward-directed length is much larger (around 3 μm at 5 ns) when the ambient pressure is lower (0.051 MPa), which is visible both in Fig. 3.7a and in Fig. 3.6c. It is justifiable that the shock wave expands further when the pressure drops because the ambient gas constrains its expansion less. Furthermore, the shock wave propagation velocity becomes higher when the ambient pressure declines and it can reach an immense initial Mach number of 7 for 0.051 MPa pressure (Fig. 3.7b). The reason is that the shock wave expands more freely under low ambient pressure, and gains higher velocity in lower background pressure due to the less collisional interaction between the gas atoms trapped in the shock front and the ambient gas.

It can also be observed that the shock wave slowing down effect is stronger when raising the ambient pressure. As the background pressure increases the shock wave front

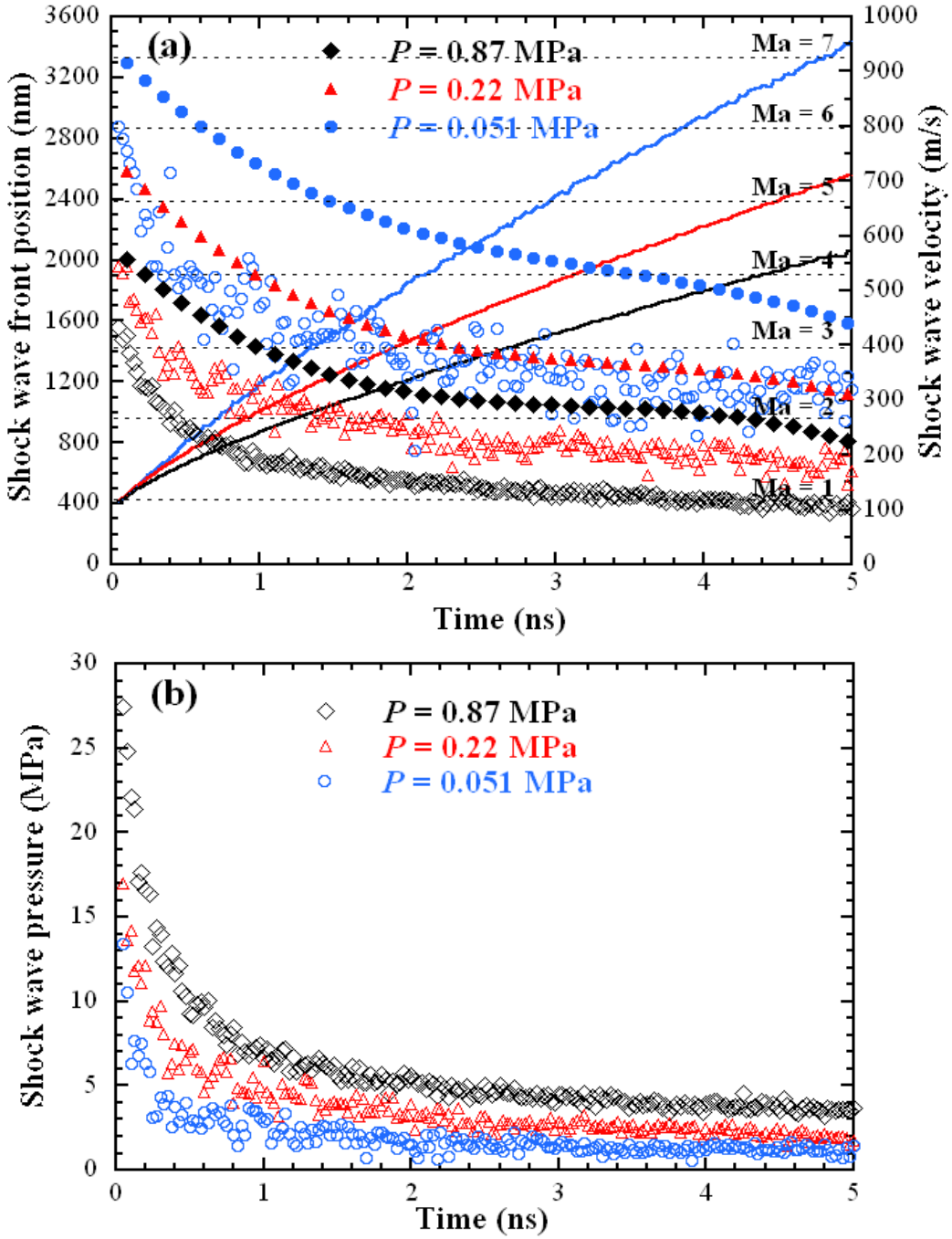

Figure 3.7 (a) Position, shock wave propagation velocity and the mass velocity of atoms in the shock wave front for three ambient pressures: 0.87 MPa, 0.22 MPa, 0.051 MPa (E=5 J/m^2, τ=5 nm). (Solid symbols: shock wave front propagation velocity; hollow symbols: mass velocity in the shock wave front; solid lines: shock wave front position); (b) Shock wave front average pressure distribution in time for three ambient pressures: 0.87 MPa, 0.22 MPa, 0.051 MPa (E=5 J/m^2, τ=5 nm).

undergoes larger scattering and is more attenuated by background gas collisions. When the ambient pressure is higher, the formed shock wave front features a much higher pressure, initially close to 30 MPa under the ambient pressure of 0.87 MPa. As the expansion progresses, the velocity in the shock wave front continues to decrease, the shock pressure is reduced noticeably, and the shielded slower components propagate to coalesce with the slowed material on the contact plume front (Chrisey and Hubler, 1994). This results in increase of the interaction zone thickness which is presented in Fig. 3.8.

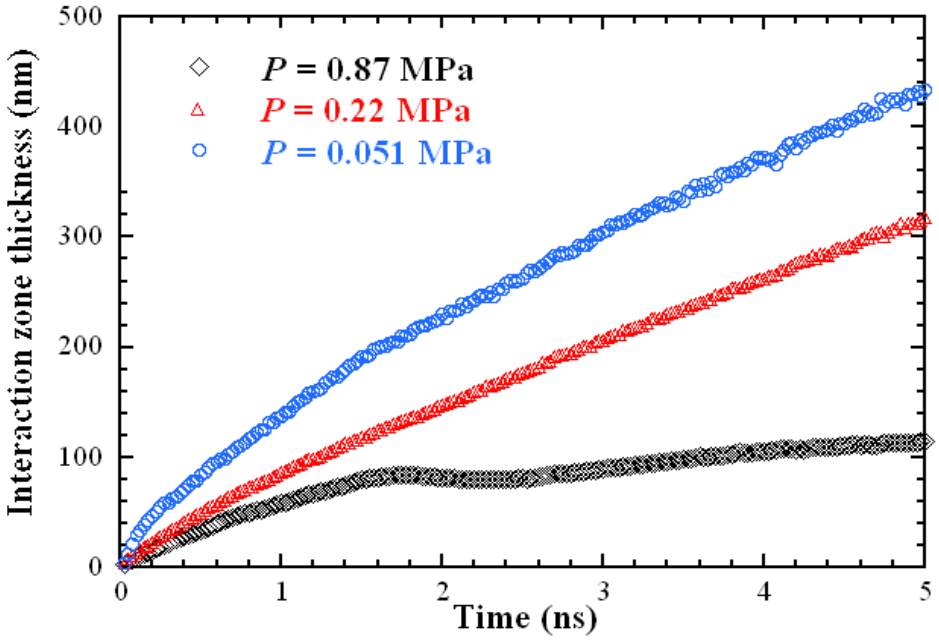

Figure 3.8 Interaction zone thickness between the target and the ambient gas for three ambient pressures: 0.87 MPa, 0.22 MPa, 0.051 MPa (E=5 J/m^2, τ=5 nm).

In general, the mixing length (interaction zone thickness) is larger when the ambient pressure declines. This is because of the higher plume propagation velocity and consequently higher recombination process of the plume constituents with shielded slower components of the shock wave. Despite almost linear increasing character of the mixing length at lower

pressures (0.051 MPa and 0.22 MPa), very surprising things occur for the higher pressure 0.87 MPa. It looks like that the process of mixing is somehow interrupted at 1.5 ns. A closer look at Fig. 3.6a reveals that at 1.5 ns, a large amount of plume is pushed back to recombine with the liquid surface. Therefore, this reduces the interaction zone thickness between the plume and the ambient gas. The increase of the interaction zone thickness after 1.5 ns is mainly attributed to the slow diffusion of the plume species into the ambient gas. The experimental work of the pressure influence on the laser ablation process has been widely covered in literatures (Chrisey and Hubler, 1994; Harilal *et al*., 2003: Eason, 2007). This work shows sound agreement with the experiments in terms of the shock wave and plume characteristics and behavior.

3.5 Comparison with Laser Material Interaction in Vacuum

For the purpose of comparison, the situation resembling the plume expansion in a vacuum is presented. This represents the extreme situation of the pressure effect (zero ambient pressure). The material plume expands freely in the vacuum since there is no medium to constrain its propagation. Figure 3.9 illustrates the spatial plume development in a vacuum combined with evolution of the target velocity along the *z* direction for similar laser ablation process parameters as previously applied: laser fluence of 5 J/m^2 and optical absorption depth of 5 nm. It can be noticed that the furthest flying out material particles can reach a length range of 16 μm at 5 ns from the target surface. To be able to attain so far distance within an ultrashort period of time, they must have very high velocity. As it can be seen in Fig. 3.9, the fastest traveling plume components can achieve extremely high expansion velocities near 3200 m/s, which approaches closely the experimental velocity

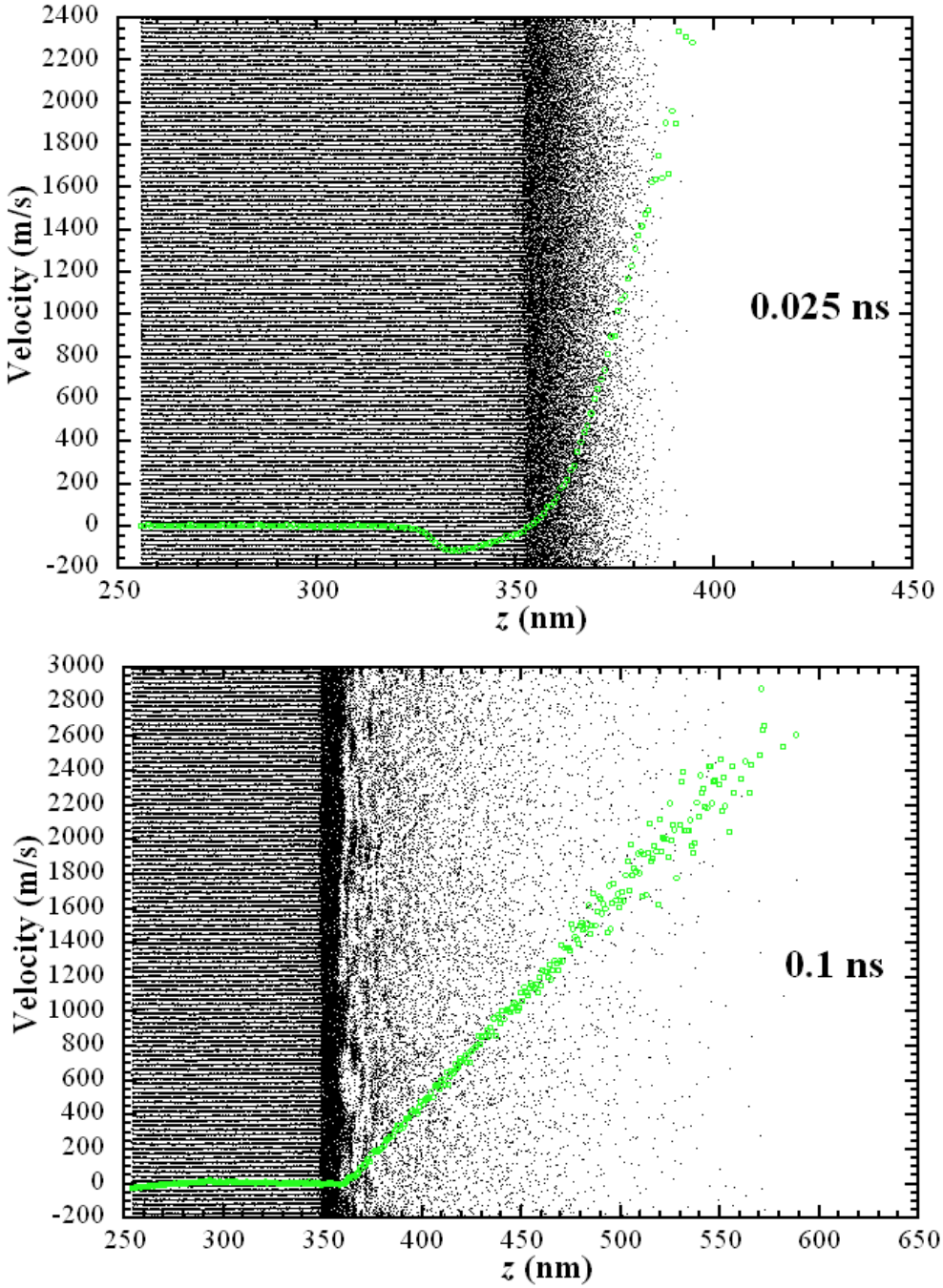

Figure 3.9 Snapshots of atomic positions combined with the evolution of target velocity distribution along the *z* direction in vacuum (E=5 J/m^2, τ=5 nm). Green color: target material velocity; black dots: target atoms.

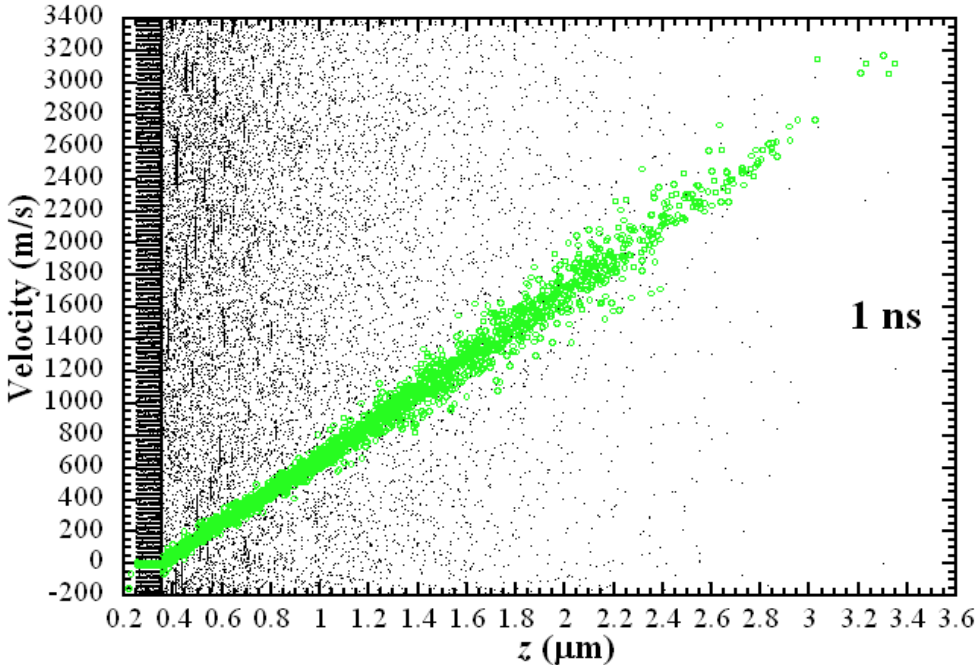

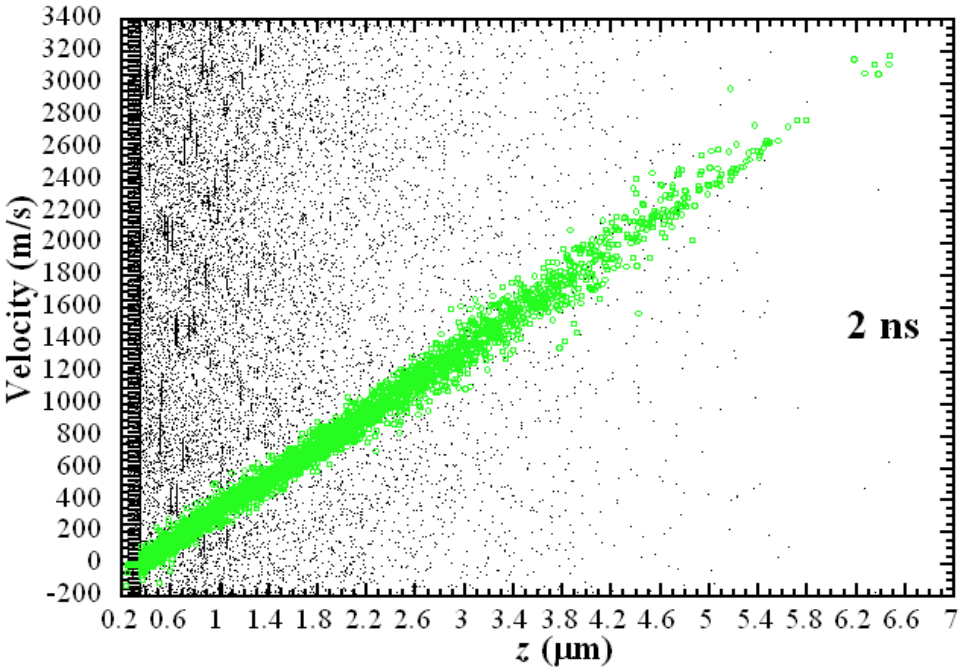

Figure 3.9 Continued.

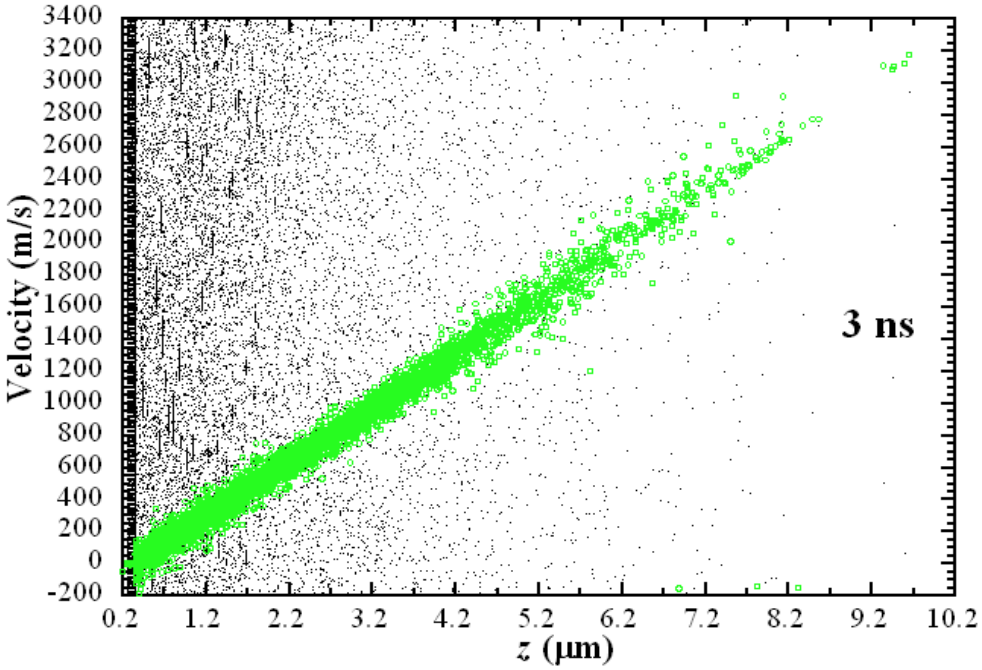

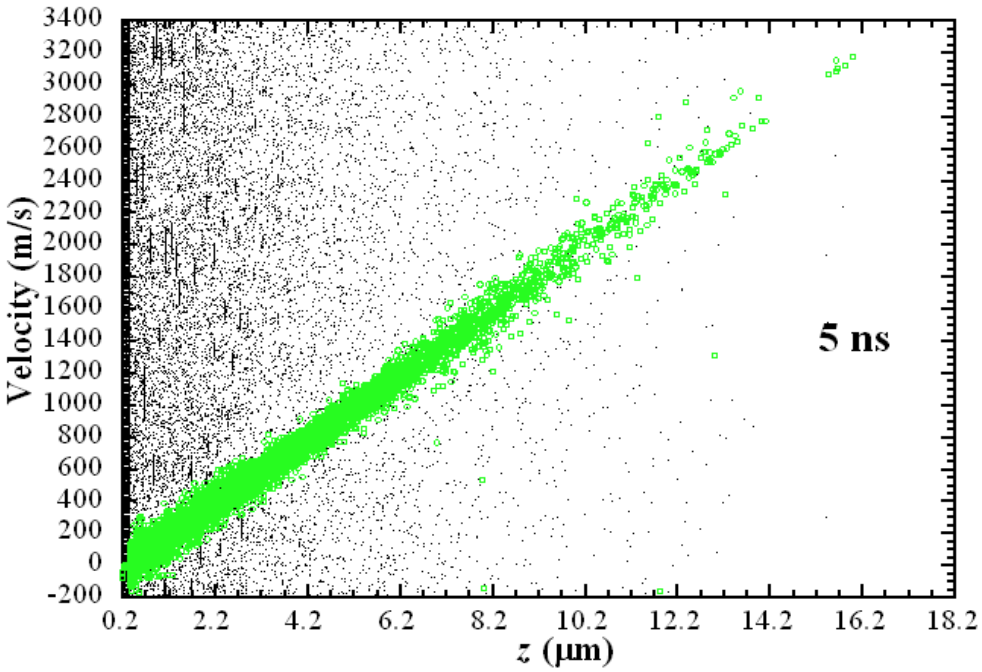

Figure 3.9 Continued.

range for instance in Voevodin *et al.* (2000).

Having shown knowledge of shock wave expansion and evolution it would be of considerable significance to also gain an insight into plume dynamics. Figure 3.10 displays the position of the plume front at three background pressures and under vacuum conditions. In this work, the plume front has been determined on the basis of plume density.

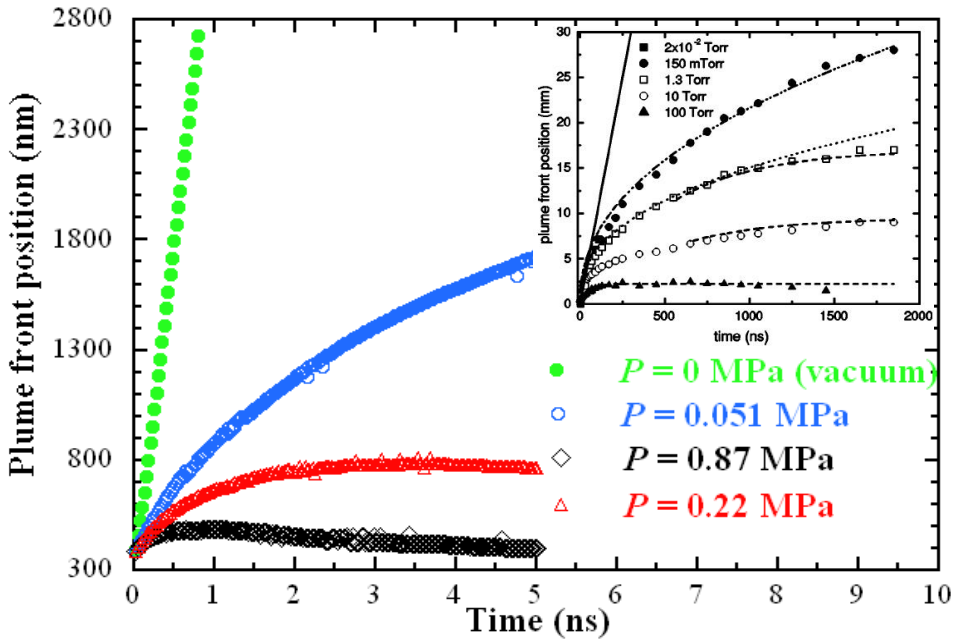

Figure 3.10 Position of the plume front (E=5 J/m^2, τ=5 nm) for three ambient pressures: 0.87 MPa, 0.22 MPa, 0.051 MPa and comparison with vacuum conditions. The inset in the figure shows position-time plots of the luminous front of the aluminum plume produced at different background air pressures taken from Harilal *et al.* (2003).

When scanning layer by layer from the top of the whole domain it will encounter the increasing number of ejectants from the target material. By selecting the criterion (dependent on the specific case since the number of atoms in plume front will vary when the ambient condition changes) the position of the plume front can be determined. It is visible that

apparent difference arises between plume expansion in vacuum and in the presence of ambient gas. The plume front in vacuum rises very fast in comparison to the cases of ambient pressure, indicating linear free expansion in vacuum. On the other hand, as the pressure of the ambient gas increases, the plume becomes more constrained which results in reduction of the effective length of the plume. These results show a perceivable analogy to the experimental outcomes described by Harilal *et al.* (2003) for nanosecond laser-material interaction (Nd:YAG laser, 8 ns pulse width). The inset in Fig. 3.10 may serve for comparison purpose. Although this work's simulation conditions differ from those of Harilal *et al.* (2003) in time scale and material, close agreement is observed between them in plume's propagation trend considering the effect of ambient pressure. Evidently, the plume development using MD simulations is not complete due to the high computational cost and can be tracked only up to a few nanoseconds. However, similarity at the early stage of evolution can be attributed, when comparing the P=0.051 MPa curve with the experimental curve at 100 Torr (0.015 MPa), the closest pressure condition, where one can quickly notice the apparent, and expected for later times, analogous behavior. Moreover, even though the timescale in MD simulation is three-order smaller than that in experiment using nanosecond laser, the reported dynamic evolution of shock waves reveals the early stage physics for shock wave formation and evolution in picosecond laser-material interaction.

For pressure 0.051 MPa the plume expands invariably forward from the surface within the computational time, which can be observed in Fig. 3.10 or in Fig. 3.6c. When the background gas pressure increases the strong shock wave stops the movement of plume and makes it move toward the target surface. As the plume expands, the counteraction of the

higher pressure ambient gas increases and the contact surface slows down, resulting in backward motion. This is observed for the background gas pressure of 0.87 MPa and 0.22 MPa in Fig. 3.10. For the ambient gas pressure of 0.22 MPa the plume starts being pushed to the surface at 3.5 ns. Very perceivable backward movement is observed for the case with the highest ambient pressure (0.87 MPa). Just after 1.5 ns the plume is mercilessly knocked back and recombines with the target surface. The plume backward motion can lead to intensification of the surface redeposition process. As observed in experiments (Singh, 2005), the mass of the redeposited debris goes up with increase in the background pressure. This is because for a higher pressure, the entrapment of the particles is stronger due to the higher gas density, consequently dragging more ablated mass back to the target surface. As long as the backward movement of plume makes it to redeposit on the target surface, a series of thermodynamic processes will occur (e.g., condensation and solidification). The local temperature and pressure play important roles in these processes. Further study is underway to investigate the phase change after plume redeposition.

3.6 Effect of Laser Fluence on Shock Wave

In laser ablation process it is important to efficiently ablate material without excessive overheating and melting of the sample. The fact is that for different materials there exists a certain level of laser energy often called as a threshold fluence of ablation, above which the material is expelled from the target surface. With increased irradiance above the ablation threshold, the ejected plume becomes more intense and the generated shock wave becomes stronger. In this work, dependence of the ablation process on the laser fluence is shown on the basis of three laser energy levels: 3, 5, and 7 J/m^2 when τ=5 nm, and P=0.22 MPa. The

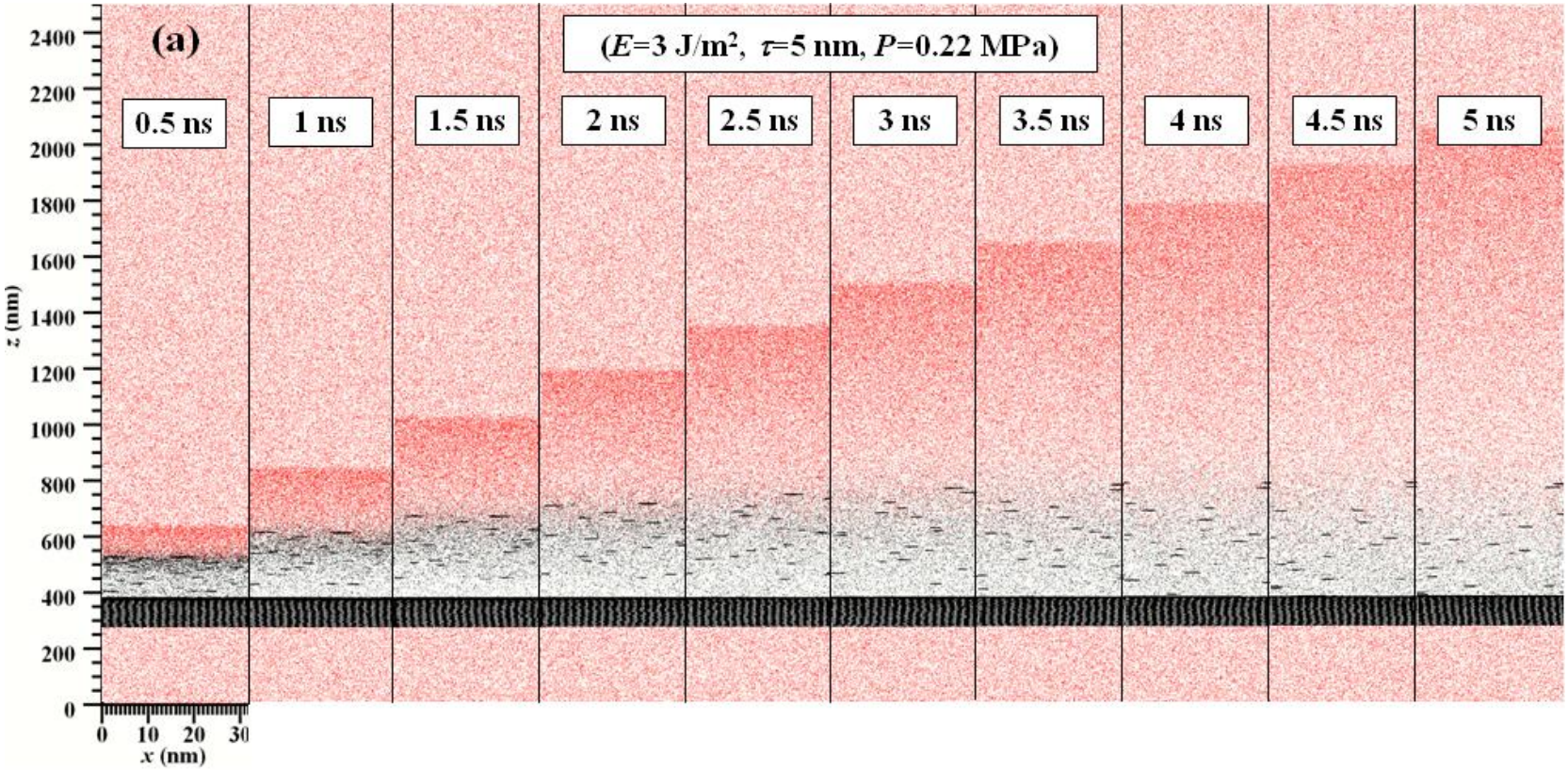

Figure 3.11 Comparison of snapshots for the dynamics of shock wave formation and evolution for P = 0.22 MPa, τ=5 nm, and three different laser fluences: (a) E=3 J/m^2, (b) E=5 J/m^2, and (c) E=7 J/m^2.

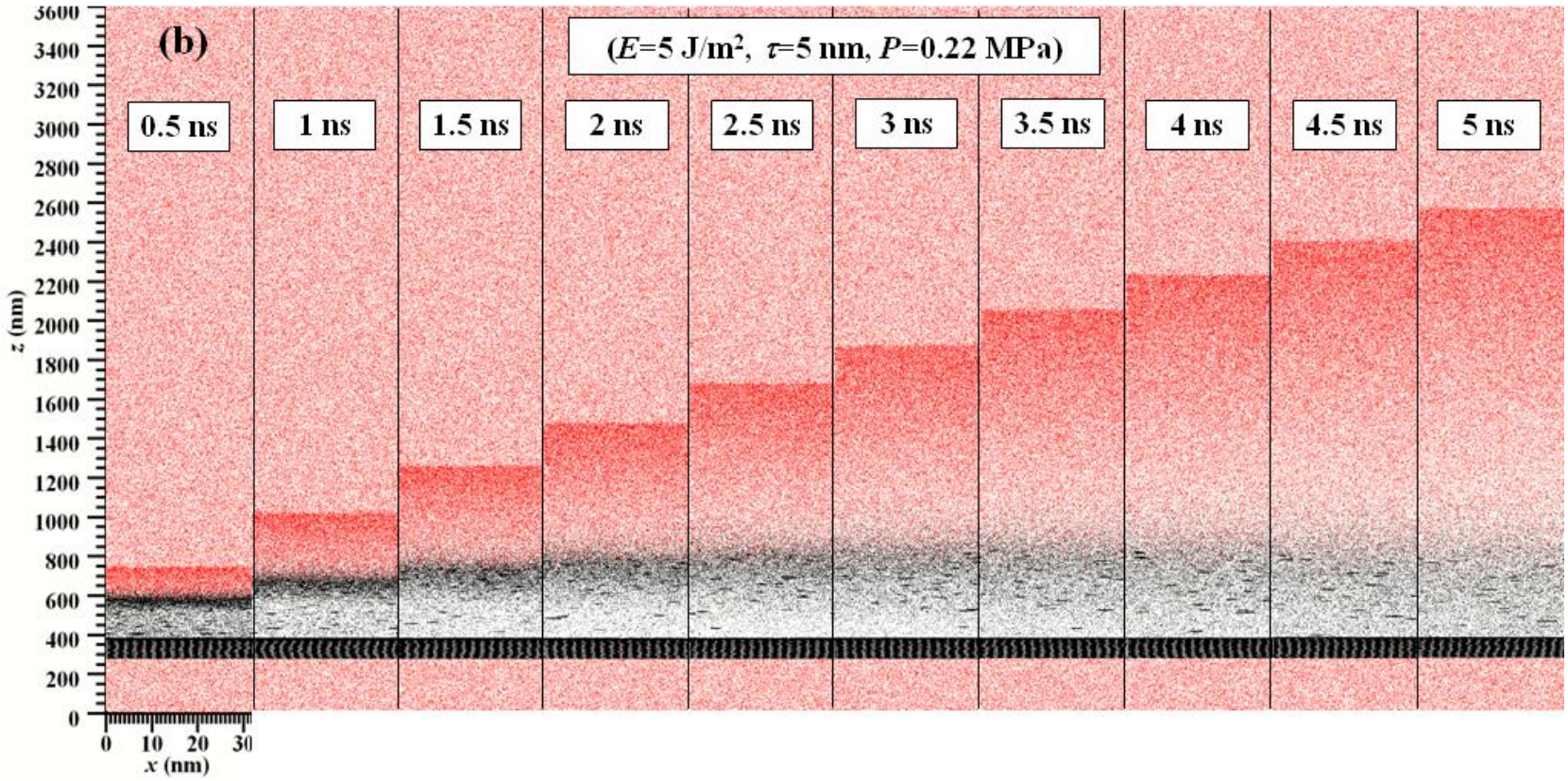

Figure 3.11 Continued.

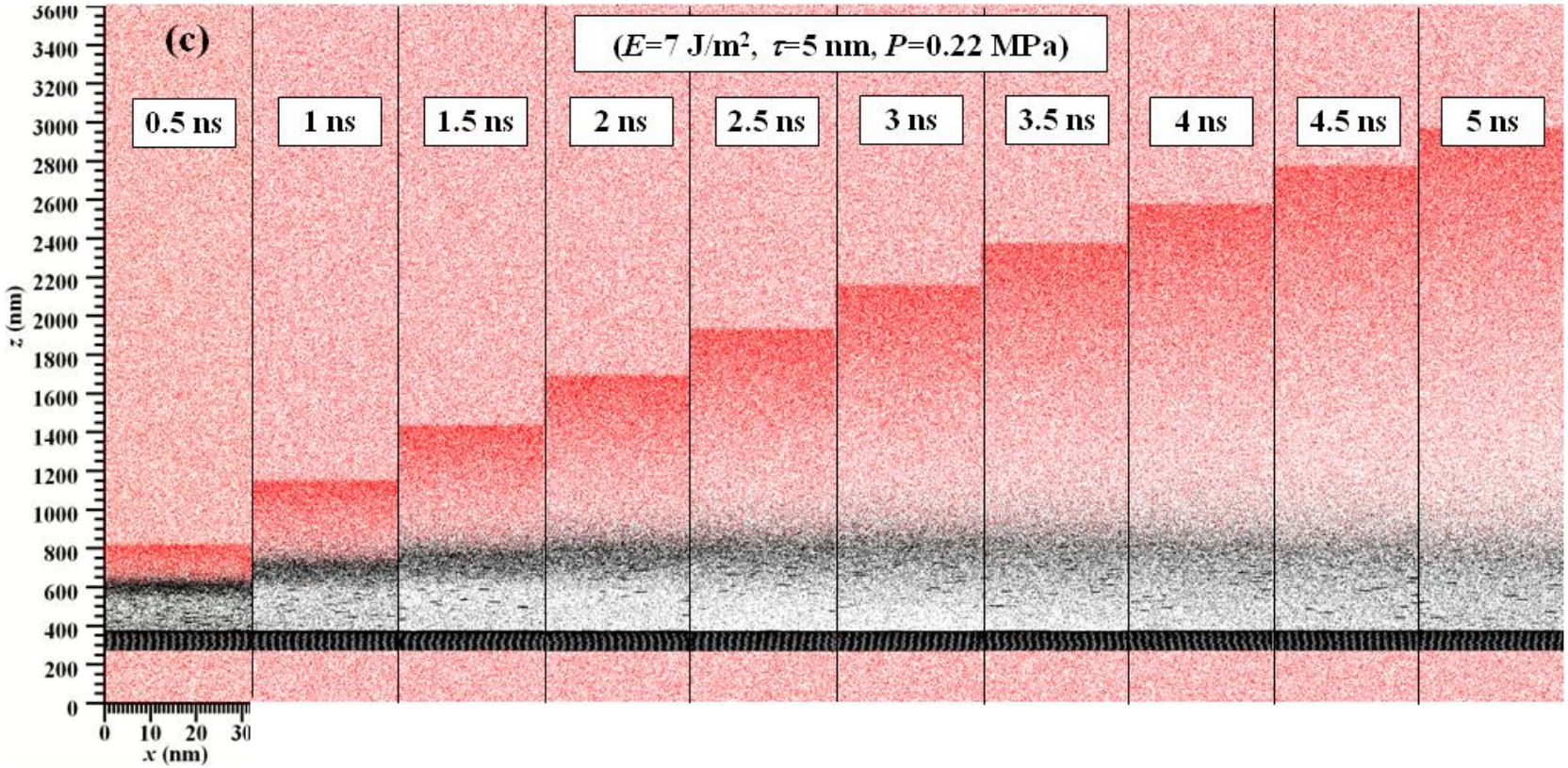

Figure 3.11 Continued.

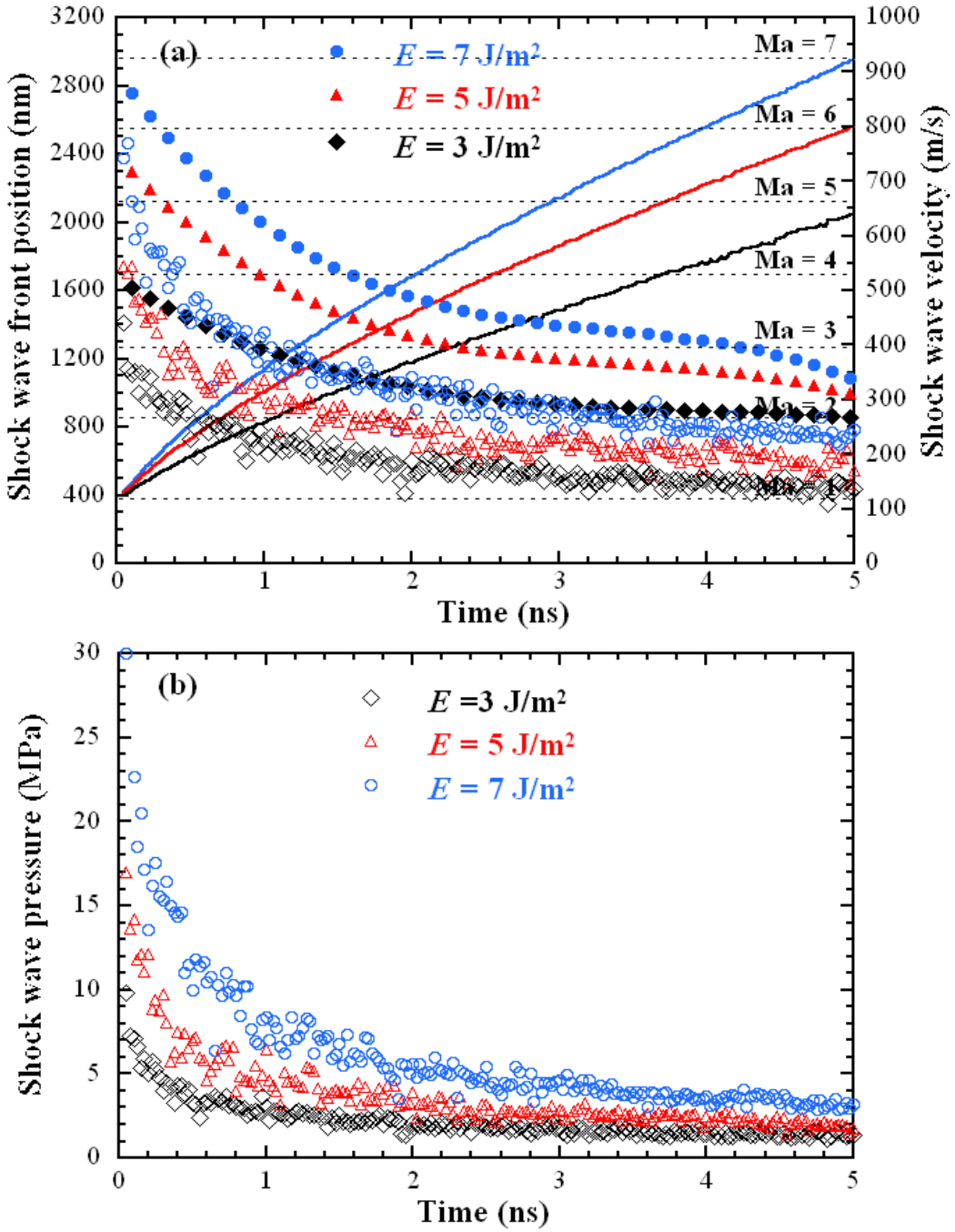

Figure 3.12 (a) Position, shock wave propagation velocity and the mass velocity of atoms in the shock wave front for three laser fluences: 3 J/m^2, 5 J/m^2, 7 J/m^2 (P = 0.22 MPa, τ=5 nm). (Solid symbols: shock wave front propagation velocity; hollow symbols: mass velocity in the shock wave front; solid lines: shock wave front position); (b) Shock wave front average pressure distribution in time for three laser fluences: 3 J/m^2, 5 J/m^2, 7 J/m^2 (P = 0.22 MPa, τ=5 nm).

atomic positions and dynamics of plume and shock wave evolution are presented in Fig. 3.11. Figure 3.12 shows the velocity (Fig. 3.12a) and pressure evolution (Fig. 3.12b) at the shock wave front for the scenarios shown in Fig. 3.11. From Figure 3.11 it is observed that with increasing laser energy input, the plume becomes more uniform with fewer large particles ablated out. When the laser fluence is higher, the material is ablated out suddenly in a more concentrated time, leading to a more concentrated plume front. More distant shock wave propagation is visible when the laser fluence is higher (Figs. 3.11 and 3.12a). Furthermore, a higher shock wave propagation velocity and pressure for 7 J/m^2 case indicates that the larger amount of laser energy generates a much stronger shock wave (Figs. 3.11 and 3.12). The interaction zone thickness also increases when the laser fluence is increased. This is due to greater relative movement of the plume and gas particles (Fig. 3.13).

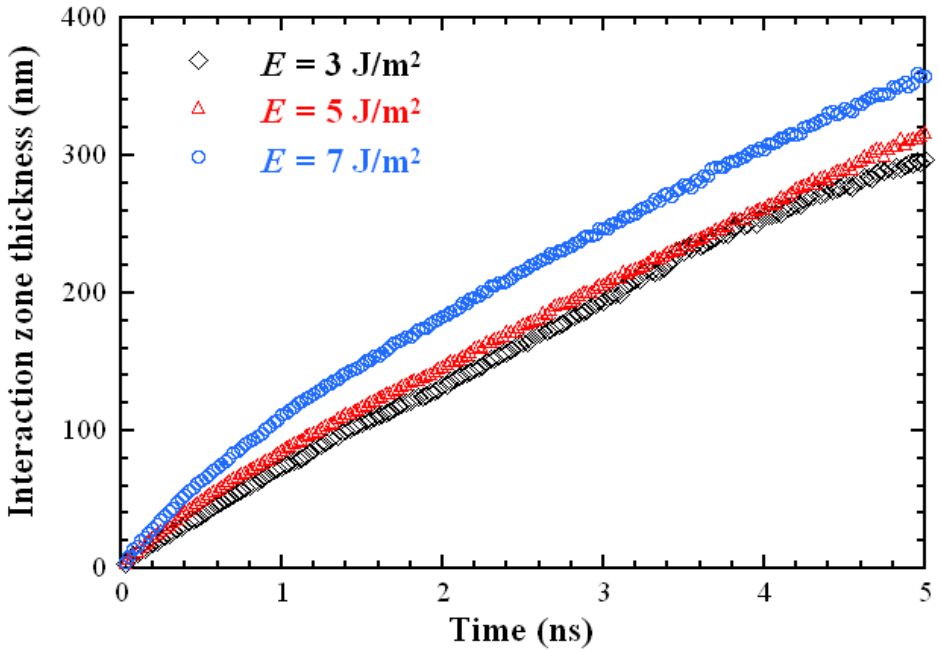

Figure 3.13 Interaction zone thickness between the target and the ambient gas for three laser fluences: 3 J/m^2, 5 J/m^2, 7 J/m^2 (P = 0.22 MPa, τ=5 nm).

It can also be inferred that, the higher laser pulse energies cause an increase in the ablated mass, additionally resulting in a larger material depth removed. That occurrence is presented experimentally in work by Mason and Mank (2001) or Singh *et al.* (2005) with close agreement with our results. Related analysis of the composition and density of the ejected plume on the laser fluence dependence has been also recently performed using MD simulations (Zhigilei *et al.*, 2003). For applied fluences range the results obtained here and observations are correspondingly reasonable.

4. SECONDARY SHOCK WAVE IN LASER MATERIAL INTERACTION

The atomic position with evolution and propagation of the primary and secondary shock waves in the background gas is presented in Fig. 4.1. Additionally, the velocity and pressure distributions are also superimposed in that figure for ease of discussion. At the first of displayed pictures, one of the initial stages of the process is shown at 0.2 ns. As it can be seen the main/primary shock wave front is already formed and is characterized by the high pressure (around 21 MPa) and velocity almost 3 times the speed of sound (around 390 m/s). The plume at this stage is propagating forward with supersonic velocity, having been ejected from the target surface after application of the laser energy pulse. An important occurrence starts to happen at 0.5 ns when the velocity of the plume front has a substantial decrease. Because of the ambient gas high pressure, the plume undergoes volumetric confinement, and in result is being bounced back. The interpretation of this harsh volumetric constraint is the extremely high pressure gradient from the compressed ambient gas front to the target surface. While the shock wave front expands further, the plume starts to move backward heading to the surface, which is justified by the negative velocity of target material at 1 ns. The same trend of the velocity is still visible at 1.5 ns; however with significant difference in the behavior of the adjacent gas molecules. Due to the backward motion of the plume material, the under-pressure zone created in vicinity of the plume front (right side) results in suction of the ambient gas atoms, with analogy to the retracting movement of the ultrafast piston. Therefore, the sucked background gas molecules are being dragged to the target surface, leading to the change in the velocity direction (1.5 ns). At this moment, a negative velocity at the rear of the background gas is observed. At 2 ns the large amount of the plume particle

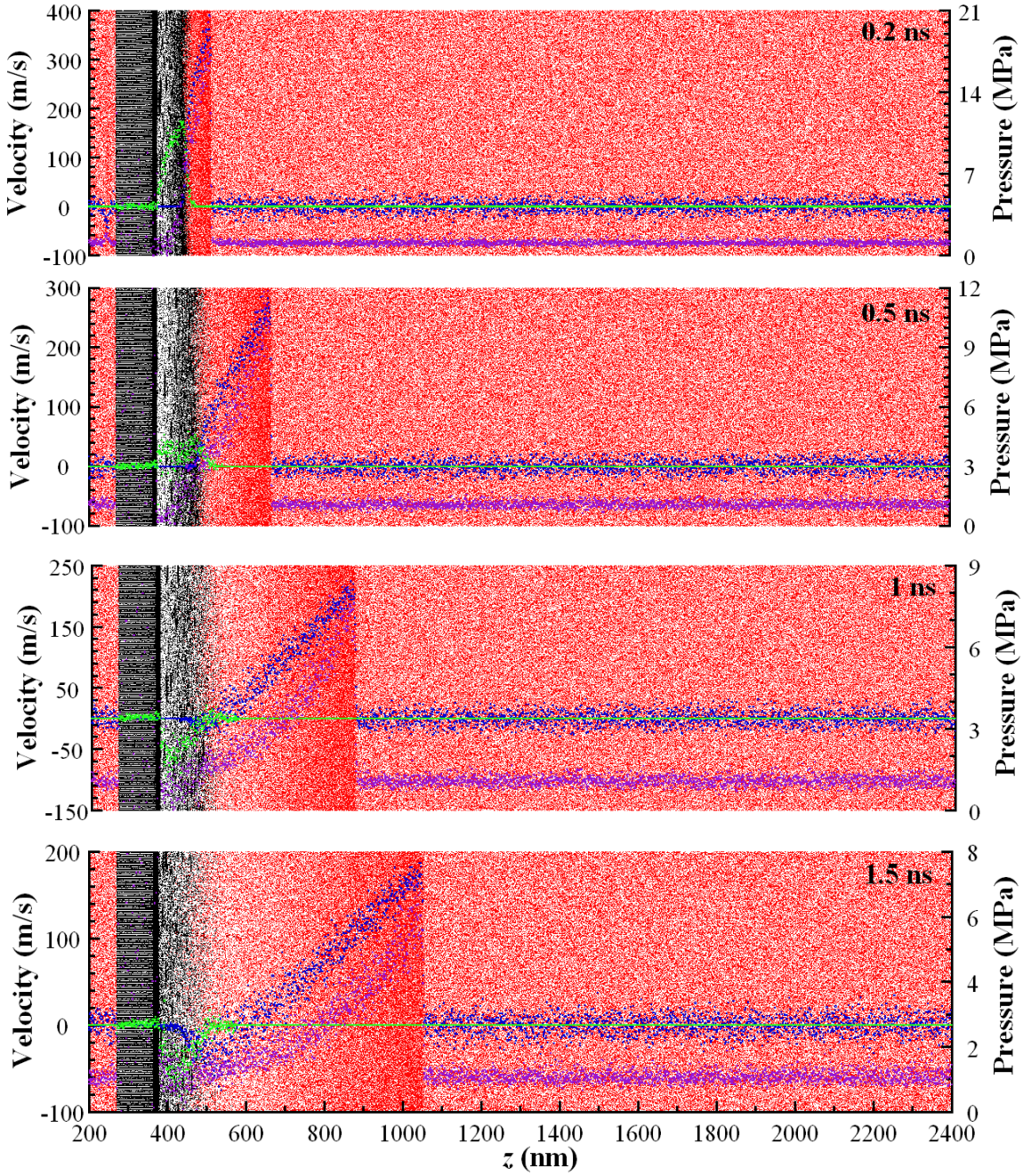

Figure 4.1 Snapshots of atomic positions combined with the evolution of target and gas velocity, alongside with pressure distribution in the *z* direction (E=5 J/m^2, τ=5 nm, P=0.87 MPa). Green color: target material velocity; blue color: background gas velocity; violet color: pressure; black dots: target atoms; red dots: ambient gas atoms.

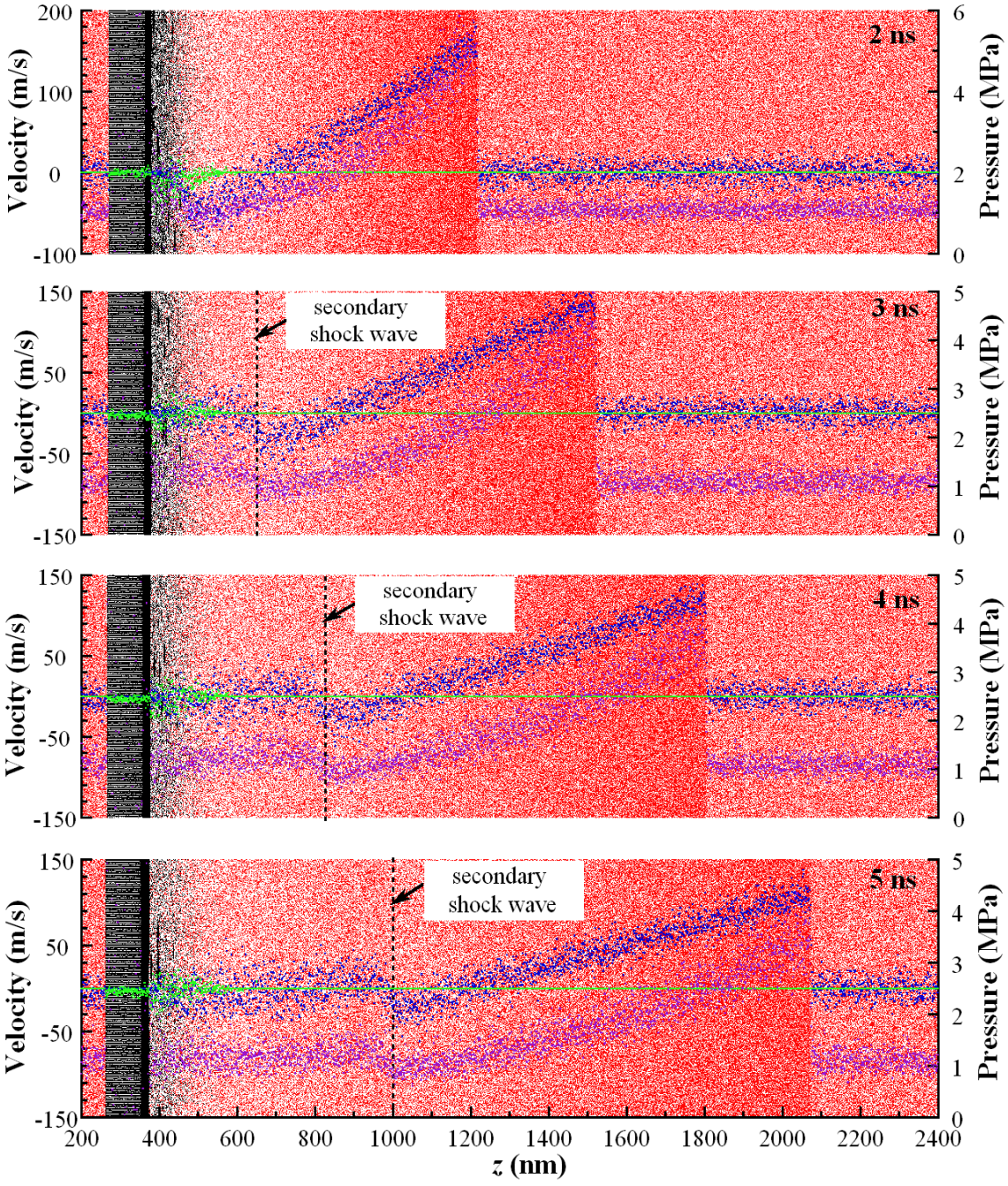

Figure 4.1 Continued.

cloud is already pushed back where it recombines with the liquid surface, and the velocity of the plume becomes almost zero. In contrast, after being dragged toward the target surface, the ambient gas is reflected from it and begins to propagate in the direction leaving the material surface, ultimately forming the secondary shock wave. At 3 ns, this internal shock wave front is fully discernible, and it is marked (as well as at 4 and 5 ns) in order to improve visual detection, since it is rather weak due to the strong dissipation. At 5 ns its velocity does not exceed the value of 50 m/s, meaning it moves almost 3 times slower in comparison with the main shock wave front. Although, in Fig. 4.1 the secondary shock wave is practically hard to observe in the atomic configuration due to its weak strength, it is clearly visible in the velocity and pressure distribution enclosed, where at the front of the secondary shockwave, a peak of the pressure and velocity is very visible. Similar behavior has been observed in TOF measurements for various plume species analyzed by mass spectroscopy (Bulgakov *et al.*, 1996), and successful attempt of modeling has been performed by the gas dynamic model (Bulgakov and Bulgakova, 1995). These results show remarkable good agreement with those scientific output on the velocity and pressure distribution, despite the difference of the inspected materials and slight disparity in the values.

In order to have a better understanding of the secondary shock wave formation and evolution, it is necessary to analyze its generation from the bulk mass and thermal point of view. For this reason, Fig. 4.2 is provided to present time sequence of the density and temperature profile along the *z* direction. As can be seen the shock wave front density and temperature is the highest at the initial stages due to compression. At 0.2 and 0.5 ns, as

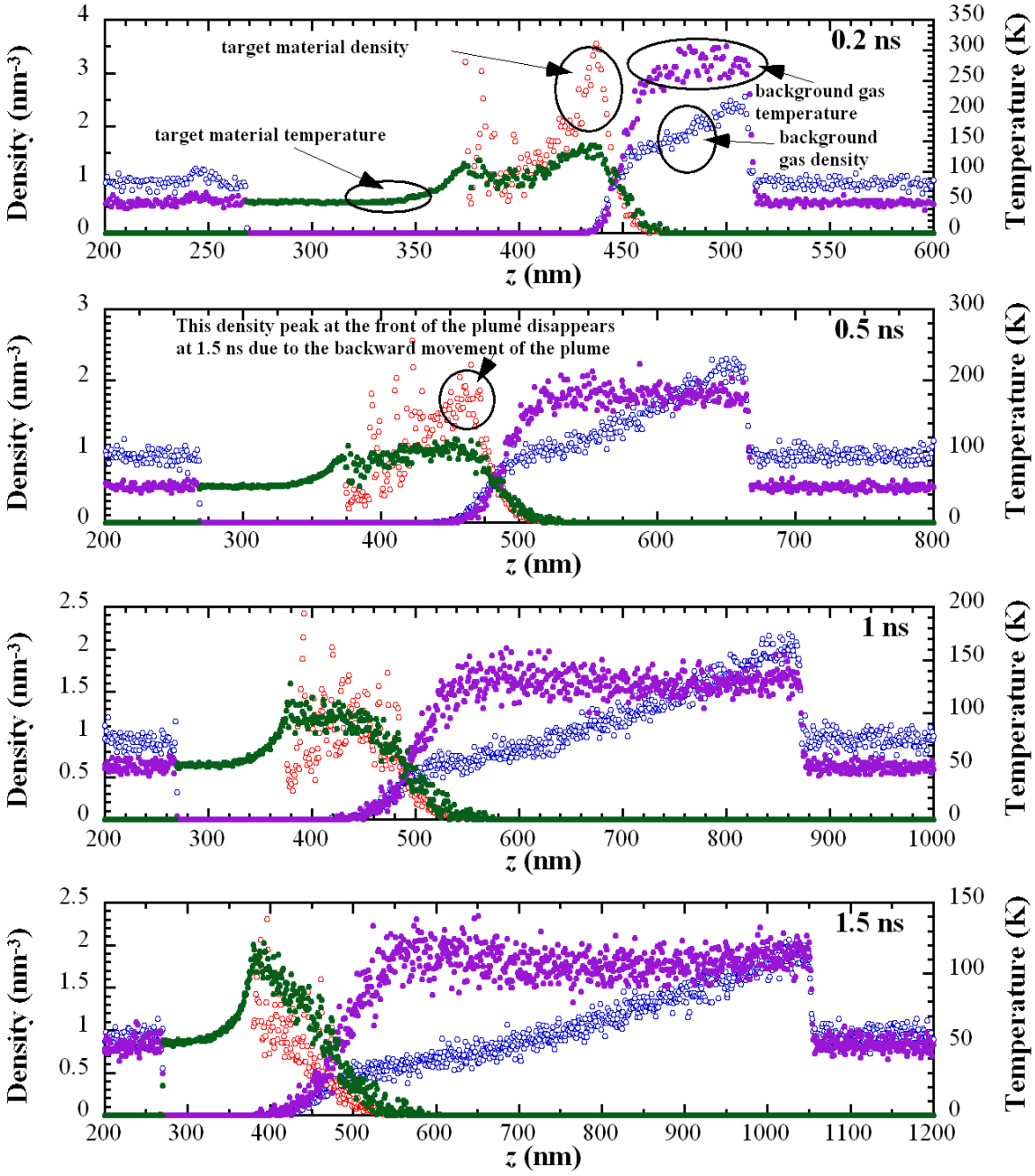

Figure 4.2 Evolution of density and temperature distribution along the *z* direction at different times (*E*=5 J/m^2, τ=5 nm, *P*=0.87 MPa). Red color: target material density; blue color: background gas density; green color: target material temperature; violet color: background gas temperature.

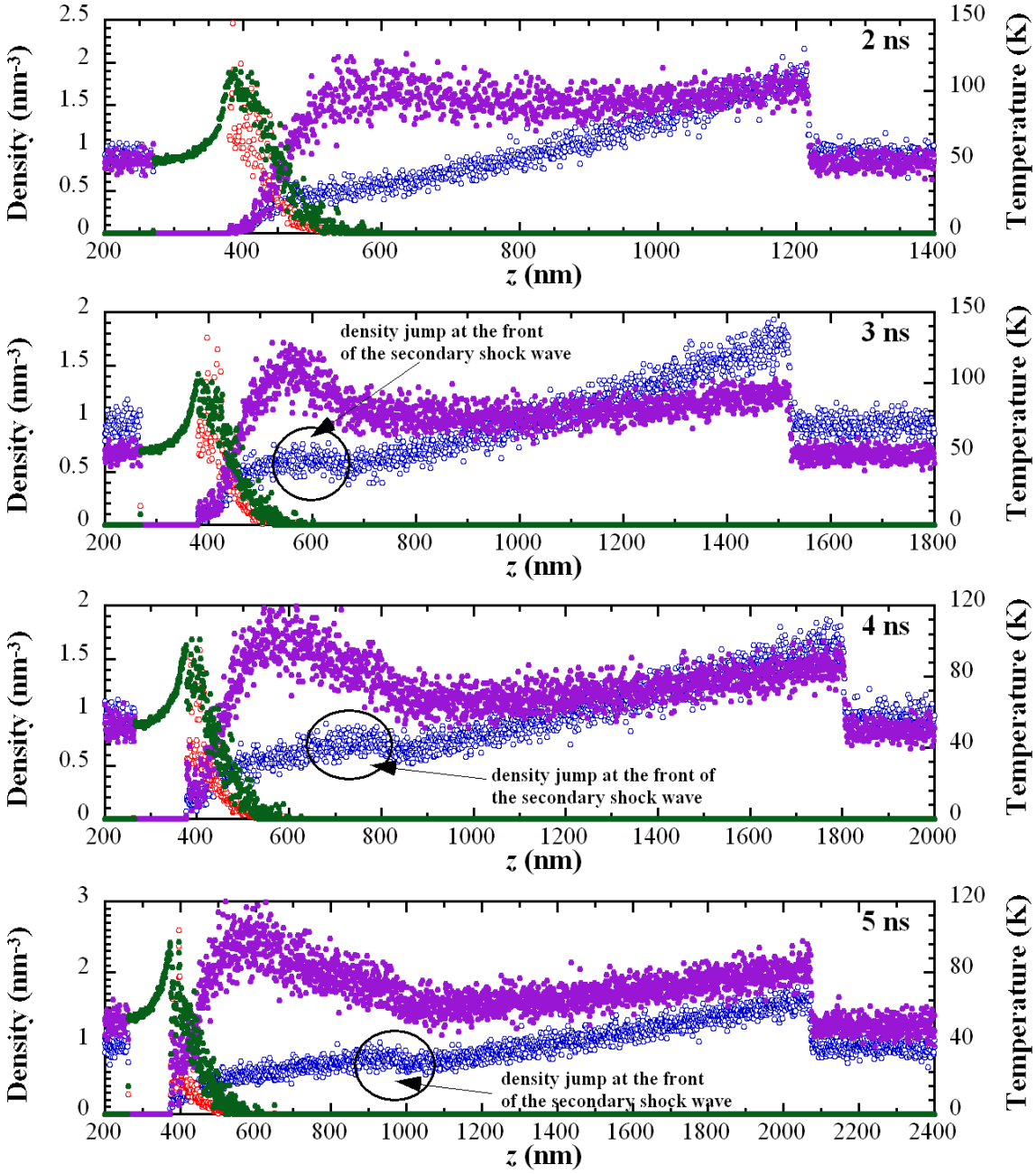

Figure 4.2 Continued.

indicated in the figure, there is a density peak at the front of the plume. Due to the high pressure gradient, the plume front is forced to move back toward the target surface. Such backward movement of the plume quickly reduces the density peak, which disappears at 1.5 ns. As we described based on Fig. 4.1, some of the ambient gas is also pushed back toward the target surface. Since the ambient gas molecules cannot coalesce with the target surface, they are reflected and the gaseous cloud induces the formation of a second shock compression. As marked in figures of 3~5 ns, there is a density jump at the front of the secondary shock wave, which is a direct consequence of the reflected background gas from the target surface. Such density jump justifies the existence of the secondary shock wave. During propagation this internal shock front keeps a distribution width of several mean free paths (5 ns). Likewise, backward motion of the ablated particles was observed in several experiments by TOF spectroscopy or time resolved imaging (Leboeuf *et al.*, 1996; Harilal *et al.*, 2003; Singh *et al*., 2005) providing considerable close agreement with this result.

In Fig. 4.2 it is observed that at the front of the main/primary shock wave, there is a significant temperature jump. On the other hand, it is noteworthy that at the front of the secondary shock wave, the temperature jump is very weak, almost negligible. For the primary shock wave, its front temperature experiences quick dissipation, from 250 K at 0.2 ns to 80 K at 5 ns. In opposite, the temperature of the ambient gas in the rear region (close to the target surface) has very slow dissipation since no stationary low temperature background gas is in contact with it.

5. PLUME SPLITTING IN LASER MATERIAL INTERACITON UNDER THE INFLUENCE OF SHOCK WAVE

In this chapter, work is focused on the physical process during the early stage of laser ablated plume propagation (up to 2 ns). In figure 5.1, the spatial evolution of the plume through the background gas at different times is presented. The combined pressure distribution with generated processes in the ambient gas is imposed to account for the interpretation of the splitting effect. As can be noticed the highest pressure in the system is generated at the front of the produced shock wave. However, not the compelling shock wave characteristics, but primarily the intriguing pressure gradient across the plume material is the aspect of concern in here. At initial expansion stages, the ejected material consists of very high pressure gradient in the front of the plume (0.2 ns), which later on attenuates significantly due to the dissipation with the background gas. On the other hand the pressure gradient in the plume's tail region is not so steep and afterwards becomes rather uniform. Although the pressure carries lots of valuable information, the plume splitting explanation must be linked simultaneously with the velocity and density profiles. In contrast to Fig. 5.1, figure 5.2 shows the target atoms transport in the two peak regions, which corresponds to temporal evolution dynamics of the plume up to 2 ns.

The plume splitting effect is perceptible with the formation of clear twin-peak behavior in the plume velocity profile (0.5~2 ns). Let us move to the elucidating of the reason of plume splitting whose configuration mechanism has to be recognized from the early time steps. The question is: Where do the atoms within the two peaks of velocity

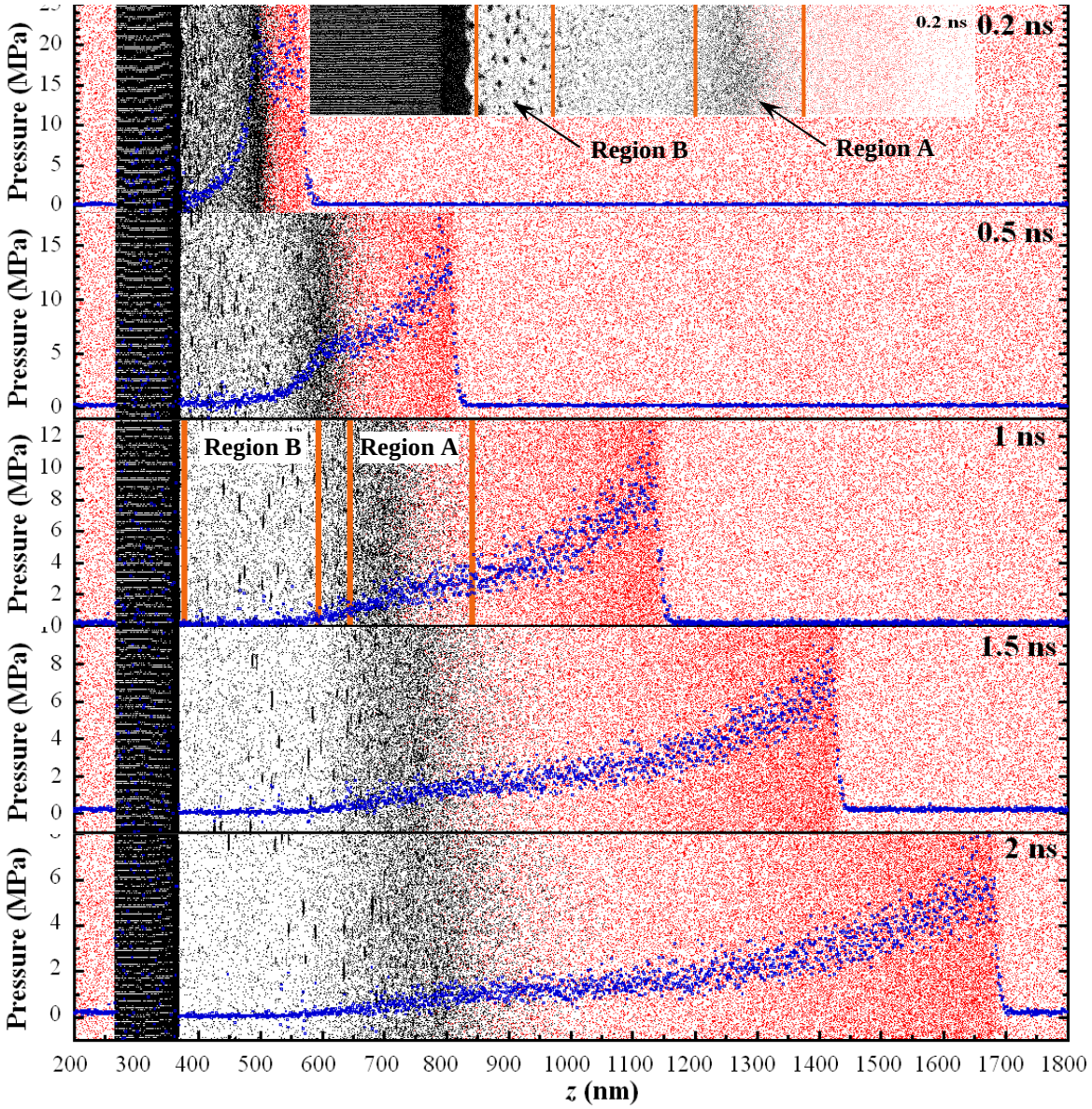

Figure 5.1 Snapshots of atomic positions combined with the pressure distribution in the *z* direction (E=7 J/m^2, τ=5 nm, P=0.22 MPa). Blue color: pressure; black dots: target atoms; red dots: ambient gas atoms.

distribution come from? The track the history of these atoms has been performed, and found that the atoms in the front peak (Peak I) (t= 1 ns) come from the front of the plume at 0.2 ns. The second peak (Peak II) at 1 ns corresponds to atoms that are ejected having slower initial

velocity at 0.2 ns. In figure 5.2, the black dots represent the atoms flying out slowly at 0.2 ns, and the violet dots are the fast atoms in the front of the plume. The atoms in these two regions (region A and B) are marked in the inset in the figure at 0.2 ns in figure 5.1. The evolution of the velocity in the regions of interest can be explained inclusive of the pressure distribution shown in figure 5.1 in order to justify the formation of plume splitting. Upon laser irradiation, phase explosion will take place. The faster ejected particles (monomers, dimers, and smaller particles) quickly move out and interact with the ambient gas and feel the strong constraint from the ambience. These atoms form Region A (marked in figures 5.1 and 5.2). As shown in figure 5.1, in that zone, there is a very steep pressure gradient due to the strong constraint of the ambient gas. This large pressure gradient plays a critical role in slowing down the atoms in Region A. This velocity deceleration can be viewed clearly in figure 5.2. The velocity of atoms in the front of the plume zone reduces from the level of 500 m/s at 0.2 ns down to less than 100 m/s at 2 ns.

In the phase explosion vicinity section, at the early times (0.2 ns), on the contrary, the larger particles have lower velocity and are left behind in the tail of the plume (Region B), as shown in figure 5.1. In that zone the pressure gradient is very small (almost flat pressure distribution). Therefore, the atoms in Region B experience much less deceleration. In fact, since some particles still have phase change (vaporization) and their velocity is picking up from less than 100 m/s at 0.2 ns to more than 200 m/s at 0.5 ns. The deceleration of Region A and acceleration of Region B give strong contribution to the formation of plume splitting, which emerges starting from around 0.5 ns. At 2 ns, it is found most of the atoms in Region B have moved quite close to the ambient gas and their velocity reduces to less than 100 m/s.

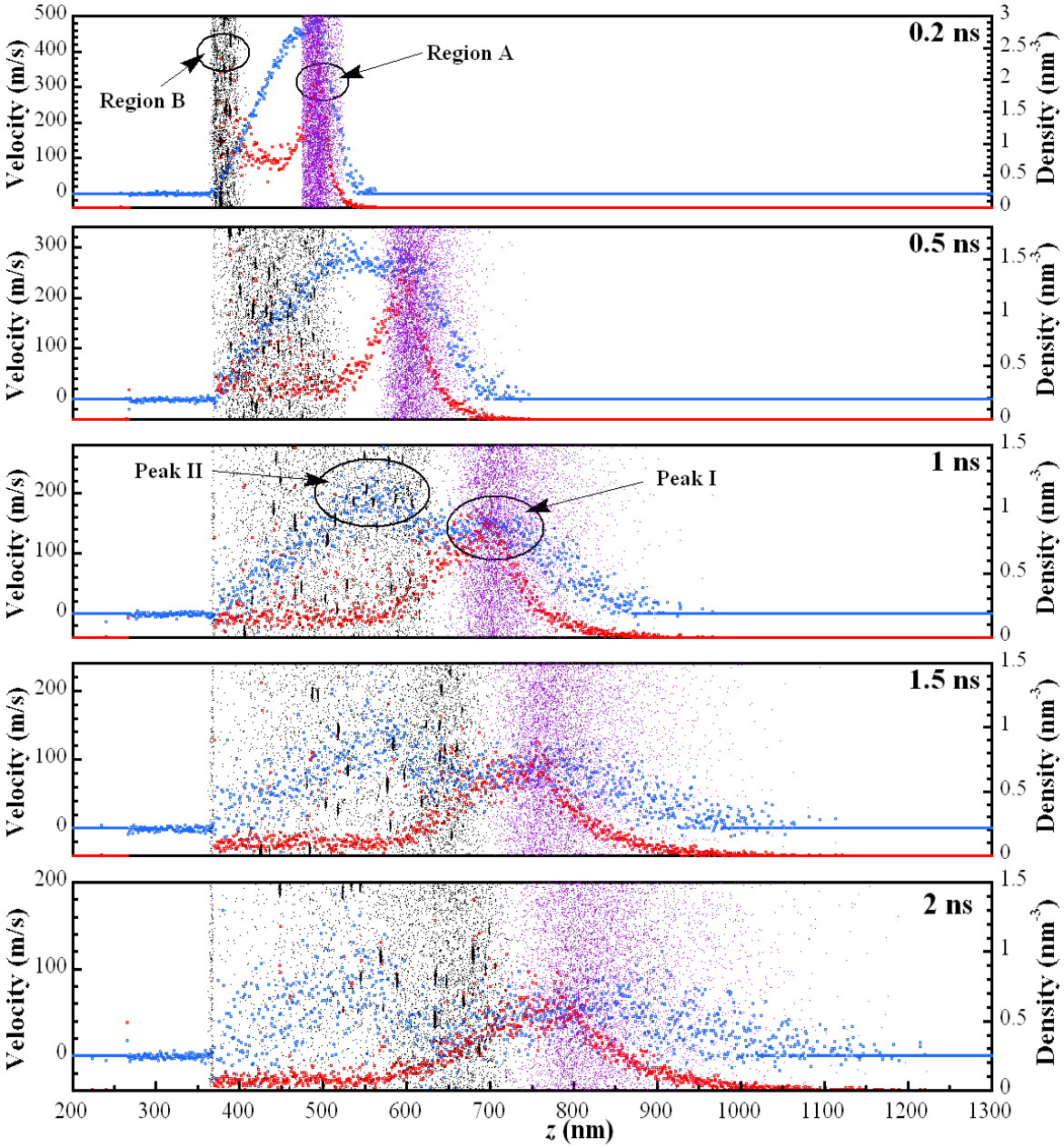

Figure 5.2 Velocity and density distribution of the target material plume and the indication of the position of the plume two-peak propagation in the *z* direction (*E*=7 J/m^2 , τ=5 nm, *P*=0.22 MPa). Blue color: plume velocity; red color: plume density; violet dots: plume's first peak atoms position; black dots: plume's second peak atoms position.

It is pertinent to notice that the double peak density formation of the plume can be observed at very early expansion times (0.2 ns in Fig. 5.2). It is believed that this occurrence is not just coincidence but it brings significant impact to the mechanism of the plume splitting. The leading density peak (Region A) characterizes the highest content of the atoms and is located in the front of the plume. During the plume expansion it retains its peak looking shape but 'snowplowing' of the background gas causes to diminish and broaden it. The other density peak initially being adjacent to the target surface (Region B), spreads over in the plume's shroud and exhibits sporadically spikes indicating appearance of nanoclusters (for example at 2 ns in Fig. 5.2).

The plume velocity decay can also be viewed clearly in figure 5.3, where velocities of atoms in both peaks are presented against time. These curves represent the average atom velocity from regions belonging to each peak. As one can perceive the plume splitting starts at 0.5 ns. Both velocity peaks decelerate very quickly from about 280 m/s at 0.5 ns to about 100 m/s and 50 m/s for peak II and peak I, respectively (2 ns). The moment when the split starts to appear can be also discerned from the propagation position of peak location (figure 5.3). While peak I moves out with time, peak II appears almost as a standing wave, showing little change of its location against time. This is clearly shown in Figs. 5.2 and 5.3. Such phenomenon holds on for about 1.5 ns during our simulation. Such standing-wave feature of Peak II is due to the strong relaxation of large particles/clusters and atoms in the plume. Similar velocity behavior has also been observed in the prominent computational study by Amoruso *et al.* (2006) at pressure of 70 Pa. The plume splitting has also been observed experimentally in the vacuum (Bulgakov and Bulgakova, 1995; Harilal *et al.*, 2002). It seems

that the phenomenon is more general in laser material interaction regime. It may indicate that the photomechanical effects with thermal desorption, melting, overheating and explosive boiling processes of the irradiated material plays important role in formation of fast atomic plume followed by a slower plume of aggregates.

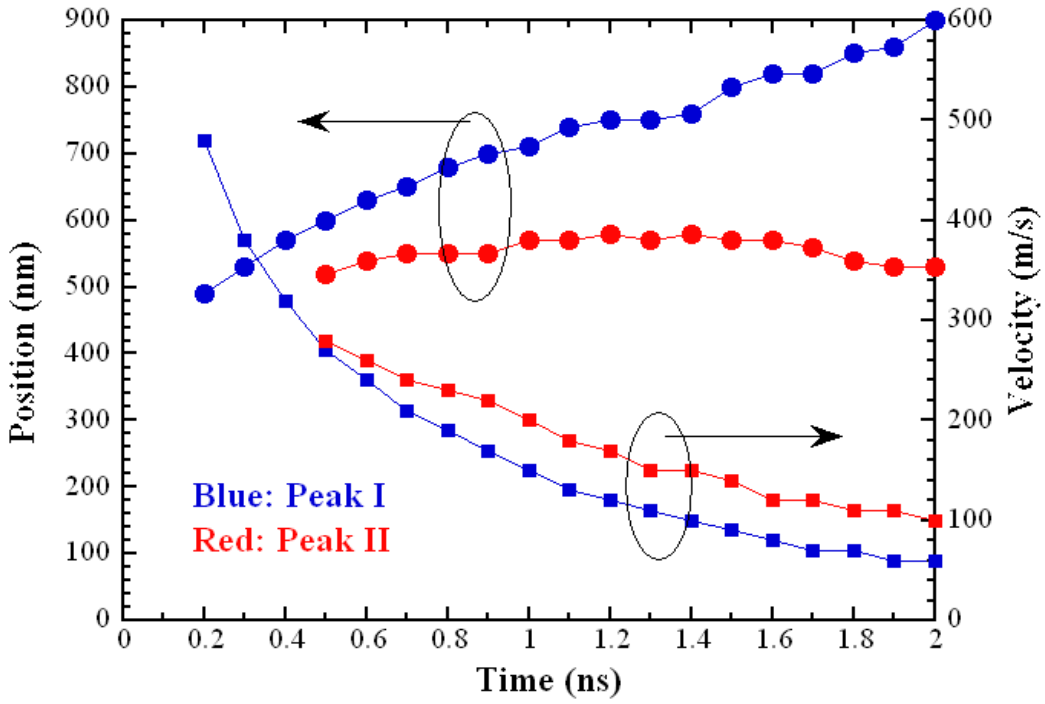

Figure 5.3 Evolution of the position and the average atomic velocity within the two peaks.

The dependence of plume splitting on background gas pressure and laser fluence has been studied as well in this simulation. It is found the plume penetration depth into the background gas decreases when the ambient pressure is higher. When the ambient pressure is increased, the plume expansion dynamics along with expansion velocities of the peaks are strongly affected by the interaction with the background gas and the plume stopping occurs at progressively earlier times and shorter distances from the target surface. The plume splitting is clearly observable but occurs much earlier and is much closer to the target surface under

the ambient pressure 0.87 MPa, whereas for 0.051 MPa the plume with vague splitting occurs spatially at a longer distance from the target and generally later in time.

The evolution from single-peaked to double-peaked plume has been investigated for two other laser fluences: 3 and 5 J/m^2. By increasing the irradiation level we observe that the plume propagation under higher fluences becomes more energetic and the plume splitting and plume sharpening is more noticeable. For irradiance in value of 3 J/m^2 the splitting effect is barely distinguishable and it occurs few tens of the picoseconds later than for 5 J/m^2 or 7 J/m^2. Under the fluence 5 J/m^2 the produced splitting of plume can be clearly noticed. Generally speaking, one can observe the apparent trend of the earlier occurrence of plume splitting when increasing the laser irradiance. To a large extent, since higher laser fluence results in more energetic particle formation, the velocity of those atoms and by that the peaks velocities are respectfully higher when increasing the fluence.

6. CONCLUSIONS

6.1 Summary and Conclusions

In this work, thermal and thermophysical phenomena induced by single picosecond laser pulse irradiation in the presence of background gas were studied using MD simulations.

For laser material interaction, the dynamics, internal structure, and evolution of shock waves were studied while emphasis was placed on the effect of the laser absorption depth, ambient pressure, and laser fluence. The study showed that the initial shock wave propagation velocity can reach an enormous value close to 7 Mach, and the initial pressure can go even over 25 MPa. The MD results on shock wave propagation and mass velocity were in sound agreement with the theoretical prediction, demonstrating the validity of MD approach for studying shock waves in laser-material interaction. At the interface between the plume and the compressed ambient gas, a velocity discontinuity was observed. Owing to the strong constraint from the compressed ambient gas, in late stage the ablated plume either stopped moving forward and mixed with the ambient gas, or moved backward to the target surface, leading to surface debris redeposition. It was found that smaller laser absorption depth, lower ambient pressure, or higher laser fluence will lead to stronger shock waves, which were featured with faster propagation in space and thicker interaction zone between the target and ambient gas.

Furthermore for picosecond laser ablation process, the secondary shock wave formation in a relatively high pressure background gas environment was investigated. The

primary shock wave evolution and especially reflection phenomenon of the internal shock front from the substrate was uniquely explored at nanoscale, giving forerun insight in its thermophysical and dynamical properties. It is found the significant pressure gradient inside the shock wave pushed the plume and some of the gas atoms in the rarefield to move back toward the target surface. The plume clusters re-deposited on the target surface while the ambient gas atoms were reflected back, leading to the secondary shock wave. Within the secondary shock wave range, the gas has relatively higher pressure, velocity, and density, but somewhat less rise of temperature. It is conclusive that the strong pressure gradient inside the main shock wave overcomes the forward momentum of the plume and some compressed gas, which leads to backward movement and re-deposition on the target surface. In result of ambient gas backward movement and reflection from the target surface, the secondary shock wave is formed.

Also for laser material interaction up to 2 ns, the physics of plume splitting was studied. Detailed atoms track allows to specifically look into the behavior of atoms within the peaks and reveals the mechanisms of peak formation. The observed plume velocity splitting came from two distinguished parts of the plume. The front peak of the plume came from the faster moving atoms and smaller particles during laser-material ablation. This region experienced strong constraint from the ambient gas and had strong velocity attenuation. The second (rear) peak of the plume velocity originated from the larger clusters in laser-material ablation. These larger clusters/particles moved slower and experienced very little constraint, eventually picked up their velocity during the early evolution. At the very beginning of laser-ablation, two density peaks emerged and quickly disappeared due to the spread-out of the

slower moving part. While the front peak propagated out against time, the second peak behaved as a standing wave and did not propagate but rather had a little trend towards the target surface. When the ambient pressure was increased, the plume splitting happened much earlier and occurred at a distance closer to the target surface. However when the ambient pressure was reduced, the plume splitting became weak and barely visible. Under stronger laser fluence irradiation, the plume splitting will happen earlier.

6.2 Contributions and Recommendations for Future Work

The fundamental information which consists of this dissertation's contents is essential for achieving a detailed understanding of the physics of shock waves in laser material interaction processes. It contributes to better understanding the phenomena occurring in early stages of laser ablation up to 5 ns. It needs to be noted this is the first study of shock wave in laser-material interaction at the atomic level. This atomic level study reveals very critical phenomena of shock waves in laser-material interaction, such as plume-back ground gas mass penetration, atomic velocity distribution inside the shock wave front, and the evolution of the plume in the background gas. Such information has never been obtained in the past.

The MD simulations were used to study the subject. The FORTRAN code has been developed with application of the parallel computation. I was a successive contributor in development and modifications to this code. Many new parameters were derived and had to be computed such as atomic velocity inside the shock wave, front propagation velocity, and mixing length parameter between expanding plume and shroud of propagating shock wave, which are very hard to obtain experimentally. Numerous simulation cases were conducted to

show the influence of external factors on the processes during laser material interaction. Notably, how ambient gas pressure, laser fluence, and laser absorption depth affects the laser material interaction was investigated. The validity of the approach and results has been verified previously in theoretical and experimental literature. It is demonstrated that MD technique is relatively fast and robust enough to perform accurate laser-material interaction simulations, especially for nano shock waves.

The reported results are designed to study the early stage shock wave dynamic, formation of the internal shock wave and plume's peculiar behavior rather than to recover an experimental condition. Laser-argon crystal interaction was studied which is different from the commonly used materials such as copper, silicon or carbon. The laser type and wavelength has not been specified. However the simulations were framed in the way that laser beam can resemble universal situation of the laser material interaction.

The meritorious significance of this study comes with broad purpose for the optimization of the experiments and itself can serve for controlling the laser material interaction process, optimizing the efficiency of laser assisted micro-machining, and minimizing the laser induced material damage. Moreover, unprecedented results can serve in improving our understanding of molecular energy-transfer processes and new presented findings successfully resulted in journal publications and conference paper.

In addition to the research conducted in this work, further investigation in laser material interaction and resulting physical phenomena requires to be performed.

Due to the immense progress in development of the ultrafast laser technology, and increasing application of this technique in recent years, femtosecond laser pulse duration should be investigated. The shorter time of the laser beam creates totally different processes when interacting with matter. The electrostatic ablation takes significant portion of the conventional thermal evaporation causing additional complexity in ongoing phenomena. Alike, the processes for nanosecond laser impulse should be studied for comparison purposes.

For the deposition of thin films it is necessary to control the composition of the laser produced plume. Plumes containing macroscopic particles and liquid droplet result in a poor quality deposited films. When, the plume cloud is ejected, nanoparticles very often combine and form nanoclusters as well as source of the liquid droplets in the plume is condensation of vapor during expansion. The process of solidification and condensation of these species should be studied and the way how the shock wave influences their creation.

Another very important occurrence in laser material interaction is melting and consecutive stress development in the target structure. It deserves more attention how the shock wave affects these processes and it would be of deliberate significance to pursue the investigation to that subject.

REFERENCES

Allen, M. P., and Tildesley, D. J., 1987, *Computer Simulation of Liquids*, Clarendon Press, Oxford.

Amoruso, S., Toftmann, B., Schou, J., 2005, "Broadening and Attenuation of UV Laser Ablation Plumes in Background Gases," *Applied Surface Science*, 248, 323-328.

Amoruso, S., Sambri, A., Vitiello, M., Wang, X., 2006, "Propagation of $LaMnO_3$ Laser Ablation Plume in Oxygen Gas," *Applied Surface Science*, 252, 4712-4716.

Amoruso, S., Bruzzese, R., Wang, X., Xia, J., 2008, "Propagation of a Femtosecond Pulsed Laser Ablation into a Background Atmosphere," *Applied Physics Letters*, 92, 041503-1-3.

Anisimov, S. I., Luk'yanchuk, B. S., Luches, A., 1996, "An Analytical Model for Three Dimensional Laser Plume Expansion into Vacuum in Hydrodynamic Regime," *Applied Surface Science*, 96-98, 24-32.

Arif, A. F. M., 2003, "Numerical Prediction of Plastic Deformation and Residual Stresses Induced by Laser Shock Processing," *Journal of Materials Processing Technology*, 136, 120-138.

Arnold, N., Gruber, J., Heitz, J., 1999, "Spherical Expansion of the Vapor Plume into Ambient Gas: an Analytical Model," *Applied Physics A*, 69, S87- S93.

Ashfold, M. N. R., Claeyssens, G. M. F., Henley, S. J., 2004, "Pulsed Laser Ablation and Deposition of Thin Films," *Chemical Society Reviews*, 33, 23-31.

Belonoshko, A. B., 1997, "Atomistic Simulation of Shock Wave-Induced Melting in Argon," *Science*, 275, 955-956.

Belonoshko, A. B., 1997, "Shock Wave-Induced Melting in Argon by Atomistic Simulation," *Science*, 278, 1474-1475.

Berendsen, H. J. C., Postma, J. P. M., van Gunsteren, W. F., DiNola, A., Haak, J. R., 1984, "Molecular Dynamics with Coupling to an External Bath," *Journal of Chemical Physics*, 81, 3684-3690.

Bulgakov, A. V., Bulgakova, N. M., 1995, "Dynamics of Laser-induced Plume Expansion into an Ambient Gas during Film Deposition," *Journal of Physics D: Applied Physics*, 28, 1710-1718.

Bulgakov, A. V., Predtechensky, M. R., Mayorov, A. P., 1996, "Transport of Neutral Atoms, Monoxides and Clusters in the Plume Produced by Laser Ablation of $YBa_2Cu_3O_{7-x}$ in Oxygen Environment," *Applied Surface Science*, 96-98, 159-163.

Bulgakov, A. V., Bulgakova, N. M., 1998, "Gas-dynamics Effects of the Interaction Between a Pulsed Laser-ablation Plume and the Ambient Gas: Analogy with an Underexpanded Jet," *Journal of Physics D: Applied Physics*, 31, 693-703.

Bulgakova, N. M., Bulgakov, A. V., Bobrenok, O. F., 2000, "Double Layer Effects in Laser-Ablation Plasma Plumes," *Physical Review E*, 62, 5624-5635.

Chrisey, D. B., and Hubler, G. K (eds.), 1994, *Pulsed Laser Deposition of Thin Films*, John Wiley & Sons INC., New York.

Clauer, A. H., Holbrook, J. H., Fairand, B. P., 1981, "Effects of Laser Induced Shock Waves on Metals," in Shock Waves and High-Strain-Rate Phenomena in Metals, Meyers, M. A., and Murr, L. E., (eds.), Plenum Publishing Corporation, New York, NY, 675-701.

Clauer, A. H., 1996, "Laser Shock Peening for Fatigue Resistance," in Surface Performance of Titanium, Gregory, J. K., Rack, H. J., and Eylon, D., (eds.), TMS, Warrendale, PA, 217-230.

Darke, S.A., Tyson, J.F., 1993, "Interaction of Laser Radiation with Solid Materials and Its Significance to Analytical Spectrometry: A review," *Journal of Analytical Atomic Spectrometry*, 8, 145-209.

Dijkkamp, D., Venkatesan, T., Wu, X. D., Shafeen, S. A., Jishraw, N., Minley, Y. H., McLean, W. L., Croft, M., 1987, "Preparation of Y-Ba-Cu Oxide Superconductor Thin-Films Using Pulsed Laser Evaporation from High-T_c Bulk Material," *Applied Physics Letters*, 51, 619-621.

Dlott, D. D., 1999, "Ultrafast Spectroscopy of Shock Waves in Molecular Materials," *Annual Review of Physical Chemistry*, 50, 251-278.

Dyer, P. E., Issa, A., Key, P. H., 1990, "Dynamics of Excimer Laser Ablation of Superconductors in an Oxygen Environment," *Applied Physics Letters*, 57, 186-188.

Eason, R. (ed.), 2007, *Pulsed Laser Deposition of Thin Films: Applications-Led Growth of Functional Materials*, John Wiley & Sons, INC., Hoboken, NJ.

Etcheverry, J. I., Mesaros, M., 1999, "Molecular Dynamics Simulation of the Production of Acoustic Waves by Pulsed Laser Irradiation," *Physical Review B*, 60, 9430-9434.

Everett Jr., R. A., Matthews, W. T., Prabhakaran, R., Newman Jr., J. C., Dubberly, M. J., December 2001, "The Effects of Shot and Laser Peening on Fatigue Life and Crack Growth in 2024 Aluminum Alloy and 4340 Steel," *NASA/TM-2001-210843, ARL-TR-2363*.

Feng, X., Wang, X., 2007, "Nanodomain Shock Wave in Near-field Laser-material Interaction," *Physics Letters A*, 369, 323-327.

Fogarassy, E., and Lazare, S (eds.), 1992, *Laser Ablation of Electronic Materials*, North-Holland, Amsterdam.

Geohegan, D. B., Puretzky, A. A., 1995, "Dynamics of Laser Ablation Plume Penetration through Low Pressure Background Gases," *Applied Physics Letters*, 67, 197-199.

Geohegan, D. B., Puretzky, A. A., 1996, "Laser Ablation Plume Thermalization Dynamics in Background Gases: Combined Imaging, Optical Absorption and Emission Spectroscopy, and Ion Probe Measurements," *Applied Surface Science*, 96-98, 131-138.

Hakkinen, H., Landman, U., 1993, "Superheating, Melting, and Anealing of Copper Surfaces," *Physical Review Letters*, 71, 1023-1026.

Han, M., Gong, Y., Zhou, J., Yin, C., Song, F., Muto, N., Takiya, T., Iwata, Y., 2002, "Plume Dynamics during Film and Nanoparticles Deposition by Pulsed Laser Ablation," *Physics Letters A*, 302, 182-189.

Hansen, T. N., Schou, J., Lunney, J. G., 1999, "Langmuir Probe Study of Plasma Expansion in Pulsed Laser Ablation," *Applied Physics A*, 69, S601-S604.

Harilal, S. S., 2001, "Expansion Dynamics of Laser Ablated Carbon Plasma Plume in Helium Ambient," *Applied Surface Science*, 172, 103-109.

Harilal, S. S., Bindhu, C. V., Tillack, M. S., Najmabadi, F., Gaeris, A. C., 2002, "Plume Splitting and Sharpening in Laser-Produced Aluminum Plasma." *Journal of Physics D: Applied Physics*, 35, 2935-2938.

Harilal, S. S., Bindhu, C. V., Tillack, M. S., Najmabadi, F., Gaeris, A. C., 2003, "Internal Structure and Expansion Dynamics of Laser Ablation Plumes into Ambient Gases," *Journal of Applied Physics*, 93, 2380-2388.

Hill, M. R., DeWald, A. T., Demma, A. G., Hackel, L. A., Chen, H. L., Dane, C. B., Specht, R. C., Harris, F. B., August 2003, "Laser Peening Technology," *Advanced Materials & Processes*, 65-67.

Holian, B. L., 2004, "Molecular Dynamics Comes of Age for Shockwave Research," *Shock Waves*, 13, 489-495.

Hu, Y., Yao, Z., Hu, J., 2006, "3-D FEM Simulation of Laser Shock Processing," *Surface & Coatings Technology*, 201, 1426-1435.

Itina, T. E., Hermann, J., Delaporte, P., Sentis, M, 2002,"Laser-Generated Plasma Plume Expansion: Combined Continuous-Microscopic Modeling," *Physical Review E*, 66, 066406-1-12.

Ivanov, D. S., Zhigilei, L. V., Bringa, E. M., De Koning, M., Remington, B. A., Caturla, M. J., Pollaine, S. M., 2003, "Molecular Dynamics Simulations of Shocks Including Electronic Heat Conduction and Electron-Phonon Coupling," in Shock Compression of Condensed Matter, AIP Conference Proceedings, Furnish, M. D., Gupta, Y. M., Forbes, J. W., (eds.), 706, 225-228, 2004.

Le, H. C., Zeitun, D. E., Parisse, J. D., Sentis, M., Marine, W., 2000, "Modeling of Gas Dynamics for a Laser-generated Plasma: Propagation into Low-pressure Gases," *Physical Review E*, 62, 4152-4161.

Leboeuf, J. N., Chen, K. R., Donato, J. M., Geohegan, D. B., Liu, C. L., Puretzky, A. A., Wood, R. F., 1996, "Modeling of Plume Dynamics in Laser Ablation Processes for Thin Film Deposition of Materials," *Physics of Plasmas*, 3, 2203-2206.

Lichtenwalner, D. J., Auciello, O., Dat, R., Kingon, A. I., 1993, "Investigation of the Ablated Flux Characteristics during Pulsed Laser Ablation Deposition of Multicomponent Oxides," *Journal of Applied Physics*, 74, 7497-7505.

Lorazo, P., Lewis, L. J., Meunier, M., 2003, "Short-Pulse Laser Ablation of Solids: From Phase Explosion to Fragmentation," *Physical Review Letters*, 91, 225502-1-4.

Lorazo, P., Lewis, L. J., Meunier, M., 2006, "Thermodynamic Pathways to Melting, Ablation, and Solidification in Absorbing Solids under Pulsed Laser Irradiation," *Physical Review B*, 73, 134108-1-22.

Lukes, J. R., Li, D. Y., Liang, X. G., Tien, C. L., 2000, "Molecular Dynamics Study of Solid Thin-Film Thermal Conductivity," *ASME Journal of Heat Transfer*, 122, 536-543.

Mason, P. R. D., Mank, A. J. G., 2001, "Depth-resolved Analysis in Multi-layered Glass and Metal Materials using Laser Ablation Inductively Coupled Plasma Mass Spectroscopy (LA-ICP-MS)," *Journal of Analytical Atomic Spectrometry*, 16, 1381-138.

Miller, J. C., and Haglund, R. F. Jr. (eds.), 1998, *Laser Ablation and Desorption*, Academic Press, San Diego, CA.

Pathak, K., Povitsky, A., 2007, "Modeling of Plume Dynamics with Shielding in Laser Ablation of Carbon," *Applied Surface Science*, 253, 6359-6365.

Perez, D., Lewis, L. J., 2004, "Thermodynamic Evolution of Materials during Laser Ablation under Pico and Femtosecond Pulses," *Applied Physics A*, 79, 987-990.

Phipps, C., (ed.), 2007, *Laser Ablation and Its Applications*, Springer Science + Business Media LLC, New York, NY.

Robertson, D. H., Brenner, D. W., White, C. T., 1991, "Split Shock Waves from Molecular Dynamics," *Physical Review Letters*, 67, 3132-3135.

Russo, R. E., Mao, X. L., Borisov, O. V., Liu, H., 2000, "Influence of Wavelength on Fractionation in Laser Ablation ICP-MS," *Journal of Analytical Atomic Spectrometry*, 15, 1115-1120.

Russo, R. E., Mao, X., Gonzales, J. J., Mao, S. S., 2002, "Femtosecond Laser Ablation ICP-MS," *Journal of Analytical Atomic Spectrometry*, 17, 1072-1075.

Schou, J., 2006, "Laser Beam-Solid Interactions: Fundamental Aspects," in Materials Surface Processing by Directed Energy Techniques, Pauleau, I., (ed.), Elsevier, 33-62.

Scott, K., Huntley, J. M., Phillips, W. A., Clarke, J., Field, J. E., 1990, "Influence of Oxygen Pressure on Laser Ablation of $YBa_2Cu_3O_{7-x}$," *Applied Physics Letters*, 57, 922-924.

Singh, S., Argument, M., Tsui, Y. Y., Fedosejevs, R., 2005, "Effect of Ambient Air Pressure on Debris Redeposition during Laser Ablation of Glass," *Journal of Applied Physics*, 98, 113520-1-7.

Voevodin, A. A., Jones, J. G., Zabinski, J. S., 2000, "Characterization of ZrO_2/Y_2O_3 Laser Ablation Plasma in Vacuum, Oxygen, and Argon Environments," *Journal of Applied Physics*, 88, 1088-1096.

Wang, X., 2001, *Thermal and Thermomechanical Phenomena in Laser Material Interaction*, Ph.D. Thesis, Purdue University, West Lafayette, IN.

Wang, X., Xu, X., 2002, "Molecular Dynamics Simulation of Heat Transfer and Phase Change during Laser Material Interaction," *ASME Journal of Heat Transfer*, 124, 265-274.

Wang, X., Xu, X., 2003, "Molecular Dynamic Simulation of Thermal and Thermomechanical Phenomena in Picosecond Laser Material Interaction," *International Journal of Heat Transfer*, 46, 45-53.

Wang, X., Xu, X., 2003, "Nanoparticles Formed in Picosecond Laser Argon Crystal Interaction," *ASME Journal of Heat Transfer*, 125, 1147-1155.

Wang, X., 2005, "Large-scale Molecular Dynamics Simulation of Surface Nanostructuring with a Laser-assisted Scanning Tunneling Microscope," *Journal of Physics D: Applied Physics*, 38, 1805-1823.

Watanabe, I., McBride, M., Newton, P., Kurtz, K. S., 2009, "Laser Surface Treatment to Improve Mechanical Properties of Cast Titanium," *Dental Materials*, 25, 629-633.

Wood, R. F., Chen, K. R., Leboeuf, J. N., Puretzky, A. A., Geohegan, D. B., 1997, "Dynamics of Plume Propagation and Splitting during Pulsed-laser Ablation," *Physical Review Letters*, 79, 1571-1574.

Zel'dovich, Y. R., Raizer, Y. P., 2001, "Physics of Shock Waves and High-Temperature Hydrodynamic Phenomena," Academic Press Inc., New York and London (Hayes, W. D., Probstein, R. F., eds.).

Zhang, Z., Gogos, G., 2004, "Theory of Shock Wave Propagation during Laser Ablation," *Physical Review B*, 69, 235403-1-9.

Zhang, L., Wang, X., 2008, "Dynamic Structure and Mass Penetration of Shock Wave in Picosecond Laser-Material Interaction," *Japanese Journal of Applied Physics*, 47, 964-968.

Zhang, Y. K., Lu, J. Z., Ren, X. D., Yao, H. B., Yao, H. X., 2009, "Effect of Laser Shock Processing on the Mechanical Properties and Fatigue Lives of the Turbojet Engine Blades Manufactured by LY_2 Aluminum Alloy," *Materials and Design*, 30, 1697-1703.

Zhigilei, L. V., Garrison, B. J., 1999, "Pressure Waves in Macroscopic Simulations of Laser Ablation," *Materials Research Society Symposium Proceedings*, 538, 491-496.

Zhigilei, L. V., Leveugle, E., Garrison, B. J., Yingling, Y. G., Zeifman, M. I., 2003, "Computer Simulation of Laser Ablation of Molecular Substrates," *Chemical Reviews*, 103, 321-347.

Zhigilei, L. V., 2003, "Dynamics of the Plume Formation and Parameters of the Ejected Clusters in Short-Pulse Laser Ablation," *Applied Physics A*, 76, 339-350.

VITA

Sobieslaw Stanislaw Gacek was born on July 12, 1980 in Krynica-Zdroj, Poland. He was raised up in Andrzejowka, small mountain village, where he spent 3 happy years of elementary school. Another 5 years of middle school studies he spent in Zlockie – lovely touristic town. In the fall 1995, he was accepted to Electrical-Mechanical College in Nowy Sacz. He graduated with highest distinctions and in October 2000, he started his undergraduate study at the Faculty of Power and Aeronautical Engineering at Warsaw University of Technology in Poland. He received the Bachelor of Engineering in Mechanical Engineering in the spring 2004 and continued to the graduate study in the same department. During his final year at the University, he received an academic scholarship at Kingston University, England. In April 2006 he received his Master of Science in Engineering with specialization in Propulsion and Aircraft Engines. He joined in the fall 2006 the Micro/Nanoscale Thermal Science Laboratory directed by Professor Xinwei Wang at the Mechanical Engineering Department, University of Nebraska Lincoln to pursue his Ph.D. degree. In January 2008 he transferred to Iowa State University following Professor Wang. He has served as Research and Teaching Assistant in the Mechanical Engineering Department at University of Nebraska Lincoln and at Iowa State University. During his doctoral program he was involved in many projects investigating thermal and thermomechanical phenomena in laser material interaction. He was awarded 3 place in 1st Annual Excellence of Graduate Research Award in Design and Manufacturing Competition in the Department of Mechanical Engineering at ISU. He is expecting his Ph.D. in August 2009.